Theodor-Boveri-Institut für Biowissenschaften

Lehrstuhl für Biotechnologie und Biophysik

ASSOCIATION AND ACTIVATION OF TNF-RECEPTOR I INVESTIGATED WITH SINGLE-MOLECULE TRACKING AND SUPER-RESOLUTION MICROSCOPY IN LIVE CELLS

Dissertation zur Erlangung des

naturwissenschaftlichen Doktorgrades

der Julius-Maximilians-Universität Würzburg

vorgelegt von

Meike Heidbreder

Würzburg, 2012

THEODOR-BOVERI-INSTITUT FÜR BIOWISSENSCHAFTEN

LEHRSTUHL FÜR BIOTECHNOLOGIE UND BIOPHYSIK

ASSOCIATION AND ACTIVATION OF TNF-RECEPTOR I INVESTIGATED WITH SINGLE-MOLECULE TRACKING AND SUPER-RESOLUTION MICROSCOPY IN LIVE CELLS

DISSERTATION ZUR ERLANGUNG DES

NATURWISSENSCHAFTLICHEN DOKTORGRADES

DER JULIUS-MAXIMILIANS-UNIVERSITÄT WÜRZBURG

VORGELEGT VON

MEIKE HEIDBREDER

GEBOREN IN BIELEFELD

WÜRZBURG, 2012

Eingereicht am 14.August 2012

Mitglieder der Promotionskommission

Vorsitzender: .....

Gutachter: Prof. Dr. Mike Heilemann

Gutachter: Prof. Dr. Christian Kaltschmidt

Tag des Promotionskolloquiums: .....

Doktorurkunde ausgehändigt am: .....

EHRENWÖRTLICHE ERKLÄRUNG

Gemäß § 4 Abs. 3 der Promotionsordnung der Fakultät für Biologie der Julius-Maximilians-Universität Würzburg erkläre ich hiermit an Eides statt, dass ich die vorliegende Dissertation selbstständig angefertigt und keine anderen Quellen und Hilfsmittel als die angegebenen verwendet habe. Alle wörtlich oder inhaltlich übernommenen Textstellen, Tabellen oder Grafiken sind als solche gekennzeichnet. Desweiteren versichere ich, dass die vorliegende Dissertation weder in gleicher noch in ähnlicher Form bereits in anderen Promotionsverfahren vorgelegt wurde.

Teile dieser kumulativen Arbeit wurden publiziert und werden hier mit der Erlaubnis der einzelnen Journals verwendet bzw. reproduziert.

Würzburg, August 2012

Meike Heidbreder

IN NATURE'S INFINITE BOOK OF SECRECY, A LITTLE I CAN READ.

WILLIAM SHAKESPEARE

ANTONY AND CLEOPATRA, ACT I, SCENE II

SUMMARY

Cellular responses to outer stimuli are the basis for all biological processes. Signal integration is achieved by protein cascades, recognizing and processing molecules from the environment. Factors released by pathogens or inflammation usually induce an inflammatory response, a signal often transduced by Tumour Necrosis Factor alpha (TNFα). TNFα receptors TNF-R1 and TNF-R2 can in turn lead to apoptosis or proliferation via NF-κB. These processes are closely regulated by membrane compartimentalization, protein interactions and trafficking. Fluorescence microscopy offers a reliable and non-invasive method to probe these cellular events. However, some processes on a native membrane are not resolvable, as they are well below the diffraction limit of microscopy. The recent development of super-resolution fluorescence microscopy methods enables the observation of these cellular players well below this limit: by localizing, tracking and counting molecules with high spatial and temporal resolution, these new fluorescence microscopy methods offer a previously unknown insight into protein interactions at the near-molecular level. Direct stochastic optical reconstruction microscopy (*d*STORM) utilizes the reversible, stochastic blinking events of small commercially available fluorescent dyes, while photoactivated localization microscopy (PALM) utilizes phototransformation of genetically encoded fluorescent proteins. By photoactivating only a small fraction of the present fluorophores in each observation interval, single emitters can be localized with high precision and a super-resolved image can be reconstructed. Quantum Dot Triexciton imaging (QDTI) utilizes the three-photon absorption (triexcitonic) properties of quantum dots (QD) and to achieve a twofold resolution increase using conventional confocal microscopes.

In this thesis, experimental approaches were implemented to achieve super-resolution microscopy in fixed and live-cells to study the spatial and temporal dynamics of TNF and other cellular signaling events. We introduce QDTI to study the three-dimensional cellular distribution of biological targets, offering an easy method to achieve resolution enhancement in combination with optical sectioning, allowing the preliminary quantification of labeled proteins. As QDs are electron dense, QDTI can be used for correlative fluorescence and transmission electron microscopy, proving the versatility of QD probes.

Utilizing the phototransformation properties of fluorescent proteins, single-receptor tracking on live cells was achieved, applying the concept of single particle tracking PALM (sptPALM) to track the dynamics of a TNF-R1-tdEos chimera on the membrane. Lateral receptor dynamics can be tracked with high precision and the influences of ligand addition or lipid disruption on TNF-R1 mobility was observed. The results reveal complex receptor dynamics, implying internalization processes in response to TNFα stimulation and a role for membrane domains with reduced fluidity, so-called lipid

raft domains, in TNF-R1 compartimentalization prior or post ligand induction. Comparisons with previously published FCS data show a good accordance, but stressing the increased data depth available in sptPALM experiments. Additionally, the active transport of NF-κB-tdEos fusions was observed in live neurons under chemical stimulation and/or inhibition.

Contrary to phototransformable proteins that need no special buffers to exhibit photoconversion or photoactivation, *d*STORM has previously been unsuitable for *in vivo* applications, as organic dyes relied on introducing the probes via immunostaining in concert with a reductive, oxygen-free medium for proper photoswitching behaviour. ATTO655 had been previously shown to be suitable for live-cell applications, as its switching behavior can be catalyzed by the reductive environment of the cytoplasm. By introducing the cell-permeant organic dye via a chemical tag system, a high specificity and low background was achieved. Here, the labeled histone H2B complex and thus single nucleosome movements in a live cell can be observed over long time periods and with ~20 nm resolution.

Implementing these new approaches for imaging biological processes with high temporal and spatial resolution provides new insights into the dynamics and spatial heterogeneities of proteins, further elucidating their function in the organism and revealing properties that are usually only detectable *in vitro.*

ZUSAMMENFASSUNG

Zelluläre Antworten auf externe Stimuli sind die Basis aller biologischer Prozesse. Die Integration dieser Signale wird dabei von Proteinkaskaden ausgeführt, welche Moleküle aus der Umgebung wahrnehmen und verarbeiten. Faktoren, welche von Pathogenen oder während einer Entzündung freigesetzt werden, induzieren für gewöhnlich eine Entzündungsantwort, eine Reaktion, die oft vom Tumornekrosefaktor alpha (TNFα) vermittelt wird. Die TNFα Rezeptoren TNF-R1 und TNF-R2 vermitteln nach Ligandenbinding Apoptose oder Zellproliferation durch NF-κB. Diese Prozesse sind engmaschig durch Membrankompartimentierung, Proteininteraktionen und -transport reguliert. Fluoreszenzmikroskopie bietet eine zuverlässige, nicht-invasive Methode um diese zellulären Prozesse zu untersuchen. Allerdings sind einige Prozesse innerhalb einer nativen Membran nicht auflösbar, da sie weit unterhalb der Beugungsgrenze der Lichtmikroskopie stattfinden.

Die jüngste Entwicklung der hochauflösenden Fluoreszenzmikroskopiemethoden erlaubt die Beobachtung dieser zellulären Abläufe auf molekularer Ebene: durch das Lokalisieren, Verfolgen und Zählen von Molekülen mit hoher räumlicher und zeitlicher Auflösung bieten diese neuen Fluoreszenzmethoden bisher unbekannte Einblicke in Proteininteraktionen. Direkte stochastische optische Rekonstruktionsmikroskopie (dSTORM) nutzt die reversiblen, stochastischen Ereignisse von kleinen blinkenden, kommerziell erhältlichen Fluoreszenzfarbstoffen, während die photoaktivierte Lokalisationsmikroskopie (PALM) die nutzt Phototransformation von genetisch kodierten fluoreszierenden Proteinen nutzt. Durch das Photoaktivieren lediglich eines kleinen Bruchteils der Fluorophore innerhalb eines Zeitintervalls können einzelne Emitter mit hoher Genauigkeit lokalisiert und ein hochaufgelöstes Bild daraus rekonstruiert werden. Quantum Dot Triexciton Imaging (QDTI) nutzt die Drei-Photonen-Absorption (d.h. die triexitonischen Eigenschaften) von Quantenpunkten (Quantum Dot - QD) um eine zweifache Auflösungserhöhung mittels eines herkömmlichen Konfokalmikroskopes zu erreichen.

In dieser Arbeit wurden experimentelle Ansätze zur hochauflösenden Mikroskopie an fixierten und lebenden Zellen implementiert, um die räumliche und zeitliche Dynamik von TNF und anderen zellulären Signalwegen zu untersuchen. Zur Analyse der dreidimensionalen, zellulären Verteilung von biologischen Zielen stellen wir QDTI vor, welches eine einfache Methode zur Verbesserung der Auflösung an Konfokalmikroskopen in Kombination mit optischen Schnitten darstellt. Dies ermöglicht die vorläufige Quantifizierung von markierten Proteinen. Da QDs eine hohe Elektronendichte besitzen kann QDTI auch für korrelative Fluoreszenz- und Transmissionselektronenmikroskopie genutzt werden, was die Vielseitigkeit der QD-Sonden verdeutlicht.

Unter Ausnutzung der Phototransformation von fluoreszierenden Proteinen konnten einzelne Rezeptormoleküle mit Hilfe des single-particle tracking PALM (sptPALM) Konzepts verfolgt werden, um die Dynamiken einer TNF-R1-tdEos Chimäre auf der Membran zu beobachten. Die laterale Rezeptordynamik kann hier mit hoher Präzision gemessen, und die Einflüsse auf die TNF-R1-Mobilität konnte nach Ligandenzugabe oder die Störung der Membranzusammensetzung analysiert werden. Die Ergebnisse zeigen eine komplexe Rezeptordynamik und lassen sowohl auf Internalisierungsprozesse in Reaktion auf TNFα-Stimulation, als auch auf eine wichtige Rolle von Membrandomänen mit eingeschränkter Fluidität - sogenannten Lipid Rafts - in der TNF-R1 Kompartimentierung vor oder während der Ligandenbinding schließen. Vergleiche mit bereits publizierten FCS-Daten zeigen eine gute Übereinstimmung hierzu, aber machen auch die erhöhte Datentiefe von sptPALM-Experimenten. Zusätzlich wurde der aktive Transport von NF- B-tdEos Fusionsproteinen in lebenden Neuronen unter chemischer Stimulierung bzw. Inhibierung untersucht.

Im Gegensatz zu phototransformierbaren Proteinen, die keine speziellen Puffer zur Photokonversion oder Photoaktivierung benötigen, war dSTORM bisher für in vivo Anwendungen ungeeignet, da organische Farbstoffe auf die Einführung über Immunfärbung in Kombination mit einem reduktiven, Sauerstoff-freiem Medium für korrektes Photoschalten angewiesen waren. ATTO655 wurde zuvor als geeignet für die Anwendung in lebenden Zellen eingestuft, da das Schaltverhalten durch die reduktive Umgebung des Zytoplasmas katalysiert werden kann. Durch die Einführung von membranpermeablen organischen Farbstoffen über ein chemisches Markierungssystem konnte eine hohe Spezifität und ein geringer Hintergrund erreicht werden. Hier konnte durch die Markierung des Histon H2B Komplexes die Bewegung einzelner Nukleosome in lebenden Zellen über lange Zeiträume mit einer Auflösung von ~20 nm beobachtet werden.

Die Umsetzung dieser neuen Ansätze für die Darstellung biologischer Prozesse mit hoher zeitlicher und räumlicher Auflösung liefert neue Einblicke in die Dynamiken und die räumliche Heterogenität von Proteinen und enthüllt Funktionen im Organismus und beleuchtet Eigenschaften, die sonst *nur in vitro* nachweisbar wären.

TABLE OF CONTENTS

1. INTRODUCTION

The proper interaction of a cell with its environment is vital for its survival. Reacting to stimuli is the most important step in integrating signals from the outer environment. Monitoring environmental conditions and reacting with a change in the inner status (e.g. expression patterns) of the cell ensures its survival and proper functioning in a tissue. In response, a cell might proliferate, (de-)differentiate or migrate, after changes in protein interactions or transcription to react to outer changes (e.g. chemotaxis in response to nutrient gradients) or it might up-regulate defense mechanisms to combat influences such as infection, inflammation or lesion. Cell-cell communication and signal propagation are vital for higher-order tissues, embryonic development and signaling in the nervous system. Magnifying and imaging biological structures beyond the capabilities of the human eye has yielded countless revelations since Galileo Galilei turned his telescope from monitoring planets to insects in 1610. Antoni van Leeuwenhoek (1632-1723) perfected Galilei's technique, leading to the discovery of protozoa and bacteria and describing these *animalcules'* erratic motions in water [1]. Robert Hooke was able to reproduce Leeuwenhoek's results for *Micrographia*, the first book about microscopy [2]. Within, he described the regular structures he observed in plants, coining the term *cellula* - as the regular structures reminded him a monk's dwelling. As bright field microscopy is limited by the little contrast that biological samples offer, naturally occurring substances were developed as differential stains in the 19th century Ehrenberg, Ehrlich, Virchow, Ramón y Cajal and many more shaping today's microbiology, histology, pathology and cell biology. The discovery of fluorescence led to the development of the first fluorescence microscopes in the 20th century. Light-emitting dyes, nanocrystals and fluorescent proteins have since then acted as specific labels to study biological targets. Hirschfeld was the first to directly measure a single fluorescently-labeled antibody [3]. Since then, fluorescence microscopy has been harnessed in a variety of procedures [4].

1.1. TNF ALPHA

In 1893, the surgeon William Coley observed the regression of malignant tumours in patients exposed to *Streptococcus erysipelatis* [5], soon thereafter devising a cancer treatment - *Coley's toxin* - consisting of heat-inactivated bacteria. At the time Coley thought the bacterial endotoxins induced an immune answer, attacking the cancer. Today it is known that endotoxins indeed activate the immune response under certain conditions and attack malignant growths. However, not all tumours are susceptible to this immunogenic reaction, explaining the slim success of Coley's treatment. In 1975, the protein responsible for the sometimes occuring necrosis was discovered to be secreted by macrophages [6]. Aptly named tumor necrosis factor (TNF), it was found to be involved in septic shock, inflammation and cachexia, but also proliferation [7-9]. A similar protein from activated lymphocyte cultures had been termed Lymphotoxin (LT) a few years before [10, 11]. Both factors were found to be produced in human monocytes and the full cDNA could be obtained from the amino acid sequence of extracted proteins [12, 13]. LT was renamed to TNFβ (and TNF to TNFα) to better reflect their homology in structure and function: both bind to the same surface receptors with high affinity, yet do not induce the same signal cascades [14-17].

After translation of the TNFα mRNA, a 76 AA presequence acts as a membrane anchor, building a 26 kDa, membrane-bound TNFα pro-form (mTNFα) [18]. Cleavage by the metalloproteinase TNFα converting enzyme (TACE) releases the 17kDa soluble, mature TNFα (sTNFα) into the extracellular solution [19]. While membrane-bound - or *juxtacrine* - mTNFα signalling has been linked to beneficial effects like tumor shrinkage, sTNFα signaling has been found to induce inflammation and septic shock, an effect linked to the differing receptors of the two TNFα types [8, 18, 20, 21]. sTNFα exhibits densely packed antiparallel β-strands, a so-called *jellyroll topology*. Three monomers self-assemble at hydrophobic interfaces into a cone-shaped, 55kDa homotrimer (FIG. 1). Each trimer exhibits three possible receptor binding sites, suggesting receptor trimerisation prior or while binding [22, 23]. As a highly pleiotropic cytokine, TNFα influences a large variety of pathways, including activation of transcription factors, cytokine production; also positively influencing its own expression levels [24-27]. TNFα was found to participate in many cellular events, e.g. cell proliferation, resistance to infection, learning and embryonic development [8, 28-30]. As TNFα plays an important role in many mechanisms, it is

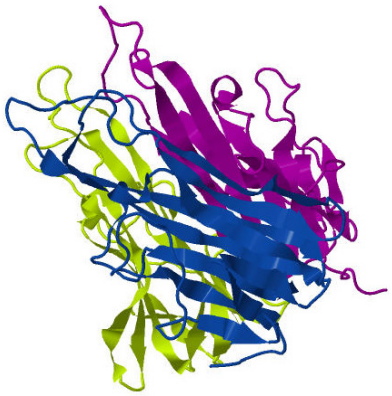

Fig. 1: Ribbon model of the jellyroll topology of single TNFα and the structure of the TNFα homotrimer, presenting each TNFα subunit in a different colour. PDB ID: 1TNF [22].

not surprising that it is also a major player in autoimmune, neurological and pulmonary diseases, but also tumor formation. As a result, TNFα antagonists have been developed for clinical use [31].

1.2. THE TNF SUPERFAMILY - STRUCTURE

The TNF superfamily (TNFSF) comprises 40 ligands and receptors, among them important mediators of growth and inflammation like CD40, TRAIL and Fas/CD95. A majority of them are expressed in immune cells and convey overlapping responses, as several ligands bind to more than one TNFSF receptor [32].

TNFSF receptors are characterized by a highly conserved extracellular motif of 2-6 repeats of a cysteine-rich domain (CRD), responsible for proper ligand binding. The CRD shows similarities to the extracellular domains of other cytokine receptors, such as nerve growth factor receptor (NGFR) and the epidermal growth factor receptor (EGFR) receptor family [33, 34]. While not directly interacting with the ligand [35], the membrane distal CRD1 is vital for ligand binding, its structure dictating a receptor's response to sTNFα [36]. CRD1 is also involved in mediating the potential pre-assembly of receptors prior to ligand binding, acting as a pre-ligand binding domain (PLAD). As the CRD1 regions of TNFSF members differ, this explains the different responses of receptors that bind the same ligand with comparable affinities: CRD1 mediates the stabilization of receptor oligomers of some receptors, thus influencing receptor responsiveness in the event of TNFα binding [37]. As an additional regulative mechanism, the extracellular part of TNF receptors can be released by enzymatic cleavage and act as a TNFα sink, binding to the ligand in the medium without eliciting a signal response [38, 39].

TNFSF receptors can be further classified by their intracellular domains: a so-called death domain (DD) - named for its importance in transmitting apoptotic signals - is typical for the intracellular terminus of some members of the TNF-R superfamily. Receptors lacking a DD can still induce apoptotic pathways, probably by ligand passing or signal amplification [40, 41]. Another group of the TNFSF exhibits a truncated cytoplasmatic domain unable to transduce a signal at all and thus acting as decoy receptors during ligand binding [42]. As TNF receptors do not transmit a signal by catalytic activity but by adapter recruitment and aggregation via present DDs, binding events in the absence of ligands must be avoided. For this, the DD interacts with an intracellular silencer of death domain (SODD), which disassociates upon ligand binding [43].

1.2.1. SIGNALLING VIA TNF-R1 / TNF-R2

TNFα mainly activates the 55kDa TNF receptor 1 (TNF-R1) and the 75kDa TNF receptor 2 (TNF-R2). While TNF-R1 is almost ubiquitously distributed on all cell types in high numbers, TNF-R2 expression is mostly restricted to cells of haematopoietic origin [34, 44, 45].

Furthermore, TNF-R2 only shows a high signal induction after binding mTNFα, eliciting different responses in the cell [45, 46]. Both receptors exhibit the four typical CRDs in their extracellular domains, while their intracellular parts show no homologies: TNF-R1 contains a typical intracellular DD, while TNF-R2 shows a TNF receptor associated factor (TRAF) motif, resulting in diverging signaling pathways [41, 47]. TNF-R1 is responsible for either induction of proliferation via activation of NF-κB, or apoptosis via activation of caspase-8 - a dichotomy largely attributed to distinct sets of recruited adapter proteins (FIG. 2): After

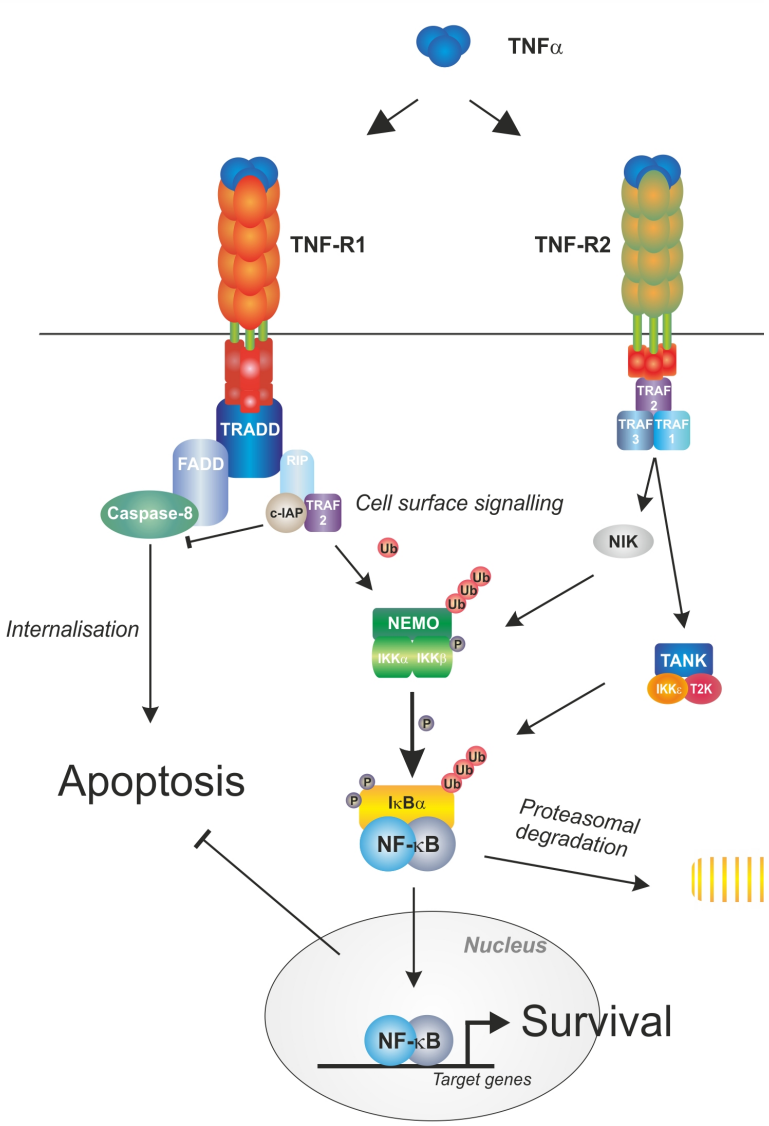

Fig. 2: Signaling pathways of TNF-R1 and TNF-R2 and their interaction. Upon TNFα binding, TRADD is recruited to the DD of TNF-R1. If the receptor is internalized, recruitment of FADD leads to the activation of caspases, resulting in apoptotic signaling. In cell surface signaling, RIP and TRAF-2 and c-IAPs are recruited, initiating the degradation of IκB via the ubiquitinylation of the IκB kinase complex. This in turn leads to the translocation of NF-κB into the nucleus, representing the canonical activation of NF-κB, usually comprising a p50/p65 heterodimer. c-IAP additionally inhibits apoptosis by influencing caspase maturation. TNF-R2 is mainly acting synergistically - in the event of TNFα binding activating NF-κB via its non-canonical pathway, inducing NIK or TANK. Induction by TNFα is usually weak via TNF-R2, full activation is only achieved by binding mTNFα, which shifts the signaling towards apoptosis for TNF-R1 signaling.

TNFα binding, TNF-R-associated death domain protein (TRADD), TRAF-2 and receptor interacting serine-threonine kinase (RIP) bind to the death domain of TNF-R1. Anti-apoptotic proteins from the inhibitor/apoptosis family (c-IAP-1 and c-IAP-2) are then recruited to the complex to suppress caspase-8 activity. The formation of this signalling complex leads to the ubiquitinylation of the subunit IKKγ/NEMO, which in turn leads to the phosphorylation and activation of its catalytic subunits IKKα and IKKβ. This results in the phosphorylation and consecutive proteasomal degradation of the inhibitory IκB, that usually retains nuclear factor kappa-B (NF-κB) it in its inactive, cytoplasmatic state. Demasking the nuclear localization sequence of NF-κB starts translocation into the nucleus, commencing transcription of anti-apoptotic proteins and also of new IκB to mask the free NF-κB. Thus, this canonical NF-κB activation is a transient process, usually lasting 30-60 minutes [48, 49]. On the other hand, recruitment of Fas-associated death domain (FADD) to TRADD leads to the commencement of the pro-apoptotic pathway: the formation of the death signalling complex (DISC) and thus the activation of caspase-8 leads to apoptosis by a release of cytochrome c [50]. In addition to the activation of caspases, TNFα has been shown to induce endolysosomal acid sphingomyelinase, which upregulates ceramide production - a second messenger known to activate apoptosis. However, TNF-R1 does not usually trigger apoptosis unless protein synthesis is blocked, as NF-κB inhibits apoptotic pathways in a healthy cell [51]. The dichotomy of pro- and anti-apoptotic functions by the same receptor is mostly orchestrated by a temporal and spatial separation of both cascades.

In contrast, TNF-R2 signaling is less well understood, usually only described to be an enhancer of TNF-R1. Signaling commences by directly binding TRAF-2 with high affinity, inducing NF-κB via its non-canonical pathways. By binding TRAF-1 and TRAF-3, the NF-κB inducing kinase (NIK) or the TRAF family-associated protein (TANK) activates IKKα and IKKβ and leads in turn to the release of sequestered NF-κB [52, 53]. However, due to a secondary TRAF-2 binding motif, NF-κB induction is usually inactive or very weak via TNF-R2 [54, 55]. On the contrary, induction of TNF-R2 usually promotes caspase-8 activity by depleting cytoplasmatic c-IAPs and TRAF-2, which leads to an enhancement of the apoptotic pathway for TNF-R1 due to the lack of survival-promoting TRAF-2 [56, 57].

1.2.2. THE ROLE OF LIPID RAFTS

The phospholipid bilayer of a cell is no static barrier to the outside world, but a dynamic space that is in constant motion, regulating uptake and disposal of molecules from and into the compartments of cells [58]. A typical membrane mainly consists of phosphoglycerids and comprising more than a hundred different lipids like sphingolipids, sterols and glycolipids that are asymetrically distributed [59]. More than half the phosphoglycerids contain at least one saturated fatty acid chain, giving the membrane a high fluidity. Due to their amphiphilic structure, lipids do not only build a bilayer in aqueous environments, but can also incorporate many proteins that exhibit at least one lipophilic domain, while additional hydrophilic or polar groups protrude from the bilayer (FIG. 3) [60]. On account of the high membrane fluidity, incorporated or attached proteins are theoretically not restricted by the surrounding phosphoglycerids and can move freely through the membrane [61]. In general, two kinds of membrane-interacting proteins can be discerned: integral proteins (high affinity to lipids) - like receptors that usually exhibit one or more transmembrane domains - span the whole

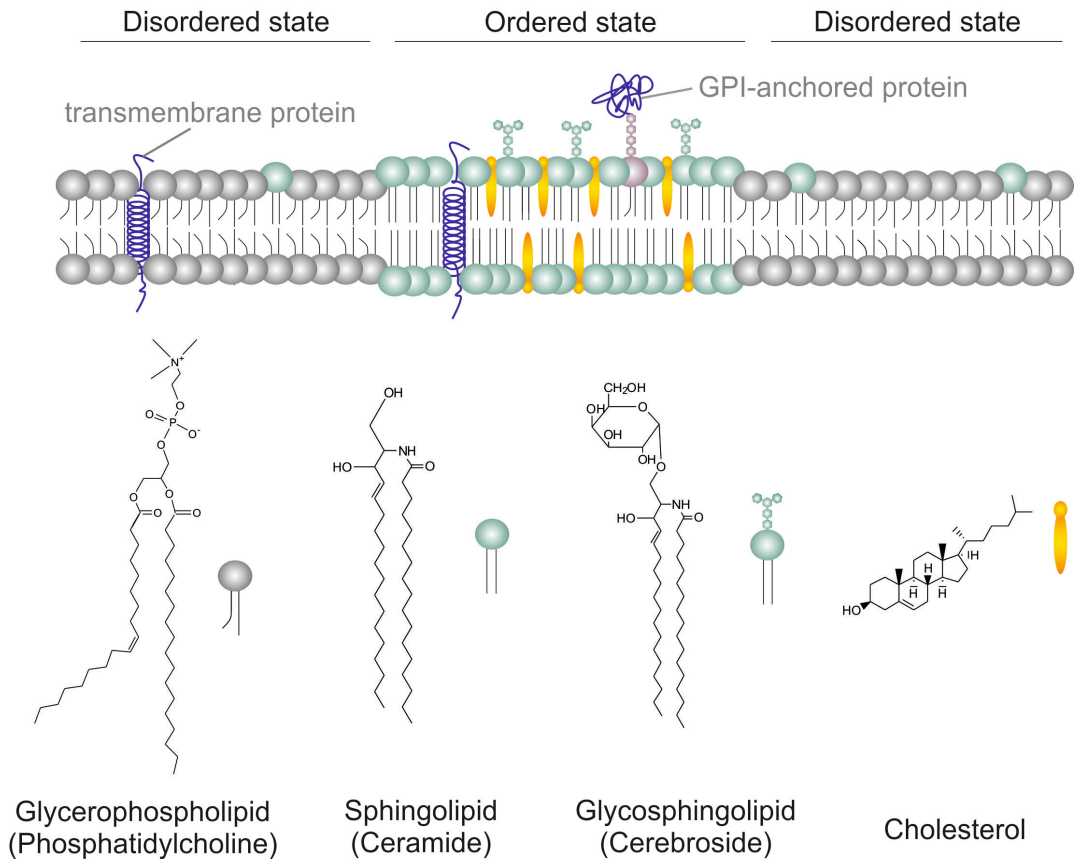

Fig. 3: Representation of the composition of the cell membrane and its membrane-relevant molecules. Liquid, disordered phases mainly comprising phospholipids host raft-like regions of ordered sphingolipids packed tightly with cholesterol. Proteins are either anchored by fatty acid anchors or transverse the membrane completely, using a hydrophobic transmembrane domain.

bilayer [62]. Peripheral proteins (low affinity to lipids) interact with only one leaf of the bilayer by anchors made of fatty acids, glycophosphatidlyinositol tails ('GPI-anchors') or interactions with integral proteins. Connections to the underlying cellular actin skeleton further stabilizes the bilayer by interactions with membrane proteins, acting as a scaffold [63, 64].

As such, the cell membrane can be described by the Fluid Mosaic Model: larger proteins move in a sea of smaller lipids which create a viscous but highly dynamic two-dimensional solution [62]. Protein interactions mediate short-ranged reactions, while at larger distances proteins are distributed randomly due to translational diffusion. While this image of a fluid membrane is still widely accepted today, the image of the membrane has since become more complex. While *Singer and Nicholson* [62] saw the lipids of a bilayer as little more than a solvent for proteins, its components have since been shown to cluster themselves. So-called lipid rafts comprise sphingolipids that are tightly packed with cholesterol, appearing as detergent-insoluble and moving through the more soluble phase of phosopholipids as ordered, rigid lipid rafts [65-67]. Thus, while the membrane is still fluid, it now exhibits two intrinsic states of order: disordered, very liquid phases and highly ordered, semi-frozen phases of packed lipids [68]. Membrane-bound proteins can be discerned by their raft affinity: many proteins have been shown to be at least temporarily raft-associated, some only moving into lipid rafts upon ligand binding or vice versa. Raft regions are mainly found on the exoplasmic leaflet of the lipid bilayer of a cell membrane, but also in intracellular compartments such as the endoplasmatic reticulum and the Golgi, as both are involved in cholesterol and sphingolipid-biosynthesis [69]. As lipid rafts change the composition of distinct areas on the cell surface, they can act as signaling platforms to segregate or accumulate specific proteins [70]. Lipid-raft associated caveolae represent flask-shaped invaginations of up to 50-80 nm for internalization, built by the polymerization of caveolins interacting with cholesterol. Like rafts, caveolae are highly abundant and dynamic [71, 72]. Thus, rafts might be an important tool in signalling and endocytosis, as they could facilitate adapter recruitment, multimerisation or internalization. Indeed, both clathrin-dependant endocytosis as well as internalisation via caveolae are dependent on the association with lipid rafts [73-75]. While widely accepted today, a direct proof for lipid rafts as such does not yet exist, as their putative diameter of 10-200 nm makes the direct, experimental visualization impossible using classic microscopic approaches. *In vitro* preparation of lipid rafts and incorporated proteins is classically done by extracting detergent-insoluble complexes from cell lysates or by using crosslinking reactions [76-78], rendering a spatial analysis of proteins on a native cell membrane impossible. Immunogold labeling and transmission electron microscopy enabled the visualization of proteins forming membrane patches, indirectly proving the proteins' raft-clustering [79].

Utilization of fluorescence microscopy and the evolution of sensitive cameras and data storage devices greatly improved the possible experimental achievements to study the cellular membrane and biological pathways. Early fluorescence recovery after photobleaching (FRAP) experiments and fluorescence correlation spectroscopy (FCS) allows the acquisition of diffusion coefficients of fluorescently labeled lipids and receptors, showing different mobilities and already hinting at protein aggregations as compared to lipids in native membranes [80, 81]. Single particle tracking (SPT) or single dye tracking (SDT) on a living cell enables the specific observation of single proteins or lipids. Other fluorescent approaches include laser trap measurements [82], revealing a high stability for rafts, and fluorescence resonance energy transfer (FRET) [83], giving an interaction diameter of 20-70 nm and a reduced mobility of raft-associated proteins. Fluorescent microscopy could prove the temporal compartimentalization of TNF-R1 after TNFα addition [84] and the dynamics of single TNF-R1 and TNF-R2 molecules were observed using FCS [84]. However, data on the live-cell dynamics and distributions of TNFSF members is still sparse. Today, super-resolution microscopy methods present new tools to dismantle lipid and protein organization *in vivo*.

1.2.3. TNF-R PRE-ASSEMBLY

Formation of signalling clusters can be observed for some members of the TNF-R superfamily, e.g. Fas/CD95 and CD40 [85, 86] and experiments regarding TNF-R1 suggest a similar reaction to TNFα binding. Crystal structures suggest the trimerisation of TNF-R1 and TNF-R2 to grasp the trimeric ligand or a dimerization, with single chain derivates suggesting a receptor dimer, both pre-assembled on the membrane due to the PLAD (FIG. 4) [35, 87, 88]. A receptor dimer binding a ligand trimer would result in a stoichiometry that enables the formation of large, stable signalling complexes [35,

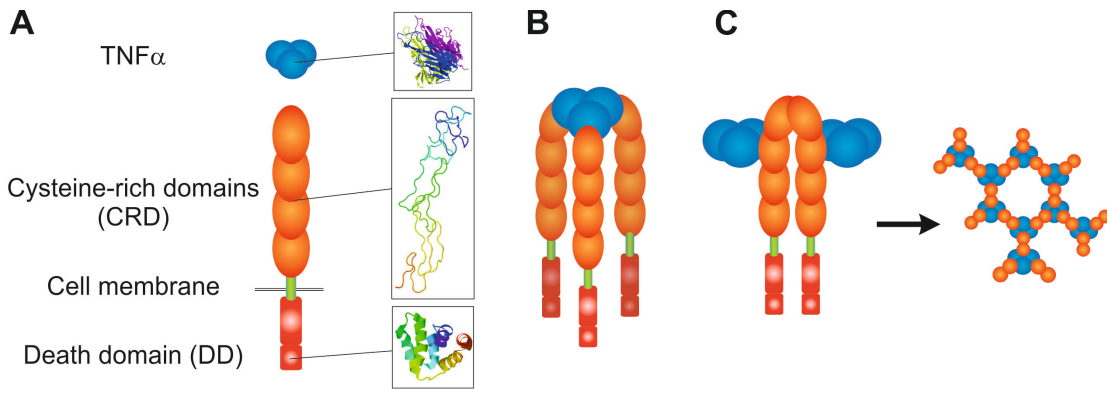

Fig. 4: Overview of structural motifs in TNF-R1 (A), including the ribbon models of TNFα (PDB ID 1TNF [5]), the extracellular TNF-R1 domain (PDB ID 1TNR [88]) and the death domain motif (PDB ID 1ICH [87]). Theories for receptor-ligand interactions (B) that might lead to trimerisation or (C) dimerization with TNFα, which could result in a higher-order cluster formation [35,90].

89, 90]. However, the close contact of many receptor trimers could also be possible, e.g. by a cytoplasmatic multimerisation of recruited (and multimeric) adapter proteins are known to oligomerize before signal initiation as well [86, 91]. Confinement zones of ~200 nm seem to be vital for TNF-R1 signal induction [92]. Not only the size of a receptor-ligand multimer, but also its localization on the cell could lead to the observed signaling outcomes in TNF-R1 - endocytosis of TNF-R1 favors apoptotic pathways, while surface signalling activates survival [23, 93]. Endocytosis has been associated mainly with clathrin-coated pits (CCPs), the DISC forming at TNF-R1 receptosomes, conveying the activation of procaspase-8 and caspase-3 [84]. Caveolae-mediated internalization of TNF-R1 exists in some cell types as well, and recruitment onto lipid rafts after ligand binding is necessary for one or both pathways [32, 84, 94, 95]. Recruitment onto lipid rafts and subsequent internalization could thus pose a vital step for TNF-R1 signaling outcome pre- or post ligand binding, the spatial distribution and the overall membrane structure the main reasons for the differing signaling outcomes. Mobility studies of TNF-R1 and TNF-R2 showed a distinct segregation of the receptors on the cell surface: While TNF-R1 shows a distinct affinity to cholesterol-containing membrane compartments, the actin cytoskeleton and cholesterol content seem to play no crucial role for TNF-R2 signaling [96]. This distinct distribution is most probably caused by differences in the receptor transmembrane region.

1.3. AIMS OF THIS WORK

As described above, signaling events in the TNFSF heavily rely on the spatial arrangement of receptor molecules on the cell surface and their interaction with adapters in concert with involved membrane microcompartments. However, the study of receptor dynamics and its distributions using the non-invasive fluorescence microscopy has previously been limited by the resolution limit of light microscopy. By applying super-resolution microscopy techniques such as stochastic optical reconstruction microscopy (*d*STORM), photoactivated localization microscopy (PALM) and quantum dot triexciton imaging (QDTI) this limitation can be circumvented and receptor distributions and live-cell dynamics that might play crucial roles in cellular signaling can be characterized. By applying single particle tracking PALM (sptPALM) and implementing live-cell *d*STORM, the movement of single receptor molecules and protein clusters can be directly followed in a live cell. By implementing and applying super-resolution techniques, new insights into the early signaling events of TNFSF members can thus be achieved, elucidating the role of receptor compartimentalization, aggregation and receptor-lipid interaction.

2. THEORETICAL BACKGROUND

2.1. FLUORESCENCE MICROSCOPY

In 1845 Herschel described the strange appearance of a blue tint that a colorless quinine solution exhibits only when irradiated with light [97]. As this phenomenon differed from the reflective properties described by *opalescence*, Stokes named the effect *fluorescence* in 1852, referring to the similar phenomenon that fluoride exhibits when irradiated with ultraviolet light. He observed that the emitted light from a sample is always red-shifted in comparison to the incident light, an effect termed *Stokes shift* today [98]. This was the first step towards fluorescence microscopes in the 20th century, which were capable of imaging only specific autofluorescent cellular structures [4]. Light-emitting dyes, nanocrystals and fluorescent proteins have since been harnessed to create specific, fluorescent labels [3]. Today, fluorescence microscopy offers non-invasive, highly specific techniques to study cellular processes even *in vivo*. However, all light microscopy is diffraction-limited due to the wave-like nature of light. Many cellular features are several orders of magnitude smaller and thus not observable with a conventional wide field setup. Recently, a variety of so-called super-resolution methods has been developed to circumvent this diffraction limit, offering insights at biological structures with nanometer resolution. Photoactivated localization microscopy (PALM) and *direct* optical reconstruction microscopy (*d*STORM) separate the fluorescent signals of single molecules in time, taking advantage of phototransformable properties or photoswitching behavior to reconstruct a super-resolved image with a resolution of up to 10 nm. Quantum Dot Triexciton (QDTI) utilizes the semiconductor properties of small nanocrystals (quantum dots) to achieve a resolution enhancement. Which method should be chosen for answering a specific biological question depends on several factors that must be taken into account before deciding on a method, a label and the appropriate labeling strategy.

2.1.1. THE DIFFRACTION LIMIT - RESOLUTION

Light microscopy of cellular structures has always been limited by a lack of contrast in biological compartments, a restriction that can be overcome by differential labeling. In fluorescence microscopy, a structure of choice is stained using a light-emitting probe which is usually excited by a monochromatic light source like a laser. In fluorescence microscopy, excitation and emission light can

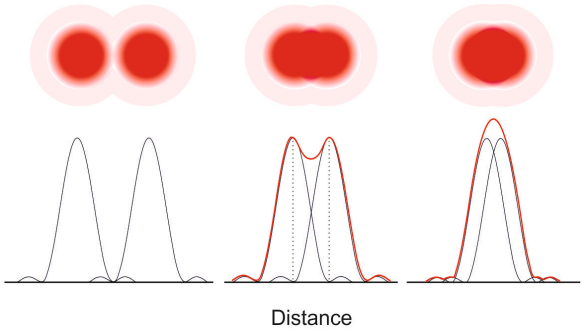

Fig. 5: Rayleigh limit, describing the distance at which two point light sources are still discernible.

be separated by the usage of dichroic mirrors due to a dye's Stokes shift, enabling the visualization of cellular compartments at a high contrast. Fluorescence microscopy is commonly used in cell biology, as it is non-invasive and offers a high specificity. However, due to light's wave-like character, the resolution of fluorescence microscopy is limited by the diffraction of light, as described by Abbe [99] by

$$d = \frac{\lambda}{2nsin \propto} = \frac{\lambda}{2NA} \quad (1)$$

Thus, the resolution (d) depends on the wavelength (λ) and the numerical aperture (NA) of the objective, which is calculated from the diffractive index of the medium (n) and the half opening angle of the objective (α). A point source appears as a circular diffracted spot (or *Airy disc*) - a bright maximum surrounded by concentric rings of decreasing intensity. The lateral radius of the Airy disc (r_{Airy}) is defined by the distance between the intensity center and its first minimum. As such, the Airy disc describes the lateral intensity distribution of a point light source, while its corresponding point spread function (PSF) also depends on the quality of the imaging system. According to Rayleigh, two point light sources are still resolvable if the main maximum of the first coincides with the first order minimum of the second (FIG. 5). Thus, the distance between two points must be ≥ r_{Airy} to be clearly separated as this causes a drop of 20% in intensity between the Airy discs and defines the resolution limit of the system [100]. This Rayleigh distance ($d_{Rayleigh}$) can be calculated by

$$d_{Rayleigh} = \frac{0.61\lambda}{NA} \quad (2)$$

for epifluorescence . This also represents the lateral Airy radius. The axial resolution is calculated from the three-dimensional Airy pattern, being the distance between the axial intensity center to the first axial minimum of the point light source, and can be defined as

$$r_{Airy(z)} = \frac{2n\lambda}{NA^2} \quad (3)$$

The typical resolution limit for visible light is 200 nm in lateral and 500 nm in axial direction. However, the resolution of a structure also depends on its labeling density. According to the Nyquist-Shannon criterion, the mean distance between two labels must be at least half the desired resolution - to achieve a resolution of 20 nm, the observed structure must be labeled regularly at least every 10 nm. The denser a structure is labeled, the better it can be resolved. [101].

As light interacts with matter, it can excite an atom's or molecule's electrons (FIG. 6). If a photon's energy is absorbed, electronic transitions from the ground state (S_0) into higher energy levels are possible (S_n). To relax back into the ground state, several pathways exist, as described by Jablonski [102]. Relaxation to the ground state can be achieved either by emission of a photon, or by non-radiatvie processes. In most substances, the absorbed energy is subsequently lost by non-radiative processes. A special case are photochemical reactions like photosynthesis, which uses excited electrons for converting light energy into chemical energy by photoinduced charge separation and consecutive electron transfer chains. Some substances act as fluorophores; they emit light during their return into the ground state. As excitation energy is lost from absorption until relaxation, the emission wavelength of the detected photons is red-shifted, resulting in the phenomenon termed Stokes shift [98]. With low probability, intersystem crossing (ISC) of an excited electron into the triplet state occurs, which can lead to a delayed non-radiative relaxation or a photon emission, called phosphorescence.

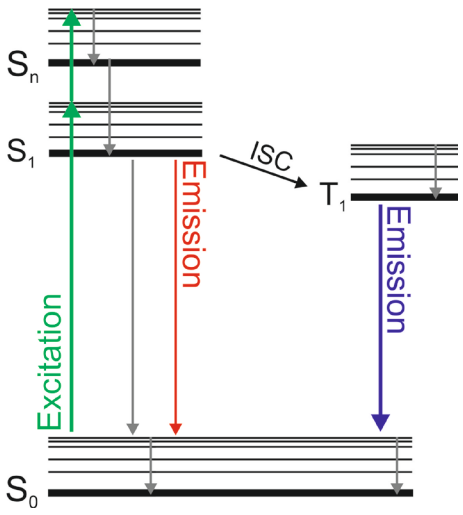

Fig. 6: Jablonski diagram, showing different energy levels of the electronic states. Relaxation by light emission from higher energy states are termed fluorescence, while the delayed emission of light after intersystem crossing results in phosphorescence.

2.1.2. MICROSCOPY METHODS

2.1.2.1. WIDEFIELD MICROSCOPY

In a wide field illumination scheme, the monochromatic light source is widened and focused onto the back focal plane of the objective, resulting in a broad illumination of the sample with parallel light. Fluorescence emitted from the sample is collected by an objective with a high NA and separated from the excitation wavelength by a dichroic mirror. Filters can be used to further confine irradiation and emission wavelengths before fluorescence detection by a single-molecule sensitive camera (e.g. an emCCD). As a large field of view is illuminated in all dimensions at once, fluorescence from above and below the focal plane results in background fluorescence. For monitoring biological samples such as cells where many axial layers of detected molecules might overlap, this dehances the contrast. Inclined illumination schemes (FIG. 7) can reduce noise by reducing the out-of-focus signal.

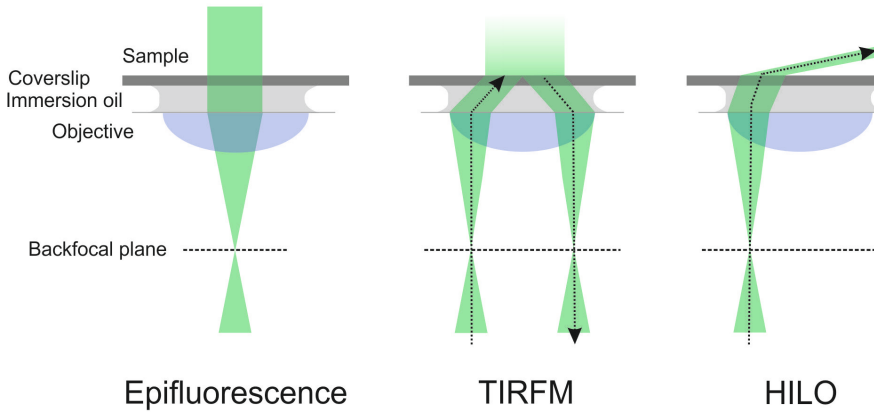

Fig. 7: Differing illumination schemes in fluorescence microscopy, the conventional epifluorescence and inclined illumination schemes TIRF and HILO.

Total internal reflection (TIR) restricts the observed area to a small volume near to the coverslip by introducing an angled illumination. Here, the incident laser beam is placed towards the edge of the objective. Thus, as the oblique incident light beam encounters the glass-sample interface, it is reflected. For incident light at a transition plane between a higher refractive index to a lower index, the beam is completely reflected if the angle is greater than the critical angle of refraction. An evanescent wave of excitation light is created at the interface, which still penetrates a short distance into the sample. As the wave's intensity decreases exponentially in axial direction, a typical excitation depth of only 100 nm is achieved [103]. A highly inclined and laminated optical sheet, or HILO approach (sometimes called *dirty TIRF*) is useful for a deeper sample penetration. As in TIRF, the incident laser is positioned at the objective's edge and refracted at the glass interface. Here, the large refraction below the critical angle results in a laminated, thin light sheet penetrating the sample

at an angle, in which fluorescence can be excited [104]. HILO and TIR fluorescence (TIRF) microscopy are widely used for localization-based super-resolution.

2.1.2.2. CONFOCAL MICROSCOPY

Confocal microscopy reduces background noise, confining the excitation and detection volume by focusing the excitation light into the sample (FIG. 8). By illuminating only a small spot of the entire volume of interest, and passing emission light through a pinhole before detection light from outside the focal spot is rejected completely [105]. The diameter of the pinhole is adjustable, the optimal value defined as 1 Airy unit (AU) or $2r_{Airy}$, which describes its dependence on the diameter of the Airy disc. As emitted light from above or below the focal plane is cut off at the pinhole, increasing the pinhole diameter will allow the detection of weaker signals, as more light is collected from outside the focal plane, but will in turn reduce resolution. Vice versa, a pinhole setting with < 1 AU will improve contrast, but only if the recorded signal is very bright [106]. By line-scanning the sample, a complete image of the sample can be reconstructed. Due the control over the focal volume in lateral and axial direction, this also allows optical sectioning, which reduces the need for thin sectioning during sample preparation [107]. The concept was since enhanced by the usage of lasers as a light source, resulting in the confocal laser scanning microscope (CLSM). Compared to a wide field microscope, where the resolution is only depending on the detection PSF, a CLSM improves the resolution by a factor of ~ ¯, as the resolution here is a product of the detection PSF and the (restricted) excitation PSF. CLSM has been used in many studies to reconstruct two- or three-dimensional images of biological samples. As a CLSM's excitation beam and can be positioned with high precision and laser intensities can be focused onto specific areas, it is often used in biological mobility studies such as FRAP or FRET.

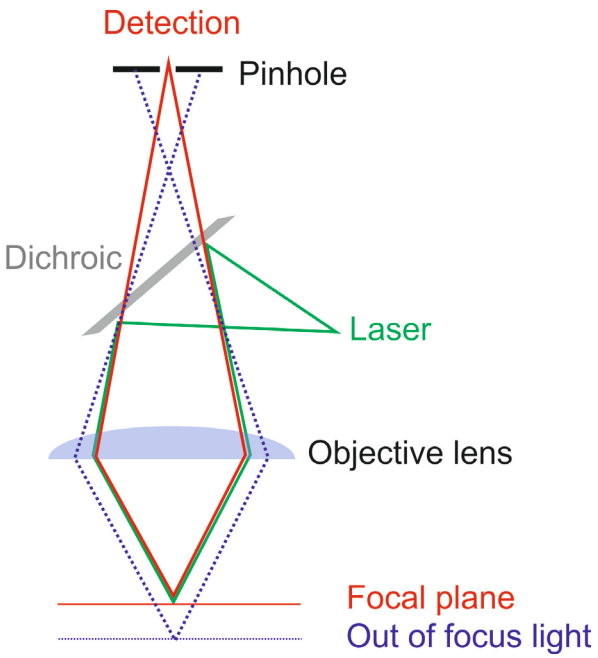

Fig. 8: Scheme of CLSM, showing the rejection of out of focus light (dotted line) at the pinhole before detection.

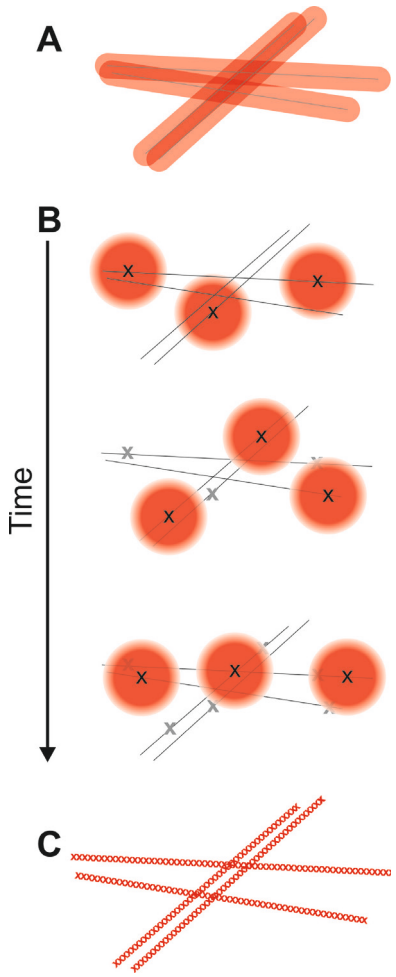

Fig. 9: The fluorescence image of a structure is diffraction-limited when imaged with a conventional WF setup (A). By temporally separating the single molecule fluorescence and localizing it with high precision (B) a super-resolved image (C) of the structure can be reconstructed.

2.2. LOCALIZATION-BASED SUPER-RESOLUTION MICROSCOPY

A fluorescently-labeled structure represents an object with many fluorophores emitting light at the same time and results in a typical diffraction-limited large image, as a great number of PSFs overlap. To circumvent Abbe's resolution limit and by localizing single fluorophores with high precision, individual PSFs of a structure must be separated in space and time (FIG. 9). This demands control over a molecule's fluorescent state, as the majority of the present probes must be transferred into a not observed, non-fluorescing state to discern single, non-overlapping PSFs. Deterministic approaches like stimulated emission depletion (STED) actively deplete the fluorescence of a probe [108], while localization-based approaches observe the stochastic fluorescence photoswitching events of a probe [109]. While *direct* stochastic optical reconstruction microscopy (*d*STORM) [110] uses synthetic fluorophores with many switching cycles, photoactivated localization microscopy (PALM) utilizes photoactivatable or photoswitchable fluorescent proteins [111]. These methods rely on monitoring only small subpopulations of emitting fluorophores, that can be localized as single PSFs become discernible. While the emission pattern of a single molecule is still a diffraction-limited PSF, its center (x_c, y_c) can be determined with high precision, using a two-dimensional Gaussian fit function:

$$I\,(x,y,A,B) = \frac{A}{2\pi\sigma_x\sigma_y}\cdot exp\left(-\frac{1}{2}\cdot\left(\frac{x-x_c}{\sigma_x}\right)^2-\frac{1}{2}\cdot\left(\frac{y-y_c}{\sigma_y}\right)^2\right)+\mathrm{B} \qquad (4)$$

Where A is the amplitude, B is the background and σ_x/ σ_y the lateral standard deviations. Precision increases with the amount of photons (N), as the Gaussian fit becomes more accurate [112]:

$$I = \sqrt{\frac{\sigma^2 + a^2/12}{N} + \frac{8\pi\sigma^4 b^2}{a^2 N^2}} \qquad (5)$$

showing that the localization uncertainty (I) is dependent on photon number (N), the pixel size (a), the background (b) and the standard deviation of the PSF (σ). At high photon numbers, this can be simplified as

$$I \sim \frac{\sigma}{\sqrt{N}} \tag{6}$$

as background noise and pixelation effects become minimal. For a fluorophore emitting ~1000 photons a localization precision of < 10 nm can be achieved, and thus representing an accuracy well below the diffraction limit. The recording of the statistical switching events of a fluorophore can then be used to reconstruct a super-resolution image by representing all centers of localized probes.

2.2.1. PROBES FOR LOCALIZATION-BASED SUPER-RESOLUTION

Super-resolution microscopy needs probes that exhibit at least two well separable states of fluorescence: in *d*STORM, photoswitchable dyes can be cycled between a non-fluorescent, dark state (*off*) and a fluorescent state (*on*) many times (FIG. 10). The achievable resolution largely depend on a probe's contrast ratio between on and off states, its switching behavior and the lifetime of the non-fluorescent dark state of a dye [113]. To increase localization precision, probes should be very bright and show a proper photoswitching behavior. In PALM, fluorescent proteins undergo phototransformation, either by photoconversion (a shift in the fluorescence emission spectrum) or photoactivation (shift from non-fluorescent to fluorescent state) by light-induced chemical reactions, also resulting in an not observed/*dark* state and a recorded on state. The contrast ratio and thus the usefulness of a fluorophore is described by its quantum yield in both switching states, comparing a molecule's absorbed and emitted photons. A high photon absorption rate, a good quantum yield, high photostability and brightness are desired for fluorescent probes to localize them precisely against the background noise.

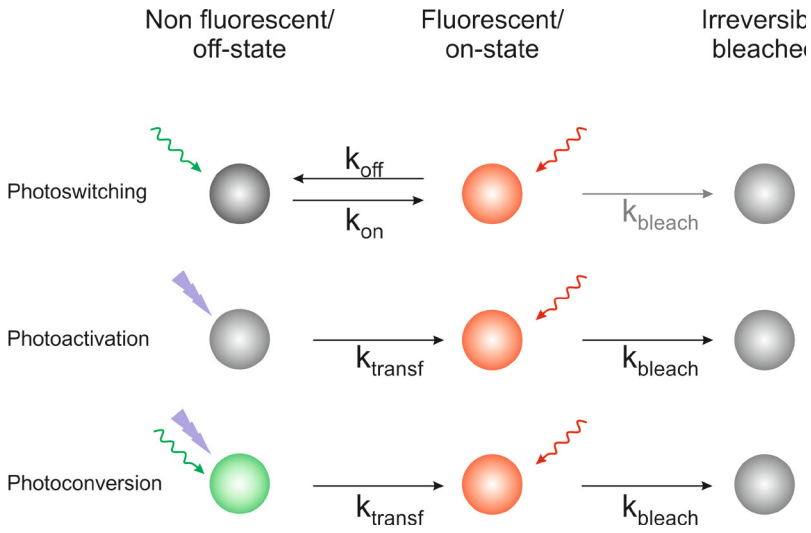

Fig. 10: Different modes for fluorophores to cycle between a non-fluorescent (or non-observed) and a bright (or observed) state. While the bleaching rate must be kept negilible for dyes, it is an essential

2.2.1.1. PHOTOSWITCHABLE DYES

Stochastic optical reconstruction microscopy (STORM) and *direct* STORM (*d*STORM) utilize conventional fluorescent dyes for super-resolution. While in STORM an activator dye and a reporter dye are necessary for switching, *d*STORM directly uses standard organic fluorophores for photoswitching, needing no activator [109, 110, 114]. As all dyes are fluorescent at the beginning of a *d*STORM experiment, they have to be transferred into a long-lived but reversible off state before the localization of single fluorescent spots can begin. If many fluorophores are present per diffraction-limited area, longer off states are needed to activate only a few fluorophores at a given time point, resulting in a sufficient low spot density with clearly resolvable PSFs. As the switching rates between the on and off-state (k_{on} and k_{off}) of a *d*STORM dye are directly influenced by irradiation intensities, the buffer pH and its redox potential, an optimal of k_{on}/k_{off} rate must be adjusted using these parameters to avoid high emitter density but record many switching events [115]. In photoswitching, a fluorophore's transient dark state is usually acquired by quenching, representing the reversible reduction of fluorescence.

Common dye classes in *d*STORM include oxazines, carbocyanines and rhodamies. The spectral properties of each molecule depends on the length of a dye's conjugated electronic system. Organic dyes show a high brightness and are very photostable, cycling between a stable dark state and the on state hundreds of times before photobleaching. Excitation of organic fluorophores containing conjugated π-electron systems leads to an electron transition from the ground state (S_0) to a higher electronic state (S_1, S_2, …) (FIG. 11). By internal conversion and vibrational relaxation, electrons relax very fast into the first excited state (S_1). By the spontaneous emission of a photon - i.e. fluorescence - the electron then relaxes back into the ground state S_0. Other relaxations into S_0 involve non-radiative processes [116]. An excited fluorophore can relax either with or without the emission of a photon -

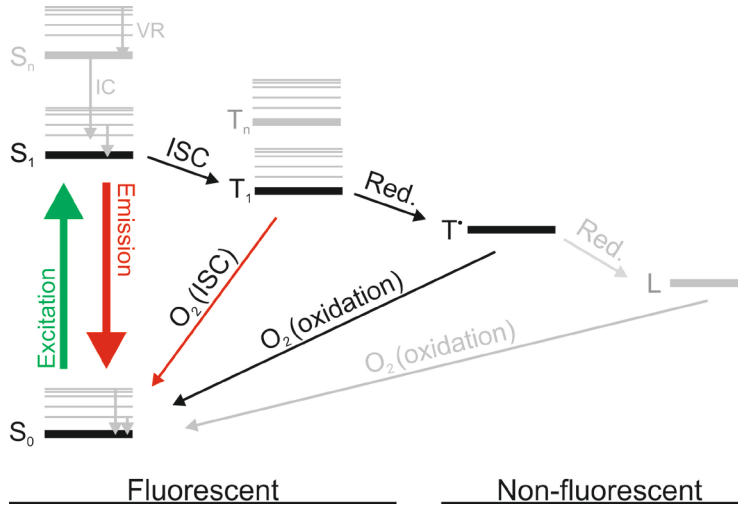

Fig. 11: Photoswitching mechanism of organic dyes shown in an extended Jablonski diagram. Relaxation into the lowest ground state of each energy level can occur by vibrational relaxation (VR) or internal conversion (IC). Intersystem crossing (ISC) into the triplet state can lead to the generation of dye radicals, which represent a stable, long-lasting, stable dark state. Further reduction leads to a leuco form (L) of the dye.

fluorescence might be quenched by interactions with oxygen or neighboring molecules. In photoswitching, a transient dark state is generated by intersystem crossing (ISC) into the triplet state (T_1). Collisions of the triplet with molecular oxygen leads to a return into the S_0 and the generation of singlet oxygen, which can induce photobleaching. Reduction of the triplet occurs if thiols are present in the medium [117], which leads to the formation of a radical anion state of the dye ($T^{\cdot-}$). While the resulting thiyl radicals quickly interact with molecular oxygen to superoxides and hydrogen peroxides, the radical is very inactive, presenting a stable off state that can last up to several hours. The reaction with molecular oxygen recovers the ground state of the dye by oxidation. In dyes with a higher electron affinity (e.g. ATTO655), a second electron can be accepted in the radical state, leading to a fully reduced leuco form of the dye. A return to the ground state can also be promoted by irradiation with short wavelengths. Thus, the stability of the radical state - and consequently the off state - can be directly controlled by the oxygen and thiol concentration, as well as the irradiation strength in a sample. However, the oxidation of dyes in the ground state via the singlet oxygen generated by collisional quenching induces photobleaching. Using an oxygen-scavenging system reduces these bleaching effects and also extends the dark state's lifetime [110]. While oxygen removal is vital for reversibly switching dyes like carbocyanines that are easily oxidized, other dyes can be photoswitched in the presence of oxygen, if millimolar concentrations of thiol-containing reducing agents are present in solution [118].

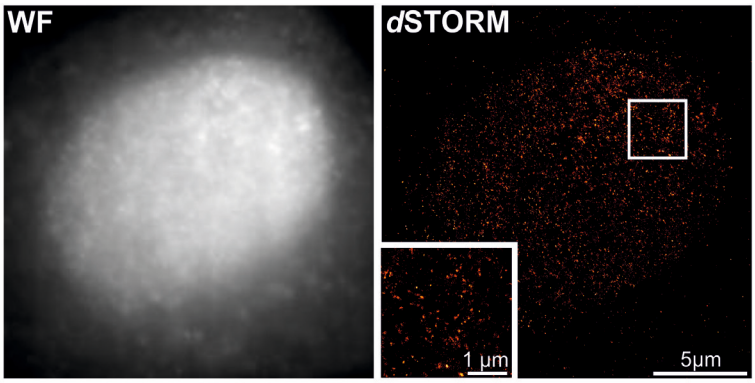

Fig. 12: Exemple of the resolution enhancement achieved in *d*STORM. A nucleus imaged in widefield (WF) that was immunostained for active NF-κB compared to the reconstructed image after *d*STORM imaging shows the increased resolution and localization of NF-κB.

2.2.1.2. QUANTUM DOTS

Quantum Dots (QD) are nanocrystals that usually consist of a semiconductor core (e.g. CdSe) passivated with an isolator (e.g. ZnS) shell. To assure biocompatibility and solubility in water, hydrophobic QDs are coated with organic polymers (e.g. PEG). Surface modifications can further functionalize QDs for biological usage - e.g. by coating them with active groups for chemical coupling, specific oligomers, antibodies or biotin. Due to their semiconductor properties, QDs have a wide absorption spectrum (FIG. 13 A): absorption of a photon above the band gap energy leads to the

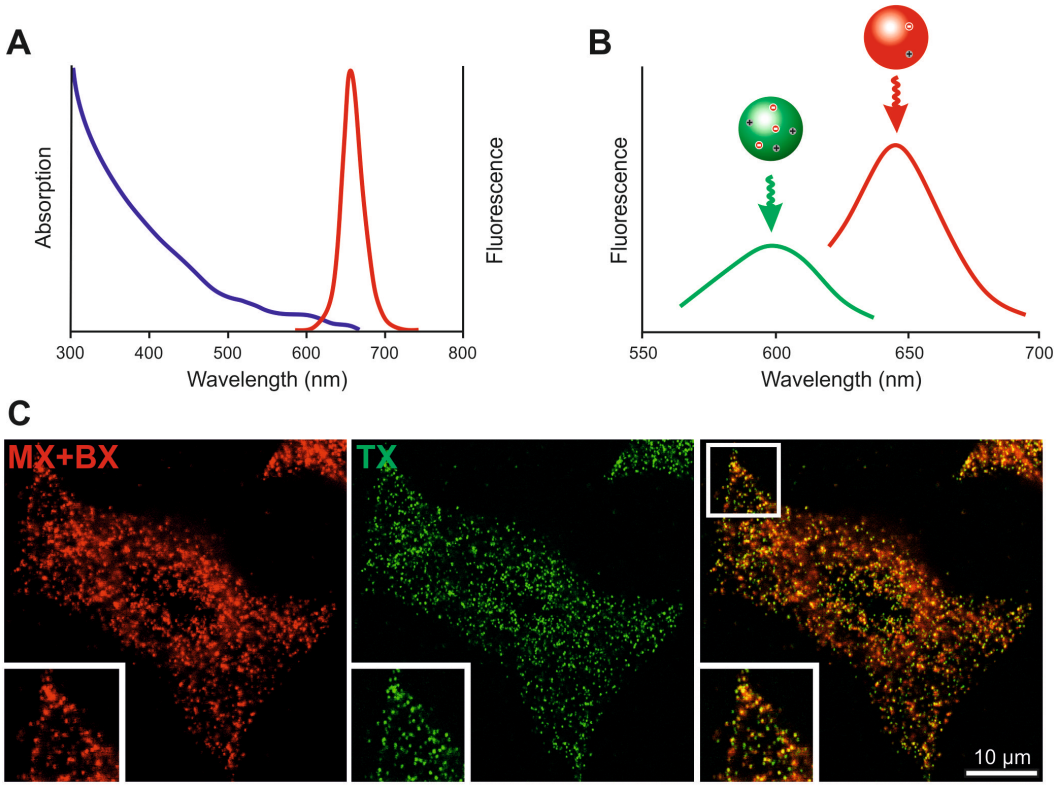

Fig. 13: Excitation and emission spectra (A) of QD655, which is known to exhibit a blue-shifted emission after simultaneous absorption of three photons (B), representing the triexcitonic state that can be used to increase the resolution in labeled cells (C). Here, TNF-R1 was immunolabeled to reveal the receptor distribution on the lower membrane of HeLa cells.

generation of an electron hole pair (i.e. exciton), recombination results in the emission of a photon. This process is more probable at higher energies (i.e. lower wavelenghts), giving QDs a broad excitation spectrum with high extinction coefficients at short wavelengths. Due to the eponymous quantum confinement of a QD's electrons, a QD can be described by the *particle in a box* model, describing an increase of the ground state energy in smaller QDs [119]. As a consequence, the QD emission is tunable by adjusting its size: a small core (2 nm) contains a large band gap, needing higher intensities for exciton creation, resulting in a shorter emission wavelength than in QDs with a

larger core [120]. Defects in the QD shell lead to the transient trapping of excitons, hindering recombination and leading to some fluorescence fluctuation [121]. In the QD655, the successive absorption of two or three photons can generate multiexcitonic states [122] similar as in multiphoton microscopy: Here, dyes are excited by wavelengths with only a fraction of the energy (i.e. half or third) of the energy needed to excite the fluorophore into the S_1 state [123, 124]. This demands rapid, almost simultaneous absorption of two or three photons, as no stable intermediate energy levels exist. This is realized by high illumination intensities and very short laser pulsing to overcome these virtual levels. Thus, multiphoton excitation (and the resulting fluorescence) is quadratically dependant on the irradiation intensity, i.e. it is more probable in the center of the irradiation radius. This restricts the effective focal volume, reducing out-of-focus light and photobleaching.

Multiexcitonic states in QDs on the other hand can be generated with lower irradiation intensities, as each exciton represents a discrete energy level before recombination occurs, which makes the method applicable for a conventional CLSM. While mono- and biexcitonic (MX, BX) states of the QD655 are spectrally overlapping, the triexcitonic (TX) state - generated by the subsequent absorption of three photons - leads to an observable blue-shifted emission of 60 nm [125]. Contrary to multiphoton microscopy, where the use of long, near-infrared wavelengths for excitation cancels out a possible resolution enhancement [126], the three-photon absorption in the visible spectrum theoretically squeezes the PSFs of TX images by a factor of $\frac{1}{\sqrt{3}}$ (FIG. 13 B,C) . Higher excitonic states might exist, but the probability of each state decreases with present exciton number. Experimentally, the blue-shift can be easily detected by proper filter adjustments and increasing resolution two-fold; a technique termed Quantum Dot triexciton imaging (QDTI) [122, 125].

2.2.1.3. PHOTOTRANSFORMABLE FLUORESCENT PROTEINS

One of the most powerful tools in fluorescent microscopy is the usage of genetically encoded fluorescent proteins (FPs). Discovered in the jellyfish *Aequoria victoria,* the 27 kDa green fluorescent protein (GFP) emits a strong fluorescence at 507 nm upon irradiation with blue light. Here, a chromophore (built in a cyclization and oxidation by residues Ser_{65}-Tyr_{66}-Gly_{67}) is surrounded by a 11-stranded β-barrel can, protecting the chromophore from denaturation [127] (FIG. 14). As the expression of GFP requires no post-translational modifications, its cDNA was soon expressed in other organisms [128]. Optimized versions (enhanced GFP - eGFP) show reduced maturation time and fluorophore aggregation and adjusted optimum folding temperatures to mammalian conditions (37°C). As genetic fusions FPs were soon used for the detection of gene expression, in labeling cellular structures and have since been used in a large variety of experiments [129]. Many derivatives of eGFP have been designed by site-directed mutagenesis of the chromophore and its surrounding amino acids, thus changing its spectral properties dramatically. A broad spectrum of new colors was derived as well as the ability of phototransformation, i.e. a light-induced change in FP emission, which can be used to generate a super-resolved image [130-132]. In general, two modes of light-induced phototransformation can be defined: photoactivation describes the transition of a non-fluorescent FP into a fluorescent form, e.g. by a cis-trans transition of the chromophore. Most phototransformations are irreversible, usually followed by photobleaching [133]. Photoconversion describes a change in the fluorescence emission spectrum of a FP, e.g. by a photo-induced cleavage of the chromophore. As a special case, some FPs combine reversible photoactivation and photoconversion [134]. EosFP (FIG. 15), a FP from the stony coral *Lobophyllia hemprichii*, is the most popular photoconvertible FP to date, as it matures at 37°C, can be expressed as a protein chimera with little influence on the labeled protein and is one of the brightest phototransformable FPs available [135]. It exhibits an irreversible photoconversion from green (516 nm) to orange-red (581 nm) after irradiation with low levels of near-UV light (~400 nm), due to an irreversible cleavage in the chromophore backbone [131, 136]. Originally tetrameric, a pseudo-monomeric, tandem form (tdEos) was designed by random mutagenesis to reduce aggregation artifacts.

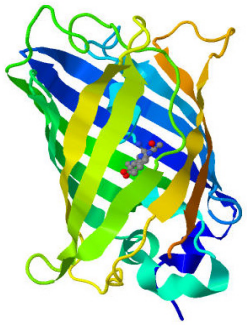

Fig. 14: Ribbon model of GFP, showing the barrel shape protecting the inner chromophore. PDB ID 1EMA [130].

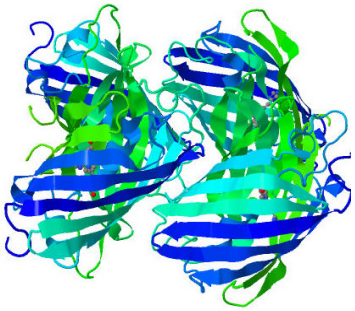

Fig. 15: Ribbon model of EosFP, showing the original, tetrameric structure of the protein. PDB ID 1ZUX [135].

2.3. MEASURING DYNAMICS IN BIOLOGICAL SAMPLES

Following the motion of a protein can reveal many aspects and properties of the underlying biological system. Since Robert Brown described the erratic movements of pollen in a drop of water [137], tracking single molecules or particles, even macroscopic cellular compartments or entire individuals has been used in a variety of scientific work to reveal spatial and temporal migration patterns. Evaluating the movement of a molecule in living cells might reveal many properties that are otherwise inaccessible. Highly controversial at their time of postulation, both fluid mosaic model and lipid raft theory have been probed with single molecule methods to elucidate types of movement, cellular organization and the influence of the cellular environment.

2.3.1. DIFFUSION, BROWNIAN MOTION AND MEAN SQUARE DISPLACEMENT

Diffusion is the movement of particles, e.g. atoms or molecules, along a concentration gradient, until two or more phases are thoroughly mixed. Fick's first law gives this current (J) as proportional to the concentration gradient, describing a particle's mobility:

$$J = -D \cdot \left(\frac{dc}{dx}\right) \tag{7}$$

Fick's second law takes into account that diffusion changes this gradient over time, which in turn influences diffusion:

$$\left(\frac{\partial c}{\partial t}\right)_x = D \cdot \left(\frac{\partial^2 c}{\partial x^2}\right)_t \tag{8}$$

The proportionality factor (D) represents the diffusion coefficient, which can be calculated according to the Einstein-Stokes equation via the Boltzmann constant (k_B), the temperature (T), the viscosity of the medium (η) and the hydrodynamic radius of a diffusing particle (α), as described by the:

$$D = \frac{k_B T}{6\pi\eta\alpha} \tag{9}$$

Measuring the diffusion coefficient is usually done by determining concentration changes, e.g. by measuring extinction coefficients or by interferometric measurements of solutions. However, even after the complete mixture of two gradients, brownian motion of particles - the temperature-dependant, erratic motion of all particles caused by collisions with the solvent and other molecules - is still observed in all samples above the absolute zero (-273°C). To examine this type of mobility of molecules without an influence of concentration gradients, a mean square displacement (r^2) of the random walk of a single molecule over time must be calculated from its coordinates r= (x,y, t).

$$MSD = \langle r^2 \rangle \tag{10}$$

Here, the mean square displacement (MSD) evaluates the overall stochastic motion of a particle during a time interval, as opposed to an overall traveled distance described by velocity. At short time scales, the MSD is calculated by

$$MSD = \frac{1}{N}\sum_{i=1}^{N}[r_i(t) - r_i(0)]^2 \quad (11)$$

Where is the distance traveled by the particle during one time interval, averaged over all the steps of the trajectory (N). The MSD of one particle then represents the mean of the sum of all movements of the particle over time. As larger time steps of a trajectory contain less data points to average over, the best accuracy of an MSD is usually achieved when calculating it from less than ¼ of the total number of points in a trajectory [138]. The slope of the MSD reports on the directionality of the movement of a particle (FIG. 16): If the particle is diffusing freely, the traveled distance is

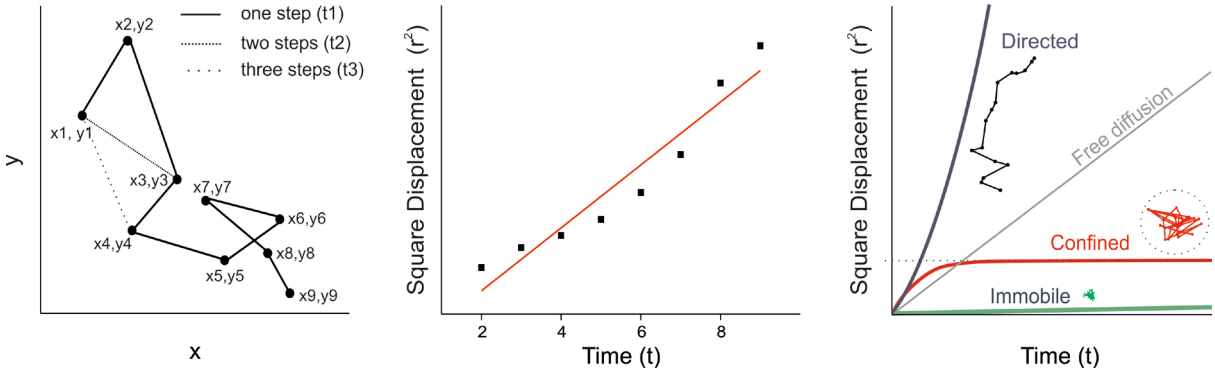

Fig. 16: Calculating the mean square diffusion of a particle. A trajectory (A) of the movement of a particle over time is calculated from its x and y positions over time. Distances between coordinates of different time lags/steps can be measured and a particles MSD can be plotted (B). The diffusion coefficient can be calculated and a particle's type of motion can be analyzed by the shape of the MSDs curve (C).

proportional to the time interval and the MSD appears linear. For a particle exhibiting only brownian motion, the MSD is directly related to the diffusion coefficient of the particle. Diffusion of a randomly moving particle can be described by the Einstein-Smoluchowski relation, in three-dimensional systems as:

$$MSD = 6Dt \quad (12)$$

For cell membranes, two-dimensionality is assumed:

$$MSD = 4Dt \quad (13)$$

However, free diffusion is uncommon in biological systems, where obstacles, active transport or confinement of molecules is common. Active transport usually manifests itself as a quadratic displacement over time, which can be described by the sum of the MSD and a mean velocity (v):

$$MSD = 4Dt + v^2t^2 \tag{14}$$

Another approach to determine directionality and thus the possible active motion of a particle is the determination of angular correlations between trajectory steps, as a directionality manifests itself in a trajectory as a persistent angle [139]. In the membrane, a maximum displacement is often reached, representing anomalous or restricted diffusion (FIG. 17 C). Here, the molecule is moving in a defined confinement zone (corral). If the MSD approaches the value L, the corral has an area of L^2. MSDs can change for a single trajectory over time - by fitting the first few points of the MSD curve, the initial mean diffusion coefficient - independent of the molecule's type of motion - can be calculated.

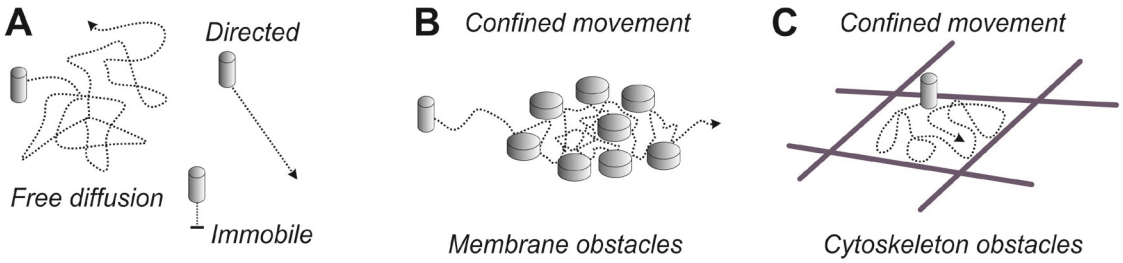

Fig. 17: Types of movement often observed in membranes. (A) Free diffusion is common if no protein-protein interactions hinder a molecule in its movement. Binding events may either immobilize a molecule on a membrane or lead to an active transport and thus directed movement. Temporally confined movement can be due to collisions or interactions with membrane obstacles (B) or cytoskeleton obstacles (C) that form a so-called corral.

2.3.2. FLUORESCENCE RECOVERY AFTER PHOTOBLEACHING - FRAP

Measuring the fluorescence recovery after photobleaching (FRAP) is one of the classical approaches to probe a molecule's two-dimensional diffusion coefficient in native and artificial bilayers. Here, a small spot (typically ~16 µm in diameter) within a fluorescent sample is irreversibly photobleached (FIG. 18). As fluorescent probes from the unirradiated surrounding diffuse back into the bleached spot and bleached probes diffuse away, the fluorescence recovery rate can be monitored as a function of time. From these rates the diffusion coefficient of a probe can be calculated by determining $\tau_{1/2}$ - the time required to recover 50% of the fluorescence intensity in the bleached spot [140, 141]. The effective diffusion coefficient (D_{eff}) also depends on the effective radius of the bleaching beam at an intensity of e^{-2} (w).

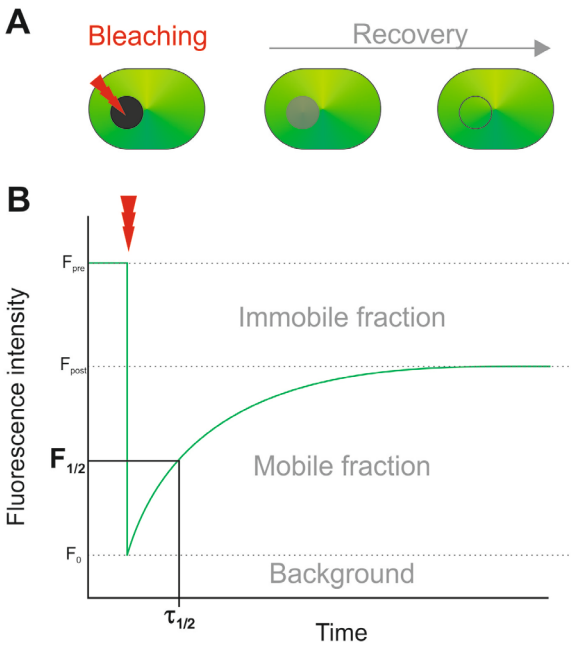

Fig. 18: FRAP recovery curve derived from bleaching a specific area of a fluorescent sample and monitoring the fluorescence recovery.

$$D_{eff} = \frac{w^2}{4\tau_{1/2}} \tag{15}$$

Irreversible bleaching depends on the applied laser intensities and beam geometry and must be factored into the above equation as a correction. The faster the fluorescence recovery, the more mobile the observed protein. Consequently, immobile molecules will not replenish the bleached area and exhibit no recovery rate, while a mobile molecule will undergo a full fluorescence recovery. In biological systems probes usually exhibit an incomplete recovery, which describes a distinct immobile and mobile fraction of the probe due to binding events or confinements. Other approaches include fitting of the recovery curve with a mono- or biexponential equation to determine $\tau_{1/2}$. Bleaching regions must be kept constant between experiments to better compare FRAP results.

2.3.3. FLUORESCENCE CORRELATION SPECTROSCOPY - FCS

Similar to FRAP, Fluorescence Correlation Spectroscopy (FCS) can be used to measure the diffusion of a fluorescent probe. Here, the intensity fluctuations of an excited probe crossing a confocal sample volume of ~1 fl is detected as a function of time (FIG. 19). The detected fluctuating fluorescence signal F(t) can be used to calculate an autocorrelation function of the fluorescence of each time delay (τ).

$$G(\tau) = \frac{\langle \delta F(t) \delta F(t+\tau) \rangle}{\langle F(t) \rangle^2} \tag{16}$$

This is averaged over many events. At longer intervals between the time lags the self-similarity of a signal diminishes and the autocorrelation goes against 0. Therefore, the autocorrelation of a photon burst represents a measure of the self-similarity of a signal over time, giving a time scale of observed fluctuation events [142]. This represents a molecule's mobility; at a given time lag, a fast molecule will only contribute to the amplitude of the autocorrelation during short correlation times, while a signal from a slowly moving probe will show a high a self-similarity over long delay times. Depending on the observed system's mode of motion, differing autocorrelation curves can be derived [143]. Similar to FRAP, the diffusion coefficient (D) of a particle is calculated from the characteristic residence time of a particle in the focus (τ_D) in relation to the sample radius (w) as:

$$D = \frac{w^2}{4\tau_D} \tag{17}$$

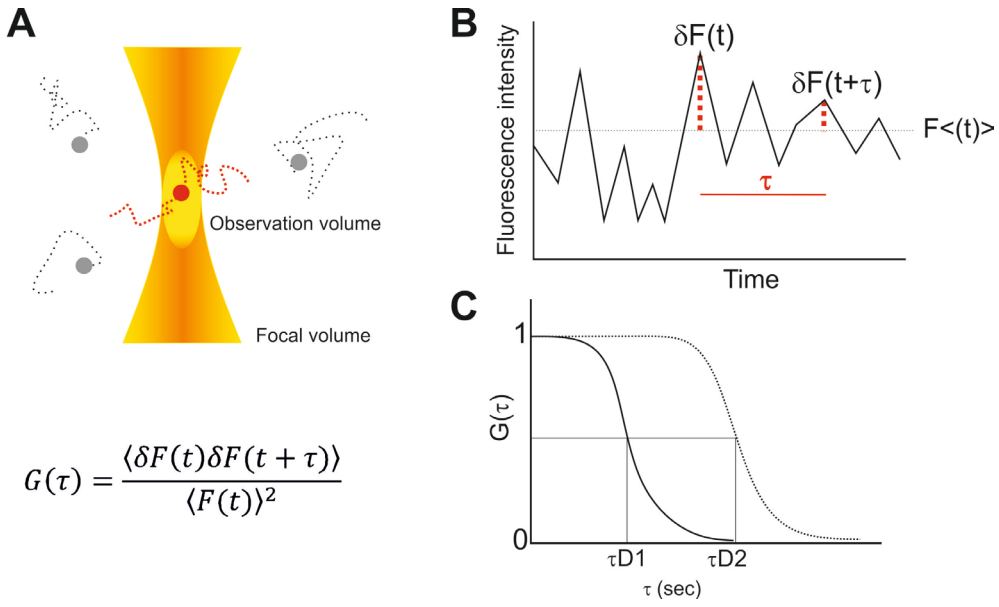

$$G(\tau) = \frac{\langle \delta F(t) \delta F(t+\tau) \rangle}{\langle F(t) \rangle^2}$$

Fig. 19: FCS monitors fluorescence fluctuations in a confocal irradiation volume over time(A, B). Calculating the autocorrelation of a signal (C) reveals a particle's specific dynamics over time.

As fluorescence fluctuations are also depending on the number of molecules in the observation volume, the concentration of probes in the sample can be determined from the autocorrelation amplitude as well as the viscosity of the medium [144]. Characteristics like conformational changes and involved kinetics or molecular binding events can additionally be determined by adding a quencher in close proximity to a fluorescent dye and observing the resulting fluorescence fluctuations. Cross-correlation of different fluorescent signals or single molecule FRET can also be applied to calculate proximity ratios of interacting proteins [145-147]. By focusing the confocal volume into or onto a cell, mobility or interaction studies can be carried out *in vivo*.

2.3.4. SINGLE PARTICLE TRACKING -SPT

Single particle tracking (SPT) measures trajectories and the diffusion coefficient of single particles, directly following the movement of a probe through time and localizing it with nanometer precision. By labeling a small subset of proteins and tracking their coordinates over long time periods, this technique is capable of revealing the mean diffusion coefficient on a cell surface as well as subpopulations with different mobilities, such as is influenced by the microstructure of the cell. SPT is thus capable of comparing the trajectories and the modes of motions and of single molecules.

Traditionally, gold beads have been used in SPT experiments, as gold gives a high contrast and does not photobleach, tracking in bright field. SPT using gold is possible with differential contrast microscopy (DIC) or using fluorescence microscopy. On account of their stability, gold particles greatly increase the observation time of single particle movements. Other probes with similar properties include quantum dots or latex beads [148-150]. In single dye tracking (SDT) a molecule of interest fused to a photostable dye (e.g. rhodamines or cyanines) that is introduced into the cell, greatly reducing the size of the probe, which enables the imaging in spatially restricted areas. This method has been mainly used for lipid tracking [151, 152]. SPT data allows the analysis of the overall MSD of particles on the cell surface, but also gives insight into possible changes in a molecules diffusive behavior. The partial analysis of tracks allows the detection of quick changes in particle movement by plotting differing MSD slopes over times. This so-called subtrajectory analysis was successfully applied in the SPT studies of particle and virus uptake, involving different uptake phases that are characterized by differing modes of motion [153]. Endocytosis or viral uptake manifests itself in a drastic change in the slope of recorded MSDs, from free or confined movement to directed movement, as the endocytotic vesicles containing the labeled probes are rapidly transported close to the membrane before traveling out of the field of view of the SPT experiment. In summary, SPT does not only give information about the properties of the tracked molecule, but - by the probes' differing modes of motion - also on the properties of the surrounding environment.

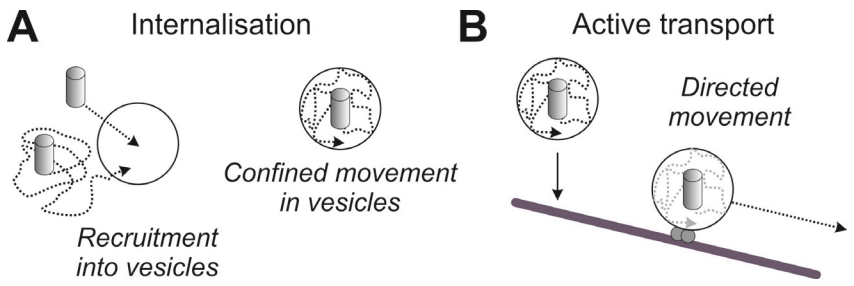

Fig. 20: Internalisation processes that influence membrane protein mobility. Upon stimulation, proteins are recruited into vesicles (A) and exhibit a confined movement in SPT experiments. Internalisation is followed by active transport in the membrane vicinity before leaving the field of view (B).

2.3.5. SUPER-RESOLUTION TRACKING

2.3.5.1. SPTPALM

Recently, a combination of the principles of PALM and SPT to sptPALM was demonstrated [154]. Here, a protein of interest is genetically fused to a phototransformable FP. By activating only a very small subset of the present fluorophores in a cell, they can be localized with high precision and individual tracks can be recorded. Bleached probes are replenished from the large pool of inactive proteins by further photoconversion. By adjusting illumination and photoconversion intensities, the optimal fluorophore density and the track lengths can be actively adjusted [154].

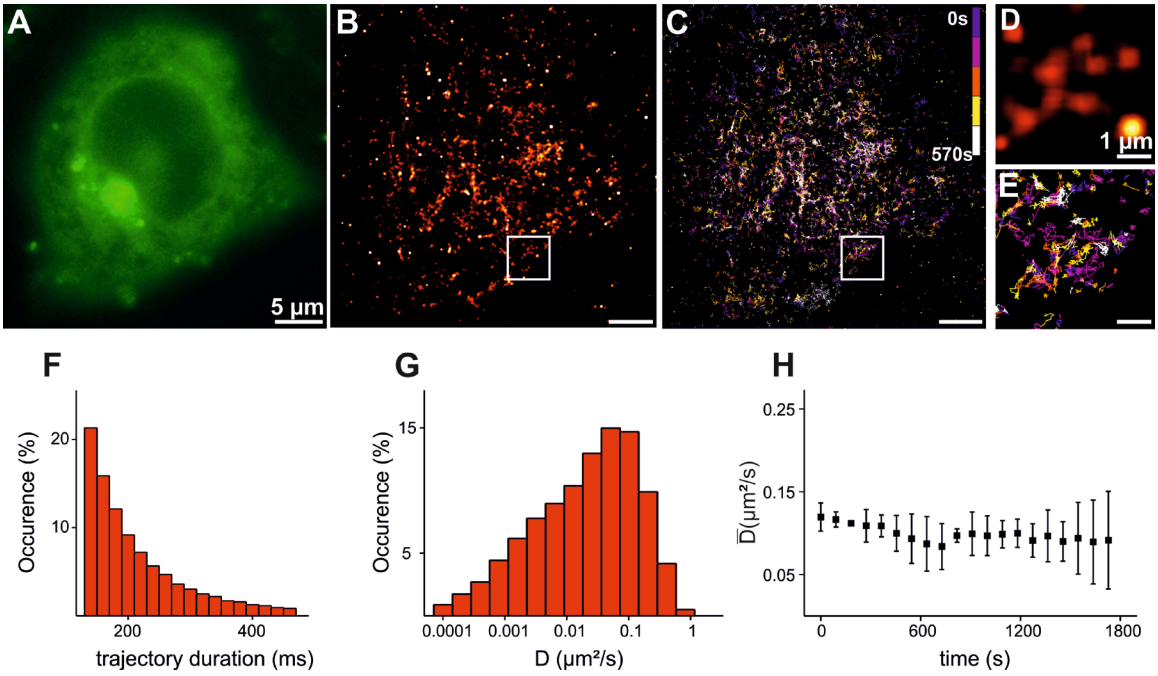

Fig. 21: Typical data set produced by sptPALM: (A) WF image of the unactivated tdEos that was fused to TNF-R1. The green fluorescence is used to identify transfected cells. (B, D) Super-resoloved intensity maps acquired from single molecule localizations during 5000 frames. (C,D) Map of single-particle trajectories can be used to calculate a mean trajectory duration (F), the mean diffusion coefficient (G) and the diffusion coefficient over time (H).

This activation-localization-photobleaching scheme together with a TIRF illumination results in a high number of observed localizations in sptPALM. As the fluorescent signals are well separated both spatially and temporally, sptPALM provides a high density of trajectories from just one measurement (FIG. 21). As in PALM, the most commonly used fluorophores in sptPALM as of today are tdEos, PamCherry1 and Dendra2 [131, 155, 156], which mature fast and are very stable in cellular environments, exhibiting a high brightness. This makes them easy to localize and track with high precision. As sptPALM achieves a high resolution, and single trajectories can be analyzed for their modes of motion, membrane compartments with differing membrane fluidity can be discerned.

2.3.5.2. PAINT/uPAINT

Similar to sptPALM, points accumulation for imaging in nanoscale topography (PAINT) utilizes freely diffusing probes that targets a surface to obtain super-resolution data [157]. Here, fluorescent probes diffuse in solution, but are immobilized for short intervals as they interact (e.g. by collisions) with a surface of interest. Using TIRF, only immobilized probes are localized with high precision. Once the probe diffuses away or is photobleached, it can be replaced by new probes from the solution. With a low probe concentration and long observation times, a super-resolution image of the entire surface can be obtained and the average residence time can be calculated. However, as residence times are in the millisecond range, no diffusive behavior of the probe can be described. The usage of PAINT has since broadened with the development of universal PAINT (uPAINT), which uses probes involved in membrane binding events as opposed to simple collisions. These include fluorescently-labeled antibodies or fluorophore-tagged ligands, which are directly added to the sample solution [158]. Thus, large sets of single-molecule data of sequential binding events can be obtained. As the underlying mechanism is a biological interaction, observed time scales are usually sufficient to calculate a probe's diffusion coefficient. This in turn allows predictions about the probe's target protein, as both should show a correlated movement during binding events without the need of photoswitching. A similar concept is realised in binding-activated localization microscopy (BALM), which uses DNA-binding dyes that show an increase in fluorescence upon intercalation [159].

2.3.6. CHOLESTEROL DEPLETION

Originally described as detergent-resistant membrane complexes, lipid rafts have been classically defined by their insolubilization in detergents like Triton-X. In live-cell approaches, the addition of cholesterol-depleting drugs is a classic tool to study the lipid raft composition of a cell and possible interaction partners. Depleting cholesterol from the membrane is generally thought to disperse all present lipid domain, as cholesterol is mainly responsible for raft stabilization by its tight interaction with sphingolipids. Additionally to dispersing microdomains, lipid-dependant internalization and recruitment processes can be perturbed by cholesterol-interacting drugs [74]. By disrupting microdomains and observing a possible disassociation of a protein by a change in the observed protein dynamics, conclusions

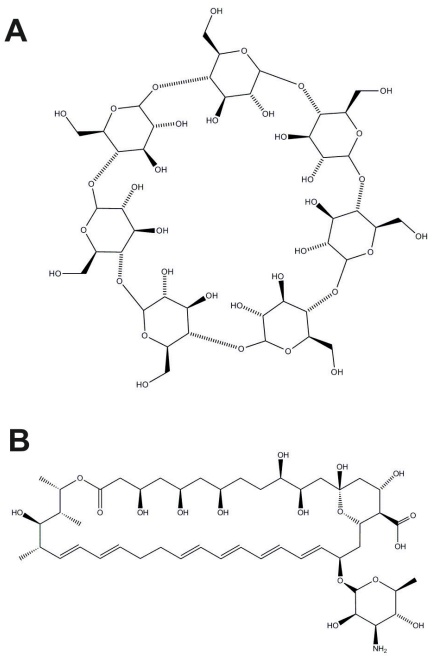

Fig. 22: Structures of (A) MCD and Nystatin (B).

about a protein's favored position in the membrane can be made. The most commonly used drugs for lipid disruption act by cholesterol-depletion, either by inhibiting the cholesterol biosynthesis directly or by removing cholesterol from the membrane and thus destabilizing the lipid rafts. The water-soluble methyl-β-cyclodextrin (MCD) extracts cholesterol from the membrane by forming inclusion complexes and thus facilitating cholesterol solubility in water [160]. However, MCD has also been shown to have a negative influence on cellular actin [161]. Like other antibiotics, the polyene Nystatin is known to bind cholesterol, sequestering it in the membrane [162].

3. MATERIALS AND METHODS

3.1. LABELING PROTEINS OF INTEREST

The observation of cellular processes needs labeling methods that have little or no influence on the biological target and need to be introduced into the cell without causing damage. Permeabilization of the membrane or crosslinking the target might influence or falsify results *in vivo*, stressing the need for membrane-permeable probes for live-cell approaches. Considerations must include a probe's brightness, photostability, the mode of labeling as well as the experimental setup. Biological assumptions should be tested carefully, as different staining techniques might be influential on the obtained results. As super-resolution is still a very young technique, the experimental results should be compared to existing data to support and verify results - or to fine-tune further data acquisition and analysis. However, super-resolution provides a large toolbox of approaches that provide insight into live-cell processes with nanometer precision.

3.1.1. IMMUNOSTAINING

As the IgG antibody type only binds to its epitope and doesn't cluster with other antibodies, it is very effective in specific labeling strategies. For visualizing cellular structures, immunostaining is the most common strategy. In direct immunostaining, an antibody that binds a protein of interest is directly coupled to a fluorophore, presenting a quick and easy method to detect specific antigens. However, direct labeling is costly and not very sensitive. For a more specific detection of proteins, indirect immunostaining, also called sandwich approach is used. Here, an antibody is raised against the protein of interest, purified and added to the sample. By targeting a secondary, fluorophore-coupled antibody against the primary antibody's host species, a highly specific cellular staining can be achieved. As several secondary antibodies can bind to one primary antibody, a signal amplification takes place, leading to an increased sensitivity of this approach. To reduce background fluorescence, samples are commonly blocked with bovine serum albumin (BSA) to block unspecific antibody reactions. Due to their size, intracellular targets can only be labeled with antibody if the cell is permeabilized beforehand.

3.1.2. DNA

A large variety of nucleic acid stains are commercially available. While some only associate weakly to the minor or major groove of DNA, others bind strongly. Many nucleic acid dyes are not membrane permeable, only passing compromised membranes. An optimal nucleic acid stain only exhibits fluorescence when bound to DNA/RNA to avoid unspecific signal in general. If the nucleus is to be observed, a RNA digestion step should be included to avoid possible RNA background fluorescence.

3.1.3. GENETIC TAGS

Contrary to encoded fluorophores, so-called tag systems use a hybrid system to introduce organic labels into the cell (FIG. 23). Here, a genetic tag is fused to a protein of interest and a specific substrate reaction is used to create a covalent bond to a fluorescent dye. The commercially available SNAP-tag is a peptide based on the human O^6-alkylguanine-DNA-alkyltransferase (hAGT), which cleaves defects in DNA repair [163]. Here, the enzyme is genetically fused to a protein of interest, while the desired fluorophore is chemically linked to an O^6-benzlyguanine using a NHS ester reaction. If this substrate is exposed to the hAGT fusion protein, guanine is cleaved and the label covalently bound via its benzyl linker. A similar method utilizes the *E.coli* dihydrofolate reductase (eDHFR), an essential enzyme in the reduction of dihydrofolate to tetrahydrofolate. The cell-permeant antibiotic trimethoprim (TMP) is used as a substrate, as it inhibits eDHFR by covalently binding to it with high affinity. As TMP is otherwise not present in cells, this tag also allows a very high specificity [164]. At last, the **biotin**-avidin/strepativin system represents a combination of tag and immunostaining system: using a biotin-labeled primary antibody, the reaction with a fluorescently-labeled strepativin produces one of the strongest, non-covalent bindings in nature. However, this method is not applicable in live cells, as mitochondria contain a large amount of biotin which must be blocked before the reaction.

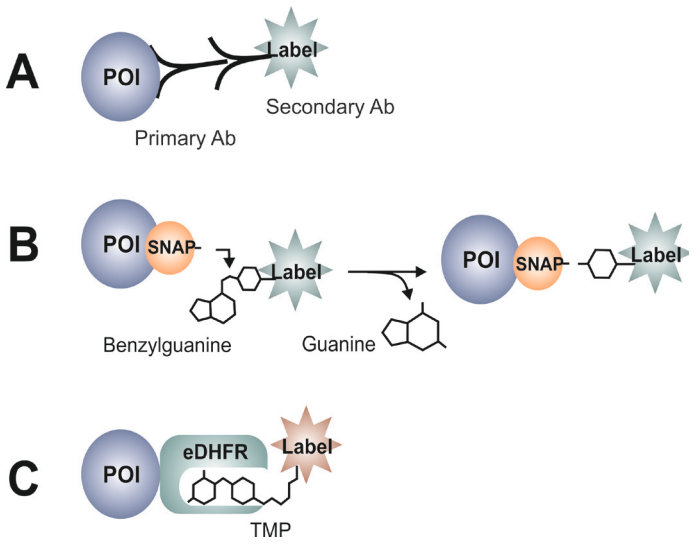

Fig. 23: Common staining methods for labeling a protein of interest (POI). Immunostaining (A) uses primary and secondary antibodies, while the SNAP tag (B) couples a probe by a chemical reaction. The eDHFR tag (C) uses covalent binging events for labeling.

3.2. ANALYZING SUPER-RESOLUTION DATA

PALM and *d*STORM recordings consist of many single-molecule localizations, generating a large dataset, demanding an automated analysis to localize fluorophores with nanometer precision. Programs such as rapidSTORM [165] or QuickPALM [166] usually consist of several discrete steps. First, the localizations of the recorded photoswitching events must be determined. For this, the raw image is noise-reduced by smoothing with a simple average mask. Using a non-maximum suppression filter, all maxima positions are then extracted from the image. Subsequently, a Gaussian function is approximated to each of the PSFs. The next step includes the quality examination of the obtained data: x,y coordinates of the Gaussian give the center of the PSF with high precision and the amplitude is proportional to the number of emitted photons. The amplitude is thus a direct parameter for localization quality: if amplitudes are too low or show an asymmetric PSF geometry, the localization is discarded. Contrary to conventional fluorescence microscopy, this does not result in a fluorescent image of the sample, but a dataset containing spatial and temporal localization coordinates of single emitters. For visualization, localizations are plotted in an artifical image.

3.2.1. DRIFT CONTROL

Sample drift can be caused by thermal fluctuations or vibrations of the microscope or the stage itself and present another limit for the achievable resolution. For drift identification and correction, a low concentration of fiducial beads are immobilized in the sample. The beads then provide a constant signal, offering a fixed point of reference to filter out lateral drift in post-processing. By plotting the coordinates of single beads, drift becomes apparent by the observed standard deviation of their temporal x,y distributions. Axial drift presents itself as a broadening of the PSF and must be addressed directly, e.g. by the usage of an active feedback loop during acquisition. The installation of a nosepiece stage (e.g. IX2-NPS, Olympus) on a microscope can help to minimize focus drift during longer acquisition times, as it abolishes distance changes between objective and sample. The overall drift of a setup can be regularly checked with a sample of beads immobilized on a glass surface. While short acquisition times are usually not prone to significant drift effects, long-term observations as live-cell imaging must always be drift corrected, especially when cellular dynamics are to be observed.

3.2.2. ANALYZING TRACKING DATA

To the observer, the motion of a particle through a sample might appear obvious, while from a non-subjective point of view the data only presents distinct positions of a particle in consecutive images. To prove an actual movement, a probe's localization must be clearly linked to that in a consecutive frame, describing the motion correspondence problem. Questions and demands regarding the analysis of tracking data have not greatly changed since the development of SPT in the 1980s [167, 168] (FIG. 24). Single objects are localized by fitting their PSF in each frame with a two-dimensional Gaussian function, from which the relative position of a probe in the sample can be obtained. A resulting pointing accuracy of 5-10 nm is common. Consecutive coordinates that belong to the same probe must then connect into a trajectory, usually by linking it to its nearest neighbour in the following frame. This creates a probe's trajectory over time from which its mean displacement and diffusion coefficient can be calculated. As a short-range MSD consists of many sample points it is very well defined, while long-range MSD values give higher errors. Thus, the MSD is more precise the more data points (i.e. coordinates in a trajectory) are available. As a PSF might appear blurred because of its motion over time and because blurring increases with acquisition time, it is vital to choose very short observation intervals. However, enough photons must be collected to allow a precise fitting.

Detection and track connection algorithms must be robust enough to define a trajectory despite fluorescence fluctuations of a molecule that is tracked in consecutive frames. In general, the concentration of probes per frame must be low enough to allow a probe's next position to be its discerned, solving the motion correspondence problem. Ideally, if only one molecule is tracked per experiment, a simple nearest neighbor approach is suitable to identify a probe's next position. By

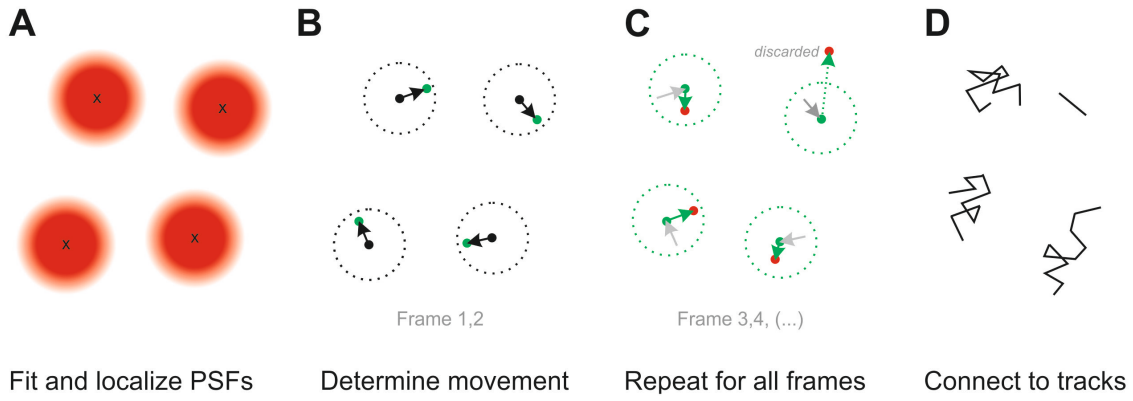

Fig. 24: Concept of SPT trajectory connection. After localizing all single molecule signals (A), displacement is determined by comparing a molecule's nearest neighbour in a consecutive frame (B). This nearest neighbour distance threshold can be adjusted to fit the experimental system. The process is repeated (C) and trajectories of the recorded movement are generated (D).

additionally calculating the difference in the positions of a fixed bead over time, sample drift can be subtracted from trajectories. By implementation of constraint parameters, such as a distance threshold of a bead between frames, an adequate representation of all tracks can be achieved. To avoid ambiguous tracking, distance thresholding must be combined with statistical approaches, testing all potential candidates against physical parameters using a score system, usually by comparing a bead's distance, intensity, size or shape [167, 169]. Florescence might fluctuate and it is impossible to ascertain probable tracks by its brightness or shape alone [170]. While Kalman filtering or joint-probabilistic data-association filters (JPDAF) define the next trajectory position after each frame according to the highest probability, a multiple hypothesis tracker (MHT) weighs all possible connection options before deciding on the most probable track result in closely-spaced targets [171, 172]. However, as tracking algorithms have been developed for aviation, they do not take biological processes like endo- or exocytosis, disassociation or clustering events into account. A tracking filter for biological events must include the probability that objects appear or disappear, as localizations might merge or split. Using a simulated annealing algorithm provides a quick and flexible way to implement this. Here, the motion correspondence problem is solved with an energy minimization method, as molecules are defined as always taking a smooth, minimal path between frames [173]. For tracking in three dimensions, e.g. automated analysis of kymograms can be applied to plot an object's fluorescence through time, analyzing its mobility from a two-dimensional projection [174]. Other methods for single-particle tracking in three dimensions include the introduction of a second focal plane via an additional objective or detector [175], or the usage of a cylindrical lens [176]. As a result, the characteristic changes in the shapes of the imaged PSFs can be used to determine the axial position of a fluorophore.

4. PUBLICATIONS

The following manuscripts were published in the frame of this thesis:

1. **Heidbreder M,** Endesfelder U, van de Linde S, Hennig S, Widera D, Kaltschmidt B, Kaltschmidt C, Heilemann M: Subdiffraction fluorescence imaging of biomolecular structure and distributions with quantum dots. Biochim Biophys Acta 2010, 1803(10):1224-1229.

2. Wombacher R, **Heidbreder M**, van de Linde S, Sheetz MP, Heilemann M, Cornish VW, Sauer M: Live-cell super-resolution imaging with trimethoprim conjugates. Nat Methods 2010, 7(9):717-719.

3. van de Linde S, Loschberger A, Klein T, **Heidbreder M**, Wolter S, Heilemann M, Sauer M: Direct stochastic optical reconstruction microscopy with standard fluorescent probes. Nat Protoc 2011, 6(7):991-1009.

4. Widera D, Heimann P, Zander C, Imielski Y, **Heidbreder M**, Heilemann M, Kaltschmidt C, Kaltschmidt B: Schwann cells can be reprogrammed to multipotency by culture. Stem Cells Dev 2011, 20(12):2053-2064.

5. **Heidbreder M**, Zander C, Malkusch S, Widera D, Kaltschmidt B, Kaltschmidt C, Nair D, Choquet D, Sibarita JB, Heilemann M: TNF-alpha influences the lateral dynamics of TNF receptor I in living cells. Biochim Biophys Acta 2012.

Submitted manuscripts

1. Zander, C, Engelen, T, Widera, D, Nair, D, **Heidbreder, M**, Sibarita, JB, Choquet, D, Heilemann, M, Kaltschmidt, B, Kaltschmidt, C: Retrograde, dynein-mediated transport of NF-kappaB p65 in hippocampal neurons occurs via heterocomplex formation with HSP90/Hsc70 protein chaperones. Journal of Neuroscience *(in preparation)*

5. DISCUSSION

5.1. SUPER-RESOLUTION FLUORESCENCE MICROSCOPY FOR THE ANALYSIS OF BIOLOGICAL TARGETS

Fluorescence microscopy is a non-invasive, highly specific technique to study the cellular processes in TNFSF signaling on the cell membrane *in vivo*. As conventional fluorescence microscopy is diffraction-limited due to the wave-like nature of light, many cellular features are thus not observable with a conventional wide field setup, as they are at least one order of magnitude smaller. Recently, a variety of super-resolution methods have been developed to circumvent this diffraction limit, offering views at biological structures with nanometer precision. PALM and *d*STORM as well as QDTI enable the study of biological targets at previously unattainable resolution. Each super-resolution technique has its unique advantages and disadvantages, which should be considered for each experimental approach. Several factors have to be taken into account before deciding on a method, a label or a labeling strategy.

5.1.1. CHOOSING A PROBE

Organic dyes are bright, photostable and exhibit robust switching cycles under redox conditions without fatigue for super-resolution using *d*STORM. Organic dyes emit on average ten times more photons in each switching cycle than a fluorescent protein. Furthermore, the switching rate can be directly controlled by irradiation intensities. The millimolar GSH concentrations found in the cell are sufficient for reversible photoswitching of some rhodamines and oxazines, making them perfect probes for live cell *d*STORM [118]. The most traditional introduction of fluorescent probes into a cell is immunostaining, the sandwich approach of primary and secondary antibody greatly increasing specificity and thus reducing background noise [177]. However, in general immunostain is not compatible with live-cell imaging, as antibodies are usually not membrane permeant and might induce unspecific crossreactions on the membrane. As a typical IgG antibody has a size of 7-10 nm, this labeling strategy already influences the achievable resolution of *d*STORM experiments (FIG. 25). This is reduced by using $F(ab)_2$ fragments as secondary labels. The degree of labeling of the secondary antibody must also be taken into account, as it might influence signal strength.

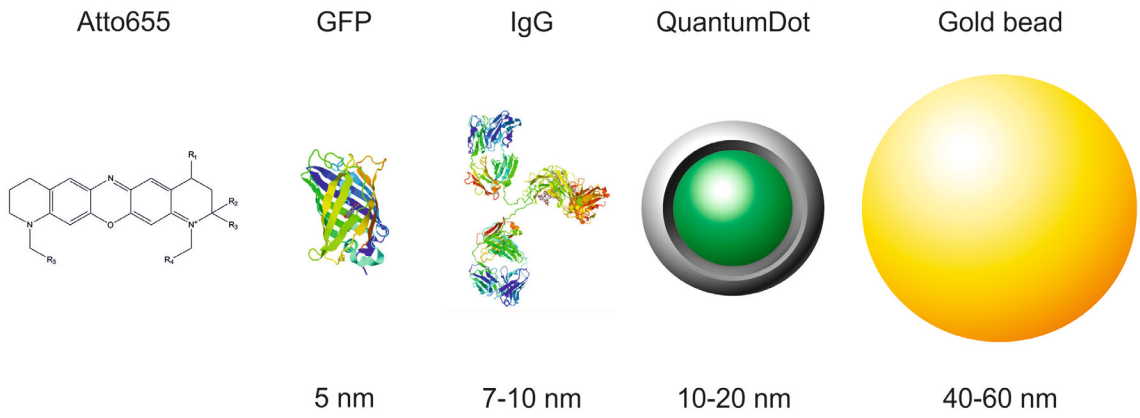

Fig. 25: Different labels for fluorescence microscopy and their relative sizes (not to scale).

Depending on the experiment design, the binding behavior of antibodies must be taken into account: As polyclonal antibodies may bind to different epitopes of the same antigen, they are best used in experiments demanding a high labeling density, e.g. for visualizing cellular structures. For quantification and distribution analyses, monoclonal primary antibodies are a better choice, as only on average one antibody binds per epitope. Secondary antibodies are often polyclonal, to achieve better signal amplification.

As an alternative to antibodies, the introduction of organic dyes *in vivo* can be achieved by using tag-technology, reducing label size, maturation time and unspecific binding drastically, as the reactions underlying all tags are highly specific and efficient. Using membrane-permeant dyes, this method is suitable for *d*STORM. The response of the cell to the probe must be minimal, allowing the probe to freely diffuse into all cellular compartments, but avoiding accumulation. While the SNAP and CLIP tags represent enzyme-based tagging approaches, the original TMP-tag relied on non-covalent binding of the probe. Despite high binding affinities, dissociation from the target is prone to produce noise and covalent TMP variations were designed to avoid this [178]. Dye concentrations in the medium must be carefully tested for all tag systems, as excess dye is prone to produce unspecific background by adsorption to the cell or the glass surface. An exception is the SNAP-tag labeling, where the guanine effectively quenches some attached dyes (e.g. ATTO488 and ATTO655) until the enzymatic reaction cleaves it off at the target protein. Consequently, the dye only becomes fluorescent when the probe is bound to its target and the guanine group is cleaved off, leading to effectively no background fluorescence of unbound probes [179].

Cellular staining with fluorescently-labeled ligands or toxins which bind specific cellular components (phalloidin-actin, α-bungarotoxin-ACh receptors) provides another method for a thorough stain of a structure of choice. However - as for antibody labeling - despite their high specificity, labeled proteins might still produce a significant background noise by adsorption effects.

Fluorescent proteins generate a fluorescent signal that is highly specific with nearly no background fluorescence, as the FP is is expressed as a fusion with the protein of interest. FPs are **small** and stable under cell culture conditions, their photoactivation or photoconversion suitable for PALM. As FPs are genetically encoded, they do not rely on binding kinetics and a high label density can be achieved, resulting in a good resolution for structural analyses. Yet fluorescent proteins are prone to photobleaching and usually exhibit only one switching event, offering a fraction of photons that are available using dyes. Furthermore, genetic tagging is time-intensive and not always feasible, as a coupled fluorophore might influence a target protein's activity, maturation or even localization in the cell. As for tags, FPs thus rely on the visualization of proteins that have been artificially entered into the cell, but contrary to organic dyes, most FPs are not phototransformable under *d*STORM buffer conditions.

In conclusion, the choice of a proper label heavily relies on the cellular target that is to be explored and the microscopy method that is to be used. While immunostain offers a quick and easy method to probe fixed cells, tags or fluorescent proteins are the better choice for monitoring cellular events at high resolution or *in vivo*. The question of labeling also heavily relies on the microscopic method that is to be used. While PALM needs encoded FPs, *d*STORM and QDTI rely on organic dyes or QDs to be introduced either by tags or immunostaining, depending if live cell or fixed cell experiments are to be conducted.

5.1.2. PALM, *d*STORM OR QDTI?

QDTI offers an easily accessible method to increase the resolution of fluorescence microscopy about twofold [180]. Contrary to *d*STORM or PALM, QDTI does not require specialized instrumentation or analysis, as it can be achieved with a widely accessible, commercially available confocal microscope. In combination with optical sectioning, QDTI allows three-dimensional, multiplexed analysis of biological samples. Because of their semiconductor nature, QDs are excellent probes for fluorescence microscopy: they exhibit a high brightness and are very photostable over long periods of time [181]. AQD exhibits a relatively small hydrodynamic radius of 15-25 nm and QDs have long been used in SPT experiments. Similar to gold beads, QDs are very electron dense - thus they can also be used to combine fluorescence microscopy and electron microscopy [182-184]. As QDTI can depict the spatial distribution of labeled molecules with an increased resolution, it might be suitable for protein quantification [184, 185]. However, QDTI relies on immunolabeling or tags and is thus dependant on labeling efficiency and thus prone to background noise. Additionally, the size of the QD might be a hindrance in labeling small substructures. Thus, dense distributions such as clusters cannot be resolved or quantified. As QDs do not rely on redox buffer conditions and can be easily implemented on a CLSM, QDTI represents one of the easiest ways to improve resolution of a sample. The

commercially available QD655, suitable for QDTI, is very photostable and bright. Their high quantum yields even in near-infrared (700-900 nm) make them the perfect probes for tracking in living organisms, a spectral area where only few dyes or proteins are currently available and only show moderate brightnesses [186].

Both PALM and *d*STORM enhance resolution to 10-20 nm, easily surpassing QDTI. However, their implementation and analysis is also far more complex. The decision if PALM or *d*STORM is to be used largely relies on the availability of suitable probes and the decision between probe brightness, specificity and labeling density. Laser intensities are by design much lower in PALM experiments: as all fluorophores are in the unobserved/dark state at the beginning of an experiment, only very low intensities have to be applied for initial photoconversion. As FPs are not very photostable, optimal read-out is also achieved with lower irradiation intensities. In *d*STORM, the first step of an acquisition is the transfer of all fluorophores into the off state before photoswitching becomes recordable. The duration of this step depends on labeling density, pH, the redox buffering and irradiation intensity. While usually negligible, the generation of radicals and superoxides during photoswitching must be taken into account and consequently high irradiation intensities but also high dye concentrations must be avoided in live cell experiments. Nevertheless, photodamage to the sample cannot be ruled out. However, for structural information, *d*STORM imaging is more suitable than PALM, as the many switching cycles of dyes offer a greater data depth during analysis than the single phototransformation recorded in PALM. Logically, discarding asymmetric or weak localizations is not as detrimental as in PALM.

In all methods, TIRF mode offers a great improvement as it reduces the observed volume, but is also prone to errors due to the limited volume of the evanescent wave: membrane invaginations only present themselves as areas without observed fluorescence signals - internalization is not directly visible in TIRF, but must be deduced from the data. Thus, a careful examination of the biological system is needed before conclusions are drawn. While HILO is useful for imaging intracellular compartments removed from the membrane (e.g. the nucleus), it introduces an inclined field of view, which must be taken into account during data analysis.

5.1.3. TRACKING PROTEIN DYNAMICS

Historically, a large amount of mobility data concerning biological targets could be derived from SPT, starting with Leeuwenhoek's observation of the erratic movements of bacteria in solution. Tracking of single reporters using SPT and QD probes was achieved in live cells, either by using immunostain or ligand labeling [187, 188].

Both *d*STORM and PALM approaches can also be used for tracking protein complexes in a living cell: by using high photoconversion and acquisition rates, a video-like reconstruction of movements is possible by grouping several frames together in a sliding-window approach. This does not increase the temporal resolution of the method, but allows the representation of temporal changes. Live-cell PALM was previously applied to adhesion complexes [189] and a comparable method was developed for *d*STORM, termed video-like *d*STORM [190]. Here, the temporal resolution mainly depends on the achievable photoswitching rate of a dye and the applied imaging frame rate, as well as the labeling density and a structure's complexity: the temporal resolution is low if a structure is very densely labeled, as more than one fluorophore in a diffraction-limited spot might be active if a very short recording interval would be chosen. By increasing excitation intensities - and thus depopulating the on-state of a dye - or the applied imaging frame rate, this can be circumvented. On the other hand, the achievable temporal resolution is high if the structure is only sparsely labeled, guaranteeing only single emitting fluorophores per diffraction-limited area at short integration times. However, a sparsely-labeled structure is not spatially well resolvable with regards to the Nyquist-Shannon criterion. Thus, temporal and spatial resolution are closely linked and depend on the imaged structure as well as on the labeling density, a structure's dynamics and the achievable photoswitching rates. In general, a spatial resolution of 20 nm with a temporal resolution of 0.1-1s is possible if the observed structure is densely labeled and a reliable, fast switching fluorophore is used [190, 191].

Tracking single proteins with high temporal and spatial precision using fluorescent proteins encompasses a number of advantages to live-cell PALM and *d*STORM: no averaging of a number of molecules is necessary, as single proteins are recorded in real time without the need for grouping frames - here, the temporal resolution is mainly dependant on the achievable speed of single-molecule sensitive cameras, today up to >1 kHz. sptPALM recently replaced the traditional usage of photostable beads in SPT, increasing the possible labeling density and thus data depth immensely. As the FP is directly fused to a protein of choice and thus no background noise from free dye molecules influences measurements, giving sptPALM a higher specificity, which is extremely important for membrane proteins, as adsorption effects of dyes usually occur on the membrane or the glass surface in direct vicinity. uPAINT depicts actual binding events on the cell surface, providing the most

biological accurate results as no genetic encoding is necessary for imaging the dynamics. On the other hand, it can produce a high background of immobile probes, as adsorption to the glass surface and even the cell surface might occur.

5.1.4. THE OBSERVER'S INFLUENCE

For obtaining an accurate depiction structure in super-resolution microscopy, a high labeling density is beneficial to satisfy the Nyquist-Shannon criterion. Antibodies and organic dyes in the medium are biologically an attack on the cell and both tag-technology and fusion proteins are usually overexpressed to achieve high labeling densities. The probe's influence on a biological system is commonly not tested, but might alter a cell's response during experiments: cellular cascades might be prematurely activated, receptors or rafts crosslinked or internalized to be targeted for degradation (e.g. by antibody binding events). The binding of dye-labeled toxins might stabilize structures that are usually in flux, resulting in aberrant reactions to other stimuli (e.g. actin-phalloidin). Laser intensities, especially at short wavelengths, might have a considerable influence on the observed processes, e.g. by the generation of reactive oxygen species. Long-term observations must always check for signs of photodamage, which manifest itself in a variety of ways. Samples must generally be checked for proper cell cycling and division before and after experiments. For the observation of native cellular reactions, stable cell cultures with FPs or tags under native promoters are optimal. Here, native reactions can be assessed independently of the imaging process and the probe's influence is minimal.

5.1.5. PROBE SIZE IN MEMBRANE TRACKING AND THE INFLUENCE OF MICRODOMAINS

The size of a label usually has little to no effect on observed membrane properties. In open spaces, the membrane viscosity is determining a molecule's mobility: the membrane viscosity is 500 times higher than that of the aqueous phase surrounding it [192]. Thus, the membrane defines the motion of the coupled molecule, while the label should have nearly no effect on the overall mobility. However, an influence on mobility in small compartments, other cells or during endocytosis cannot be ruled out if large probes are used. Additionally, bivalent binding of probes might lead to artifacts due to aberrant probe aggregation. The motion of many cellular components could be shown, proving the presence of confinement zones that might represent raft areas of 200-300 nm. Furthermore, the mobility in these confinement zones could be influenced by cholesterol depletion, hinting at lipid microdomains. The influence of the cytoskeleton on the mobility and organization of membrane proteins could also be shown [193-196].

5.1.6. TRACKING METHODS FOR MEMBRANE COMPONENTS

Diffusion is vital in biological systems; transcription, neuronal signalling and molecular transport often depends on diffusive properties of proteins. Lateral differences in two-dimensional diffusion of lipid bilayers is a common explanation for receptor compartimentalization and recruitment to microdomains. sptPALM can be used to track a photoactivatable probe at high density and high temporal and spatial resolution. Here, previously unobservable heterogeneities in protein mobilities can be observed, as single particle trajectories can be analyzed. Both FCS and FRAP are capable of revealing the presence of lipid microdomains in the membrane and as observation volumes in both FRAP and FCS can be adjusted according to the observed probe's mobility, offer a high temporal resolution even in fast processes.

Since its development in the 1970s, FRAP has been used to study protein dynamics; the discovery of GFP and development of confocal microscopy lead to a revival of the method in modern biology. Using FRAP, membrane dynamics with dye-labeled lipid components such as cholesterol [197] or phospholipids [198] were studied. The movement of transmembrane proteins [199, 200] and other intracellular membranes, such as the nuclear envelope [201] or the Golgi [202] have been probed by FRAP as well as three-dimensional systems like the transcriptional activations in the nucleus [203] or active transport along active axons [204]. FRAP generally shows incomplete recovery rates for most membrane components, suggesting an immobile phase in the lipid bilayer.

Compared to FRAP, FCS is capable of measuring very fast dynamics, even free diffusion in solution. Fluorescently labeled lipid analoga can be used as a probe to compare diffusion on native and model membranes, revealing reduced mobility in native cells, proving the prevalence of molecular interactions in the cell membrane [96, 143]. By using fluorescently labeled ligands, receptor binding, mobility studies and protein-protein interactions can be observed [205-207]. FCS can reveal small differences in the dynamics of membrane components in model membranes upon cholesterol depletion [208] or upon ligand induction of receptors in native cells [96]. However, measuring membrane dynamics with FCS might give falsified results, as the FCS volume is larger than a biological membrane, averaging data from probes diffusing below or above the membrane. Furthermore, the spatial resolution of both FRAP and FCS is limited by the diffraction of light, so the probing of native microcompartments is impossible. For studying a lipid bilayer, a membrane model system like giant unilamellar vesicles is often used. By constraining the excitation volume by using a STED beam (STED-FCS) reduces the sample volume, the Oheterogeneous dynamics of single diffusing lipids [209]. However, no statements about the immobile phase can be made in FCS or FRAP - observations are limited by the mobility of the observed probe and its availability in the surrounding areas. Furthermore, the exact alignment of the detection volume to a biological membrane poses

experimental challenges. The common cellular autofluorescence might also influence fluctuation and recovery rates. In conclusion, both FCS and FRAP represent powerful ensemble methods to probe diffusion coefficients of a cell, revealing the dynamics of a molecule with limited detail [210]. Both methods are theoretically optimal for a uniform population of molecules that exhibit the same diffusive behavior. However, determining an averaged diffusion in such a heterogenic system as the cell membrane with bulk methods is debatable [211].

Contrary to FRAP and FCS, SPT is not limited in its spatial resolution by the usage of a diffraction-limited laser beam. Localization precisions of <10 nm can be achieved by localizing the probes with high spatial and temporal precision [167, 168, 211, 212]. As in FCS, the accuracy of SPT increases with longer observation times, as a larger number of recorded molecule trajectories improves statistics. However, SPT is limited to a finite number of traceable molecules in each experiment. In contrast, the high density trajectory maps gained from sptPALM give a similar data depth to ensemble techniques like FRAP or FCS. Additionally, sptPALM also reveals spatial and temporal dynamic heterogeneities on the cell surface that are otherwise only accessible by SPT [154, 213]. Observed immobile phases can be theoretically used for clustering analyses, as sptPALM allows observations of a high-density with nanometer precision. Here, the boundary to 'classical' PALM analysis is fluent. Additionally, the stochastic activation of fluorophores with low photoconversion and illumination intensities (usually kept low to acquire a maximum trajectory length before photobleaching) are much less photodamaging than the high intensities needed for bleaching in FRAP. While sptPALM is a powerful method to track single molecules, a combination with FRAP or FCS might further verify observed dynamics: sptPALM provides information on the heterogeneity of a membrane, FRAP or FCS are the methods of choice to measure global mobilities, indispensable for comparing data between different samples and experiments. As such, a combination of methods should yield the adequate representation of a cellular dynamic; monitoring both global and local, very fast and slow changes, harmonizing the different methods' results into a biological hypothesis.

5.2. APPLIED PROJECTS - INTEGRATIVE SUMMARY OF THE RESULTS

As membrane interactions and the spatial distribution of TNF receptors play an important role in signal transduction [93], analyzing both is vital for understanding the involved signal cascades in more detail. To study the TNF cascade with nanometer resolution, several different super-resolution approaches have been implemented to analyze spatial distributions of TNF-R2 and the temporal dynamics of TNF-R1.

5.2.1. TNF RECEPTOR QUANTIFICATION

QDTI was introduced to provide an easily accessible method to increase the resolution of a biological sample twofold, facilitating three-dimensional and multicolor approaches to analyze molecular distributions and spatial organization (FIG. 26). As QDs are very bright and photostable, they are unambiguous in particle analysis. As such, QDTI can theoretically be used in the quantification of single proteins that are well separated, but also to increase the resolution of labeled structures. However, quantifying densely packed structures such as clusters is impossible with QDTI, as QDs cannot be selectively photoswitched and thus not resolved as in localization-based super-resolution. Furthermore, the complete surface of a closely spaced structure is possibly not fully accessible by the large QDs, leading to a non-representative staining. While spatially well-discernible receptors are thus theoretically quantifiable, TNF-R1 is no valid target for this method, members of the TNFSF are theorized to cluster with or without the aid of microdomains of a size below the diffraction limit [92]. TNF-R2 shows many homologies to TNF-R1, including a PLAD, but is usually representing only a fraction of the TNFSF response of a cell [214]. Additionally, the response of TNF-R2 to sTNFα is inhibited by its unique stalk region, inhibiting signal transduction. Formation of highly stable, ligand-independent TNF-R1 complexes is favored by sTNFα on the other hand [215]. As juxtacrine signaling via mTNFα is dependent on global cell-cell interactions, it is feasible to assume that TNF-R2 represents a sparsely distributed, non-clustering target on the membrane and thus a perfect model system to test QDTI quantification.

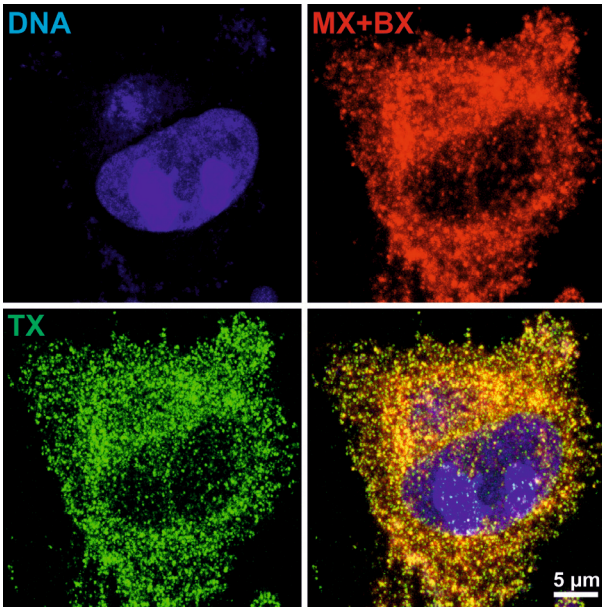

Fig. 26: Maximum intensity projection of a 3D QDTI stack. Helas were immunostained for TNF-R2 and counterstained with QD655. Adapted from [185].

To label only membrane-bound TNF-R2, cells were not permeabilized to visualize only the native membrane distribution of the receptor on a cell. Immunostaining of TNF-R2 and subsequent QDTI indeed revealed a distinct receptor distribution that is impossible to discern with common dye stains, where single TNF-R2 molecules only appear as a homogenously dispersed fluorescence blur. DNA stain provided a point of reference to define the dimensions of the nucleus. Structures can also be imaged with an increased resolution, proving the QDs high specificity, showing nearly no background stain even if a cell has to be permeabilized.

TNF-R2 expression is differentially regulated, with receptor numbers varying between 100 and 10000 copies per cell, largely depending on the cell type. The TX channel of labeled TNF-R2 reveals a well separated, distinct receptor distribution in three dimensions, allowing quantification and revealing a population of even up to ~21000 receptors in a cell [185]. However, defining a baseline expression level for a cell is difficult per se, as most - if not all - protein copy numbers are influenced by a variety of medium-dependant stimuli. While TNF-R1 expression seems to be kept under a non-inducible housekeeping promoter, expression of TNF-R2 is strongly influenced by inflammatory stimuli like TNFα, IFN-γ or IFN-α and might account for the strong fluctuations in observed receptor counts. Interestingly, TNF-R2 mediates its effects mainly by interaction with TNF-R1: the abundance of TNF-R2 detected here might be interpreted as a transitory reaction to outer stimuli, as Helas usually do not transcribe TNF-R2 in such high numbers [41, 216]. The well-distributed, large TNF-R2 population might thus be interpreted as a first step towards a global response of the cell to an unknown influence, guiding the cell towards future apoptotic pathways, as TNF-R2 is known to degrade TRAF-2 that TNF-R1 usually utilizes to induce proliferation. An increase in the global TNF-R2 population might catalyze this signalling decision by providing an equidistant network of TRAF-2 degradation [56] (FIG. 27). As no infections could be observed in the cell culture prior or after imaging, the serum-containing media such as fetal bovine serum (FBS) might here directly influence the cellular response to inflammatory stimuli, as it is usually not endotoxin-free [217]. However, as resolution is only increased twofold in QDTI, we could only rule out larger clusters, but could not define if any microclusters of TNF-R2 are present on the cell membrane, as QDTI is still a diffraction-limited technique.

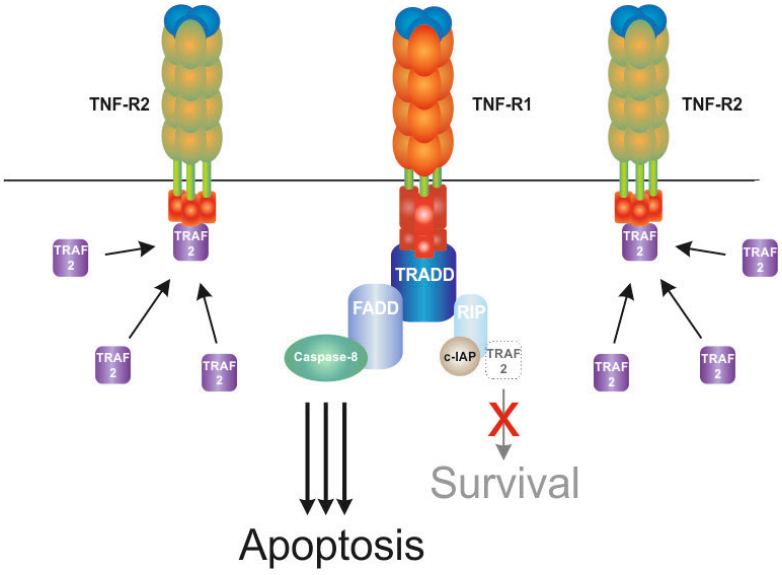

Fig. 27: Theory of TNF-R2 amplifying apoptotic signalling of TNF-R1 by higher TRAF affinities. As TNF-R2 binds all available TRAF after induction with mTNFα, TNF-R1 signaling switches to apoptotic pathways. This mechanism is enhanced by a large number of expressed TNF-R2.

In general, no absolute number of molecules should be derived from QDTI data without extensive negative controls, as QDs tend to get 'stuck' even in unpermeabilized, unlabeled cells due to their size. Unspecific binding and the tendency of QDs to cluster spontaneously before antibody binding might also lead to a high deviation in receptor counts, as QDs below the Rayleigh criterion are impossible to discern. Quantification algorithms must also be tested for their robustness, as it might misinterpret collected TX signals, especially in axial direction. Negative controls define the number of 'background' QDs in an untreated cell. Nevertheless, quantification of spatially well distributed receptors is in theory possible using QDTI, supplying an easy method for estimations of molecule numbers that are impossible to discern in conventional fluorescence microscopy. Structural information is also accessible with an increased resolution. To obtain similar results, electron microscopy would have to be used as an alternative, demanding high experimental effort. Recently, QDs have been used in combination with electron microscopy, providing a method for combining the advantages of fluorescence microscopy – i.e. multicolor imaging – and the structural, high resolution information that electron microscopy offers. Correlative microscopy proves the high specificity of QDs [184]. In theory, QDTI can also be used to track receptors on live cells. However, the necessary laser intensities – usually threefold to obtain TX – could be photodamaging for live cells if high imaging rates are used. For tracking the long-term reactions of TNF-R2, the photostable QDs could prove to be a vital tool in the future.

In conclusion, quantification of receptor molecules with QDTI can be done as a proof of principle, but demands many controls of labeling efficiency, specificity and robust particle indentification algorithms. Quantification of targets that cluster or build dense structures is difficult, but still reveal spatial structures with an~ two-fold increased resolution, as shown for microtubule filaments or

mitochondria proteins. Interestingly, TNF-R2 was found to be present in high numbers, but not found to cluster on HeLa cells, but rather exhibited a uniformly-spaced localization, a fact that might hint at its supporting role for TNF-R1 signaling. As such, QDTI is an easy method to increase the resolution usually achieved in CLSM.

5.2.2. LIVE-CELL *d*STORM

Combining video-like STORM with tag technology and using live-cell compatible dyes, the movement of nucleosome complexes using live-cell dSTORM became possible. Previously, *d*STORM was limited to fixed cellular samples, as dyes need oxygen removal and a certain thiol concentration to exhibit the stable photobleaching that is needed for super-resolution. However, some oxazine dyes like ATTO655 are compatible with oxygen. The antioxidant agent GSH is found in adequate, millimolar concentrations in the cytoplasm, where it protects the cell from the detrimental effects of reactive oxygen species. Thus, the GSH concentration is adequate reducting agent for photoswitching ATTO655, enabling live-cell super-resolution imaging with *d*STORM. To test the proper photoswitching under cellular conditions, the membrane permeant ATTO655 was introduced to histone H2B, using the eDHFR-tag [218]. Histones provided a specific and well-discernible cellular signal in a nucleus, and DNA counterstaining was used to evaluate the specificity of the tagging (FIG. 28). Histones represent the basic unit of DNA folding and are thus highly important in cell cycle progression and gene transcription. Consequently, the movement and distribution of histone components has long been probed with fusion proteins and fluorescence microscopy. In nucleosomes, DNA is tightly wound around a compact histone octamer, building the typical *beads on a string* with a diameter of 30-40 nm [219]. Highly dynamic during the metaphase, nucleosome mobility is considered to be quite static during interphase, as it is constrained by centromers and telomeres to a radius of ≥ 500 nm [220]. Consequently, tracking the short, saltatory movements inside this area that interphase nucleosomes exhibit has been difficult, as conventional approaches – e.g. using GFP fusions [220] - are diffraction-limited. FRAP could show that H2B is the most mobile histone of a interphase nucleus [221]. Using video-like *d*STORM, the spatial resolution of moving interphase nucleosomes could be improved (FIG. 29). By grouping several images, the heterogeneous mobilities of nucleosomes was revealed: while some were largely static, others exhibited slow dynamics of up to ~3 nm/s. Nucleosome movement is linked to chromatin remodeling processes that change the accessibility of DNA, facilitating transcription, replication and repair [222, 223]. As such, the recorded mobile nucleosomes could represent single DNA sections

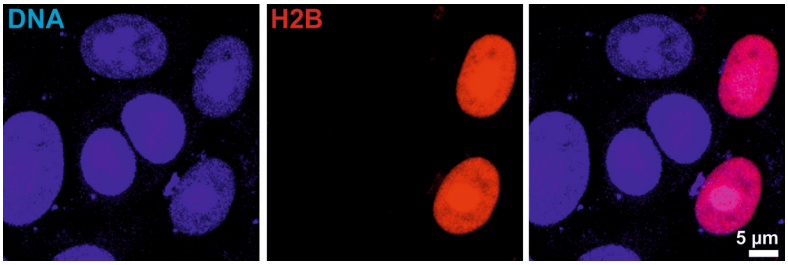

Fig. 28: Specificity test of eDHFR tag. Counterstaing of DNA after tagging H2B-eDHFR with ATTO655-TMP reveals cells transfected with an H2B stain are selectively stained with ATTO655. Adapted from [218].

where the chromatin structure undergoes conformational changes during the measurement, revealing transcriptionally active domains. It is unclear if the measuring influences these mobilities, but cells showed no signs of photodamage and divided properly after imaging and staining procedures. Even stained cells showed no negative reactions to the experiments, proving that the used tag and the dye had little to no negative influences. Nucleosomes exhibited an experimental diameter of 30-80 nm. As the grouping of several frames to obtain a video-like reconstruction of histone dynamics blurs the results, histones show a slightly larger diameter than the literature suggests.

Again, the background noise and the labeling density define the achievable resolution: the densely packed nucleosomes labeled with tag technology prove an excellent target for video-like *d*STORM, as nearly no unspecific binding events were observed in the nucleus. By imaging the nucleus in 'dirty TIRF', only a small sheet of the densely labeled nucleus was imaged, greatly increasing contrast. However, targets on the cell membrane are prone to incorporate unspecific background, as dyes

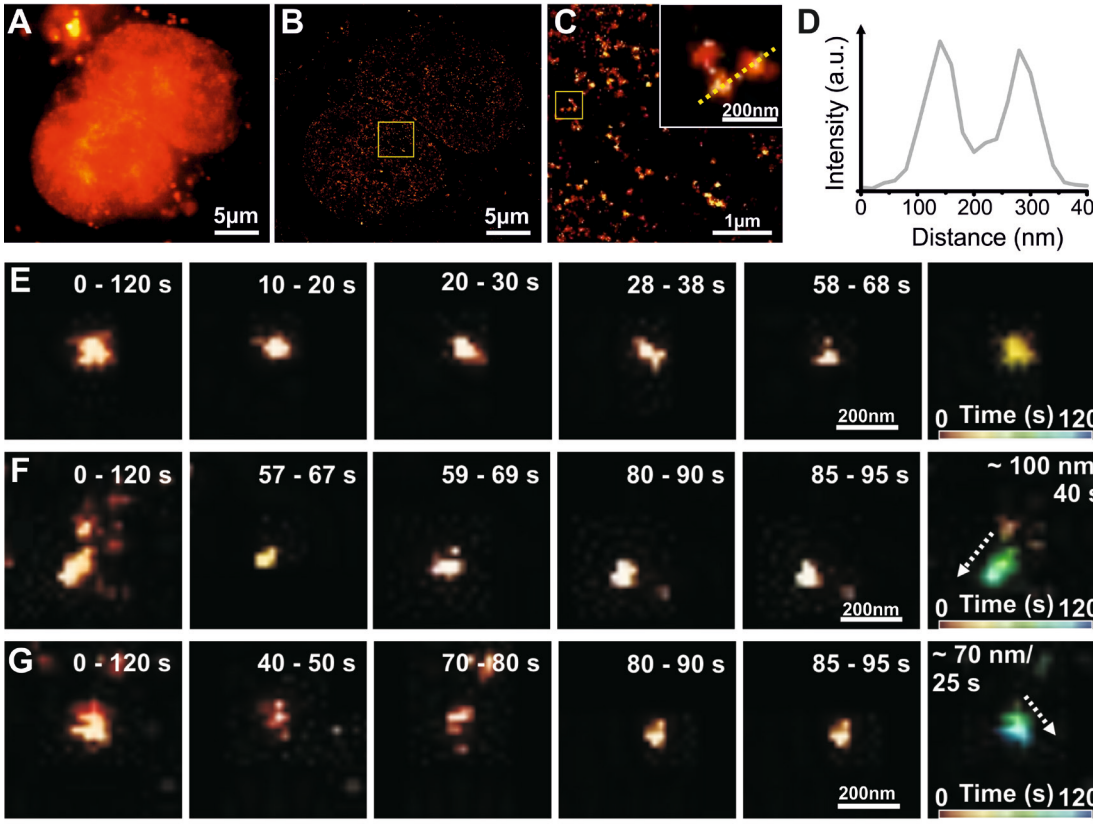

Fig. 29: Live-cell *d*STORM imaging nucleosomes. Widefield image (A) of H2B stained with ATTO655 and the corresponding reconstructed super-resolution image (B). Details and cross-sections depicted in (C,D) show the great increased resolution attainable by *d*STORM opposed to WF mircoscopy. Monitoring histone mobility (E-F) is possible by grouping 60 frames (1 s) to reveal static (E) or dynamic protein clusters (F,G). Adapted from [218].

might adsorb to the glass surface or the membrane itself. To avoid this here, cells were first stained and then transferred into new sample dishes – saturating the glass surface with BSA prior to coating has proven to have a similar effect. Nevertheless, tracking cellular and nuclear structures over long periods of time could provide insights into the changes in gene expression that TNFα is causing in the future. In conclusion, the introduction of organic fluorophores that are capable of photoswitching under native cellular conditions with tag-technology enables live-cell *d*STORM, allowing the tracing and resolving of cellular structures well below the diffraction limit. As this proof of principle suggests, other tagged intracellular proteins are valid for observation using live-cell *d*STORM – however, receptor dynamics on the cell surface might always be influenced by possible background signal, which can only be avoided by the use of the highly specific FP-protein chimeras.

5.2.3. TRACKING TNF-R1 WITH SPTPALM: THE ROLE OF LIPID RAFTS

Many proteins found on the cell surface have been shown to be at least temporarily associated with rafts, an interaction that is vital for cellular signal transduction (e.g. EGFR [224] or CD95 [225]). The distribution and the mobility of TNF-R1 on the cell surface has also long been theorized to be main influence on its signaling outcome after TNFα binding [41, 84]. If microdomains like lipid rafts are indeed involved in signalling, differing modes of motion should be observable on a live-cell membrane. Indeed, changes in TNF receptor dynamics have been monitored in live cells using FCS [96], revealing a broad, slow distribution for TNF-R1 which is not influenced by TNFα addition. Cholesterol depletion in turn increases the observed mobility, suggesting that some receptors are associated with cholesterol-containing microdomains. In contrast, TNF-R2 dynamics are unchanged after cholesterol depletion or cytoskeleton disruption, but show a marked decrease after induction with a mTNFα analogon. As this decrease of diffusion coefficients is not linked to cluster formation, membrane viscosity or adapter interaction, *Gerken et al.* suggest a sorting into cholesterol-independent compartments or the binding with other interactors.

While FCS gives an ensemble measurement of membrane mobilities, single-molecule methods can reveal additional subpopulations and heterogeneities (FIG. 30). By using sptPALM and introducing a TNF-R1-tdEos chimera, an entire cell surface could be monitored over long time periods (30 min) and a high density of receptor trajectories (> 500 tracks per cell) with a duration of at least 80 ms could be obtained [226]. The sptPALM approach could indeed reveal subpopulations of receptor molecules with differing mean diffusion coefficients (FIG. 31). Comparing sptPALM data with FCS shows a good accordance of the measured mean diffusion coefficients (TAB. 1), a native cell exhibiting a mean diffusion coefficient of 0.12 $\mu m^2/s$ in FCS and 0.14 $\mu m^2/s$ in sptPALM. A native HeLa membrane exhibits a broad, heterogeneous distribution of TNF-R1 diffusion coefficients and a well-discernible slow fraction of receptors (between 10^{-4} and 10^{-3} $\mu m^2/s$). It is unclear if TNF-R1 is present as mono- or oligomer, and if slow receptors are present in a pre-assembled form, but the overall relatively high mean diffusion

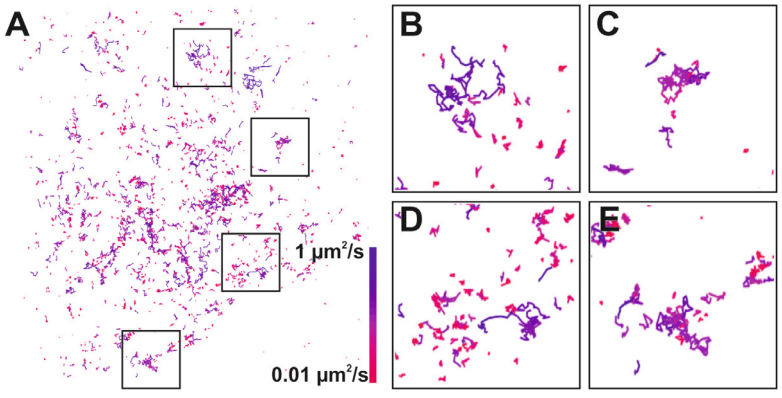

Fig. 30: Spatial heterogeneities revealed by plotting the trajectories of TNF-R1 on a native cell reveals possible regions of temporal confinement. An overview (A) shows the heterogeneity of trajectory localisations with apparent hot spots for TNF-R1 visitations (B-E).

coefficients suggests small aggregates. Diffusion maps of the receptor on the membrane revealed a heterogenic distribution of recorded receptor trajectories, but could also show that some regions are more often visited than others. Areas with a high trajectory passage could represent lipid rafts temporally decreasing a receptor's mobility. However, as no complete read-out of TNF-R1 of the cell is monitored, and cellular invaginations are only deducible by the complete absence of trajectories, it is impossible to describe the topological anatomy of the cell membrane in full detail from trajectory data alone.

5.2.3.1. TNF STIMULATION

Upon TNFα addition the overall diffusion coefficient of TNF-R1 shows no significant increase (0.16 $\mu m^2/s$), but the slow fraction is immediately significantly depleted (FIG. 31). As the disappearance of the slow fraction does not lead to an increase of the mean diffusion coefficient, a mobilization of slow receptors cannot be the explanation here. One can assume that the slow fraction of receptors is

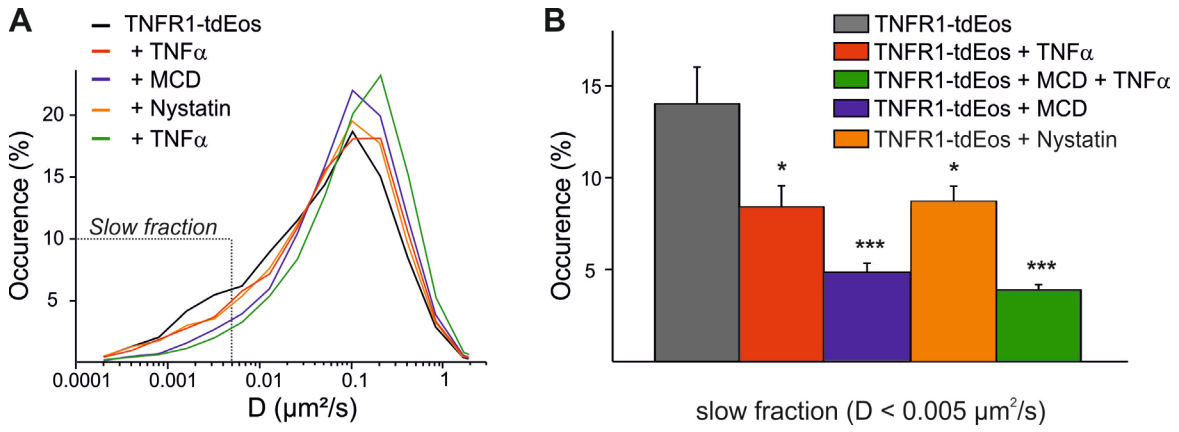

Fig. 31: Results from sptPALM trajectory analysis. The relative frequencies of mean D (A) and the percentages of the slow receptor species (B) show a significant depletion under lipid disruption and TNFα addition in comparision with the native conditions. Adapted from [226].

removed from the surface and thus the field of view during measurements. The overall diffusion coefficient remained constant over the next 30 min after the TNFα pulse and on native cells. This is in good accordance with previous studies that showed endocytosis within minutes and subsequent signal induction and degradation of TNF-R1 over the course of 60 min after an TNFα pulse [84]. If and when the cell replenishes the internalized receptors remains unclear, but as the slow fraction remains absent, it can be supposed that either no replenishment takes place or that only mobile, single TNF-R1 is returned to the membrane which do not aggregate in microdomains. As in FCS, it can be assumed that at least a portion of TNF-R1 is at least temporarily restricted in its movement, either by obstacles, interactions with other receptors or membrane microdomains like lipid rafts or cytoskeletal corrals. As microdomains are known to restrict protein mobility and facilitate

internalization, one can assume that the disappearing slow receptor fraction was internalized from lipid microdomains upon ligand induction. Unlike TNF-R2 [96], TNF-R1 shows no marked mobility reduction upon binding TNFα, ruling out a larger cluster formation. Additionally, adapter protein binding is not observable by a reduced mobility here. The theory of internalizing TNF-R1-containing microdomains is further corroborated by preliminary analyses of individual TNF-R1 MSD plots (FIG. 32:). While MSDs of trajectories extracted from a native cell membrane show a broad distribution of all types of movement that represent a variety of immobile and mobile types of motion, addition of TNFα leads to a change in MSD distributions. Here, the exponential curves of MSDs hints at the possible active transport of the receptor as it is internalized and transported away from the cell membrane [227]. As trajectories that represent caged movement of receptors also increase, this is a further hint at endocytosis of TNF-R1 happening directly after TNFα stimulation.

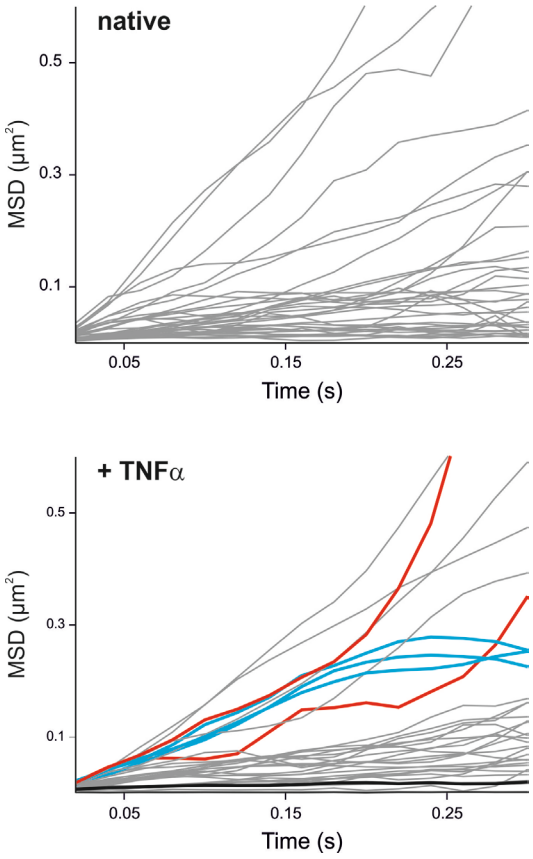

Fig. 32: Individual MSDs of TNF-R1 trajectories recorded using sptPALM. Native cells show a heterogenous distribution of receptor dynamics After TNFα induction, active transport (red) and confined movement (blue) become observable.

5.2.3.2. LIPID DISRUPTION

To examine the role of lipid rafts in TNF-R1 dynamics in more detail, cholesterol was depleted, leading to a dispersal of all putative raft regions, abrogating possible TNF-R1 interactions with microdomains and inhibiting internalization processes in general [75, 228].

Addition of the cholesterol-depleting MCD led to a significant increase of the mean diffusion coefficient for TNF-R1 (TAB. 1) to 0.20 $\mu m^2/s$ and a reduction of the slow receptor fraction (FIG. 31). Addition of the cholesterol-sequestering Nystatin has a similar, but less prominent effect on TNF-R1 dynamics and strongly resembles the depletion monitored under TNFα addition in both mean diffusion coefficient and its frequency distribution. As internalization processes are inhibited by cholesterol-depletion, they cannot be the reason for the disappearance of slow receptors under Nystatin addition. It is thus feasible to assume that immobilized TNF-R1 is released from raft regions as they are dispersed here, leading to a larger number of mobile receptors on the membrane that increase the mean D in comparison to the native conditions slightly, as observed for TNFα as well. The more drastic effect of MCD on the slow species and mean diffusion coefficient can be explained with the additive effects of MCD, which is known to negatively influence the cytoskeleton [161]. As the actin cytoskeleton is actively coordinated with lipid rafts it can be assumed that the underlying cytoskeleton plays at least a partial role in TNF-R1 dynamics as well. Indeed, it is known that both clathrin- and caveolae-mediated endocytosis requires actin [229, 230]. Which exact role the cytoskeleton plays in TNF-R1 dynamics remains unclear, but a further stabilization of microdomains seems most probable. Addition of TNFα under lipid-disrupting conditions further potentiated the effect, leading to an additional increase of the mean diffusion coefficient.

Tab. 1: Mean diffusion coefficients under differing condictions Comparison between mean diffusion coefficients obtained by sptPALM and FCS measurmeants. Data from [96,226].

	D derived from FCS ($\mu m^2/s \pm SD$)	D derived from sptPALM ($\mu m^2/s \pm SD$)
Native	0.12 ± 0.09	0.14 ± 0.02
+ TNFα	0.11 ± 0.08	0.16 **±** 0.03
+ MCD	0.16	0.20 **±** 0.04
+ Nystatin	--	0.16 ± 0.05
+ TNFα+ MCD	0.16	0.24 **±** 0.03

5.2.3.3. A REFINED MODEL FOR TNF-R1 MEMBRANE SHUTTLING

In summary, sptPALM and FCS experiments could show that TNF-R1 is apparently present in cholesterol-rich microdomains on native membranes, but is rapidly internalized upon binding TNFα. The underlying cytoskeleton plays a decisive role in either facilitating TNF-R1 internalisation or in stabilizing the microdomains responsible for later endocytosis (FIG. 33). As the pre-assembly of TNF-R1 prior to signal induction provides an easy method to amplify a signal - and a recruitment into microdomains favors this self-association by spatial segregation - a vital role of lipid rafts in receptor aggregation and signaling [76]. For the TNFSF, lipid raft-dependant pathways have been proven to exist (e.g. for Fas/CD95), which are attributed to the presence of a death domain [231]. Thus, apoptotic signaling would be directly induced by raft-association or association with raft-located proteins [232, 233]. Other approaches could reveal a TNF-R1 compartimentalization into confinement zones of ~200 nm upon ligand binding [92]. Interestingly, survival signaling has been linked to lipid rafts as well - posing the question if internalization and surface signaling might both be regulated by lipid rafts - possibly by a temporal separation into a fast survival pathway on the cell surface and a slower apoptotic pathway induced after internalization [84]. sptPALM trajectory maps revealed spatial heterogeneities, showing that some areas on the cell are more often frequented than others (FIG. 30). These regions could represent temporal confinement zones that are usually associated with microdomains. However, an interpretation of these regions is difficult, as the membrane topology is unknown and not all present TNF-R1 molecules were imaged. The sptPALM experiments done here could show that TNF-R1 signaling is indeed apparently largely depending on receptor mobilities. As TNF-R1 is internalized by caveolae-like domains or clathrin-coated pits in a cytoskeleton-dependant manner, a signaling hypothesis can be described (FIG. 34): on a resting cell, TNF-R1 is distributed all over the cell membrane, with receptors found in raft and non-raft

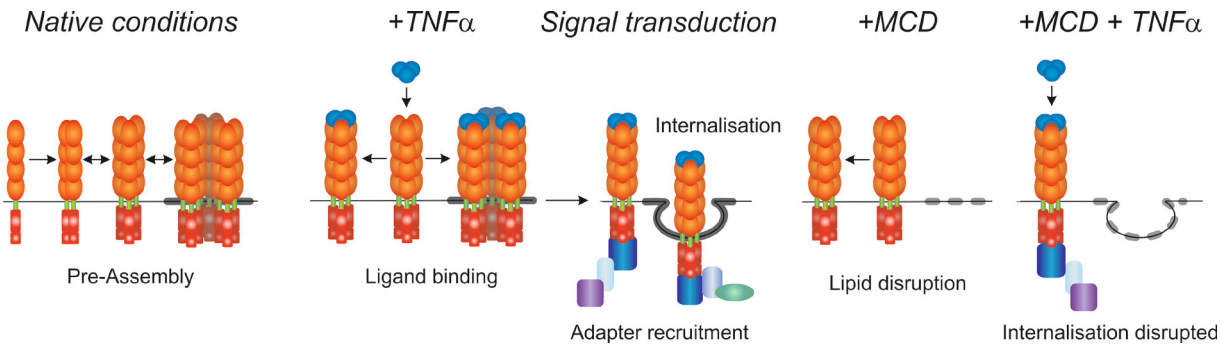

Fig. 33: A refined model for TNF-R1 shuttling on the cell membrane. Pre-assembly prior to ligand binding sorts TNF-R1 into raft domains and non-raft domains, representing the slow and the fast receptor species respectively. Addition of TNFα leads to the internalization of slow species from rafts, while raft disruption increases the slow receptor's speeds on the cell surface, as internalization is inhibited.

compartments. Due to their PLADs, receptors associate, a mechanism possibly facilitated by lipid microdomains that mediate the close contact of TNF-R1 molecules and lead to the formation of a slow receptor population. Upon ligand binding, these oligomerized TNF-R1 complexes are internalized within minutes from the microdomains to mediate death signaling, while smaller receptor aggregations of non-raft regions remain on the cell surface to initialize survival signaling. As such, the amount of receptors found on rafts or microdomains might be a direct pre-ligand signal modulator, depending on a cell's status deciding between life and death signalling in the event of TNFα binding. In contrast, TNF-R2 is heterogeneously distributed in varying numbers that depend on the cell's inner state. While TNF-R2 also contains a PLAD and can be internalized and shed, little is known about its initial response on the cell surface [234]. TNF-R2 is not strongly induced by sTNFα addition. *Gerken et al.* could show that unlike TNF-R1, TNF-R2 is not directly associated to rafts or the cytoskeleton. When binding to mTNFα, TNF-R2 slows significantly due to a recruitment into cholesterol-independent compartments. How and if the receptor is internalized after this remains unclear. TNF-1 and TNF-R2 are thus spatially segregated, possibly in raft and non-raft compartments, occupying very different membrane microdomains. How TNF-R1 and TNF-R2 interact remains largely unknown: as TNF-R2 has a markedly higher mobility than TNF-R1 in FCS experiments [96], it could act as a global and very mobile signal enhancer during or prior TNF-R1 signaling and internalization.

Comparing the results of probing TNF-R1 mobilities with other sptPALM experiments show the prowess of this new technique for studying membrane dynamics: the first sptPALM studies probed the vesicular stomatitis virus G (VSVG) and the human immunodeficiency virus (HIV)-associated Gag protein, presenting a very mobile protein on the plasma membrane (VSVG) and the consecutive slowing of multimerizing Gag [154]. As for TNF-R1, histogram of mobile and less mobile proteins depict the differing mean diffusion coefficients, while large clusters of immobile Gag-tdEos are very well discernible here, a property not observed in TNF-R1 diffusion. However, Gag clusters usually contain ~5000 of very closely-spaced proteins [235], which might not be the case for TNF-R1 aggregations. Two-color approaches using sptPALM could show a dynamic colocalization of immobilized clathrin in pit-like domains with EGFR, a receptor that is also well-known for signal amplification by cluster formation via lateral receptor interactions [236-238].

Using sptPALM and other established methods for the elucidation of receptor dynamics, it becomes apparent that a model for receptor mobility is highly receptor-specific, even when analyzing the same receptor family. Recruitment from or into specialized microdomains like lipid rafts or endosomes modulates a possible ligand-transduced signal as much as adapter binding, oligomerisation, transcription or diffusion rates in the cytoplasm of a cell, all of which is dependent on the cell type itself. A possible model for TNF-R1 signaling (FIG. 34) must incorporate all these complexities, mainly arising from the spatial and temporal diversion and the large number of possible interacting proteins. By grouping elementary reactions into functional units, and assigning reaction rates from experimental data, this can be facilitated, with life or death complex formation as the definitive steps in signaling decisions [239, 240].

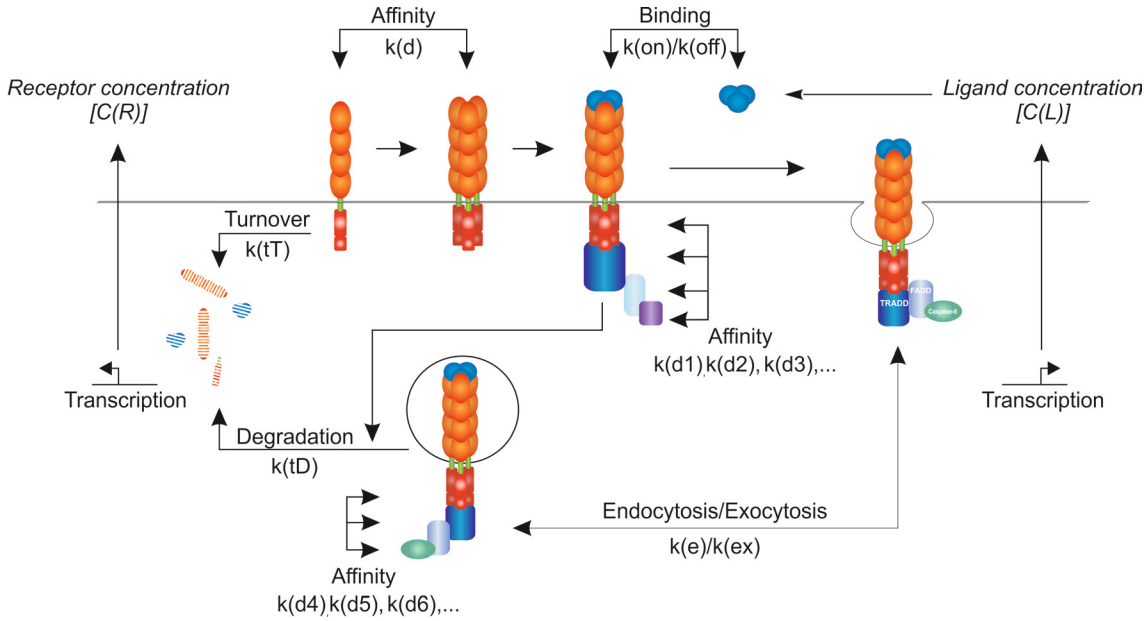

Fig. 34: Model for mathematical computing of the TNF-R1 pathway, taking differing mobilities, affinities and rates for active transport and diffusion into account.

6. OUTLOOK

Super-resolution microscopy enables quantitative and qualitative insights into biological processes, offering single-molecule, single-cell resolution and reveals heterogeneities with a near-molecular resolution. However, as biological processes usually consist of many differing protein interactions, they can - by design - seldomly be characterized with just one microscopic technique. Apart from facilitating labeling, imaging and data analysis, super-resolution techniques could be combined to obtain a larger data depth, verifying already existing data and expanding the understanding of a biological target. With these methods, an entire signal cascade, from ligand binding to the relevant adapter networks and their effectors could be elucidated.

6.1. MULTICOLOR IN SUPER-RESOLUTION

6.1.1. TEMPORAL AND SPATIAL COLOCALIZATION

As *d*STORM has been shown here to be suitable for live-cell imaging, and as some FPs tolerate *d*STORM buffer conditions [241], a multicolor approach using PALM, *d*STORM or a joined method of these two could be utilized to analyze the spatial distribution of differing proteins on the cell surface. This could e.g. elucidate the relative positions of TNF-R1 and TNF-R2 and their respective adapter proteins pre- and post ligand binding. The cholesterol of lipid raft regions can be imaged by staining with cholera toxin subunit B (CTxB). Interactions of proteins or proteins with lipid rafts would then be revealed by the colocalization of two fluorophores. Different organic dyes for different protein targets could be introduced by using several distinct tag systems, in combination with spectrally suitable fluorescent proteins genetically fused to other targets. Applying pair-correlation analysis to super-resolution data like PALM (pc-PALM) could provide vital information about cluster sizes and absolute protein numbers – comparing both lipid raft sizes and receptor distributions pre- and post induction [242]. As localization-based microscopy is not producing fluorescence images but a set of temporal and spatial coordinates, the classic, image-based approach for colocalization is not the first choice. Instead, a coordinate-based colocalization (CBC) can be implemented [243].

By using several different tag-technologies, the cells could also be pulse-chase labeled, tracking the long-term dynamics of a distinct subset of cellular compartments, receptors or adapters to reveal distinct aggregates and dynamics on the cell surface over longer time periods. By using dye-labeled ligands or receptors, the question of multimerisation events on the cell membrane before and after ligand induction could further be elucidated using staircased photobleaching of fixed cells. Here, fluorophores that are in close vicinity show a distinct two-step bleaching, revealing cellular interactions and representing another method to quantify observed interaction partners [244]. By

using fluorophores that show the proper overlapping fluorescence emission and absorption spectrum of donor and acceptor dyes, this method could also be used for single-molecule fluorescence energy transfer (smFRET) and alternating-laser excitation spectroscopy (ALEX) to measure conformation, stoichiometry and possible interactions of labeled proteins [245, 246].

6.2. LABELING STRATEGIES FOR THE QUANTIFICATION OF MOLECULES

QDs still offer an easy and reliable way to quantify well-distributed molecules on a cell surface. By comparing receptor, ligand and adapter numbers, conclusions about the inner state of a cell could be drawn. However, TNF-R1 distributions are usually too dense for quantification. Super-resolution optical fluctuation imaging (SOFI) analysis of QD-labeled TNF-R1 cells could overcome this limitation. Here, the intensity fluctuations of fluorescent probes are used to obtain a background-free super-resolved image by applying higher order autocorrelation analysis, enhancing resolution five-fold. As SOFI relies on intermittent fluorescent signals, photoswitchable probes can be used as well [247, 248]. A combination of super-resolution and electron microscopy could further be used to attain the structural information that only electron microscopy can offer, revealing receptor or adapter localization within or outside of raft regions. As an organic dye exhibits many photoswitching events, it is unsuited for quantification. An alternative could be the use of monomeric FPs with only one fluorescence event, using PALM to quantify a FP-receptor chimera under the target's natural promoter in a knockdown cell line. A stable cell line like this would then only express FP-labeled proteins, in numbers that represent the natural state of the cell, allowing quantification of the native cellular state of a protein. With long integration times and very low irradiation intensities to avoid bleaching effects, the complete protein population of a cell could be accounted for. While photoswitchable dyes are unsuitable for a direct molecular quantification, they are optimal probes to analyze larger cluster distributions and sizes. Changes in the diameters of observed TNF-R1 clusters could provide further insights into the possible multimerization events after TNFα addition.

6.3. TRACKING CELLULAR DYNAMICS

To generate a reliable mobility map of a molecule, a combination of available tracking methods would supply the greatest insight: mobilities of FP-labeled receptors, or a fluorescent ligand on a membrane using sptPALM or uPAINT could be verified by parallel analysis in FRAP or FCS. Adapter or ligand interactions, as tested in colocalization approaches of fixed cells, could be verified in sptPALM, as a coordinated movement of different proteins would prove interaction or binding events on the cell surface. Tracking intracellular compartimentalization and endocytosis events at high densities in three dimensions is the next great challenge of sptPALM. The development of photoswitchable probes that react to a change in environment with a change in emission (e.g. pH sensitivity) or act as

a timer by changing its emission over time [249, 250] would further broaden the possibilities of localizing and tracking cellular processes with high resolution. A dual-color approach for sptPALM or a combination with uPAINT could further act as a complementary method for probing ligand-receptor interactions. While simple colocalization does not prove interaction, a trajectory of coordinated movement does. By first generating a spatial colocalization map, the observed interactions could be proven in the dynamic, *in vivo* observation of both fluorophores.

6.4. TRACKING NF-κB AND TRANSCRIPTION DYNAMICS

NF-κB is one of the most important downstream targets of TNFα, its translocation into the nucleus is followed by the transcription of several proliferative genes. Mobility of NF-κB in the nucleus is modulatable by TNFα - FRAP studies revealed at least two distinct populations of promoter-bound and nucleoplasmic NF-κB [251]. Super-resolving promoter occupancy and thus transcriptional activity in combination with nucleosome movements could reveal distinct nuclear targets of NF-κB. A combination with live-cell fluorescence in situ hybridization (FISH) could further determine the transcribed genomic regions [252]. By introducing fluorescent pulse-labeling of nascent RNA or DNA using click-chemistry [253], these results could be further verified. NF-κB also plays an important role in long-term memory formation and learning, a p50/p65 NF-κB heterodimer most commonly found in the neuron. Using fusion proteins of IκB and of NF-κB, the interaction dynamics of these proteins can be used to study the response of a cell before and upon induction with TNFα (FIG. 35). Contrary to other cell types, NF-κB is actively transported towards the nucleus upon induction by a dynein/dynactin motor complex [254]. Inhibition and induction, retrograde and anterograde transport of NF-κB are well-discernible using FRAP, as free diffusion is practically non-existent in the spatially very confined axon. By using sptPALM, the axonal transport of NF-κB can be further elucidated (manuscript in preparation [255]).

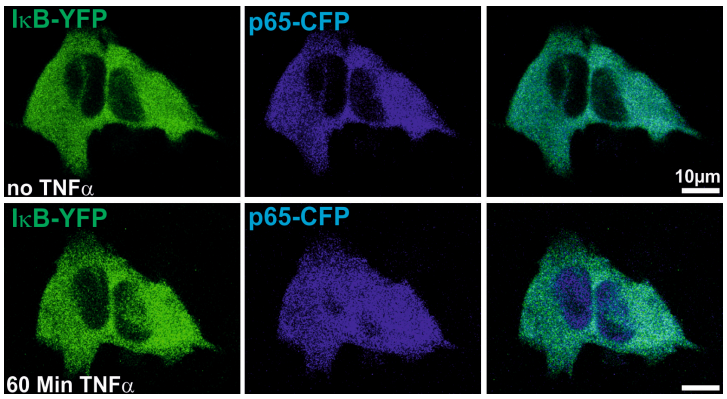

Fig. 35: CLSM images of FP fusion proteins of IκB and the NF-κB subunit p65 in a living cell before and after TNFα addition shows p65 translocation into the nucleus, while the inhibitory IκB remains in the cytoplasm.

Many ideas exist to combine established methods for analyzing biological processes with the highest possible resolution and accuracy. The development of new fluorescent probes, improvement in data

analysis and imaging further stresses the necessity of interdisciplinary cooperation to gain previously unknown insight in cellular organization. In conclusion, single-molecule data is capable of revealing binding constants, mobility and immobilization rates and thus provide a large dataset for modeling a biological signaling cascade from *in vivo* data with unprecedented specificity.

7. PROTOCOLS

7.1. VECTOR DESIGN AND DNA AMPLIFICATION

tdEos was C-terminally fused to TNF-R1 to create an intracellular FP label that doesn't interfere with the N-terminal TNFα binding domain. For p50 and p65, a C-terminal fusion limited the effects of tdEos on the NLS and heterodimer formation (FIG. 36). TNF-R1, p50 and p65 were amplified from their respective template vectors using a High Fidelity Phusion-Taq DNA Polymerase (Finnzymes) to reduce possible copy errors. Mutagenic primers were designed to add specific restriction sites for fusion into the EosFP vector. Amplificates were first ligated (blunt end) into the pJet Gateway Vector (Fermentas), from where they were digested using the previously modified restriction sites. TNF-R1, p50 and p65 were then ligated into the commercially available tdEosFP target vector (Mobitec).

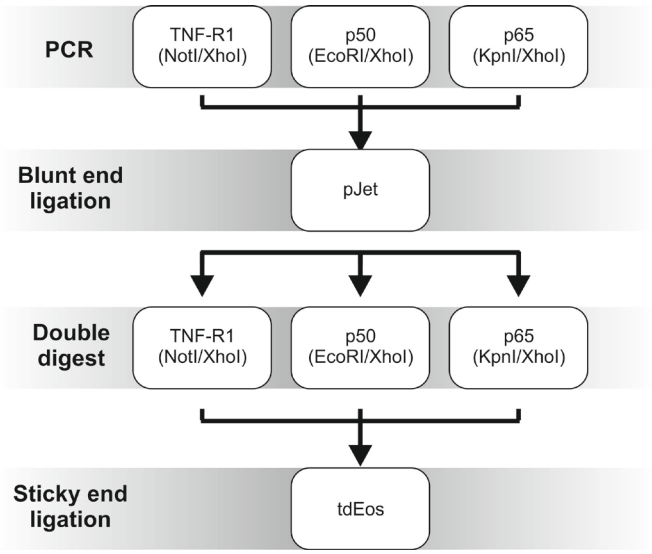

Fig. 36: Representation of the cloning paths used to obtian FP fusion proteins.

7.1.1. VECTORS

1 M Betaine was added to the reaction mix to improve specificity and yield of amplificates [256]. As the PhusionTaq polymerase generates blunt end DNA products, no additional blunting step is necessary before ligation.

pcDNA3-Flag1-td-EOSFP	MoBiTec
pOTB7-TNF-RSF1A	MGC
pJET1.2/blunt Cloning Vector	Fermentas
pCMV-p65-CFP-N1	mod. Clontech; friendly permission of C. Kaltschmidt and T. Seidel
pCMV-p50-YFP-N1	mod. Clontech; friendly permission of C. Kaltschmidt and T. Seidel

7.1.2. PRIMERS

TNF-R1 (NotI)	5' AAA AGC GGC CGC TGT CTG GCA TGG GCG GCC TCT CC 3'
TNF-R1 (XhoI)	5' TTT TCT CGA GGC CAA ATC TGA GAA GAC TGG GC 3'
P50 (EcoRI)	5' AAA AGA ATT CAA ATG GCA GAA GAT GAT CCA TAT 3'
P50 (XhoI)	5' TTT TTC TCG AGT CCA GTG CCC CCT CCT CC 3'
P65 (KpnI)	5' AAA AGG TAC CCC TAT GTG GAG ATC ATT 3'
P65 (XhoI)	5' TTT TCT CGA GTA AGG AGC TGA TCT GAC TCA G 3'

7.1.3. PCR PROGRAM AND SAMPLE CONDITIONS

DNA samples were amplified using the Phusion HF buffer system according to the manufacturer's advice. PCR programs were adjusted for the optimal DNA yield. Annealing temperatures were adjusted to 60s at 63°C and an extension time of 120 s with 35 cycles for amplification. DNA was then stored at -20°C until further use. For Colony PCR, bacteria were picked from the agar plate and directly entered into the PCR mix. Initial denaturation was then extended to 3 minutes at 95°C.

7.1.4. AGAROSE GEL

Agarose gel electrophoresis was performed in 1.8% agarose with 10 µg/ml ethidium bromide solved by heating in 1x TAE buffer. Samples were separated at 100 V for approximately 40 min. To obtain DNA from agarose gels, the Gel Extraction Kit II (Qiagen) was used according to the manufacturer's protocol. Buffer components were solved in 1l ddH_20 and diluted to working concentration (1x) with H_2O when needed.

TAE Buffer (50x)	
Tris base	242 g
Acetic acid	57,1 ml
EDTA (0,5 M)	100 ml

7.1.5. DNA DIGEST

Plasmids were cut using the optimal respective buffer conditions and incubation temperature (NEB), adjusted to a minimum activity of at least 75% for each enzyme. Blunt and sticky end ligations of target vector and cut DNA was performed after purification by agarose gel using a T4 ligase setup (NEB).

Enzyme pair	**Buffer (NEB)**	**Temp (°C)**
NotI/XhoI	3	37
EcoRI/XhoI	4	37
KpnI/XhoI	1	37

7.1.6. *E. COLI* CULTURE

Competent *E.coli* cells (TOP10; Invitrogen) were used to amplify the constructed vectors in high number before transfection into a mammalian system. Ampicillin or Kanamycin (100 µg/ml or 50 µg/ml

Agar plates	
Tryptone	8g
Yeast-Extract	5g
NaCl	5g
Agar	16g

respectively) was added to the growth medium corresponding to the antibiotic resistance (Amp^R/Kan^R) on the used vectors acted as selection marker. Transformed *E.coli* were harvested and plasmids purified using a GeneJet miniprep kit (Fermentas). Plasmids were stored at -20°C. Agar plates were prepared by diluting agar components in 1l ddH_20. Antibiotics were added after the solution had cooled to a 60°C and then poured into petri dishes. LB medium was solved in 1l ddH_20, the pH adjusted to 7.5 and autoclaved. SOB medium was prepared in 1l ddH_20 and pH adjusted to 7.0 before autoclaving.

7.1.6.1. BACTERIA TRANSFORMATION AND MAINTENANCE

For *E.coli* transformation, competent cells were thawed on ice and 5-10 µl of desired plasmid were added. The mix was kept on ice for 30 min, then heat shocked at 42°C for 90 s and again cooled on ice for 1 min. 300 µl SOC medium was added and the bacteria were allowed to grow for 30 min at 37°C. The solution was then plated on agar plates containing the relevant selection marker and grown over night at 37°C. For liquid stocks, single colonies were transferred into LB medium supplied with the relevant antibiotic and shaken at 37°C over night. For frozen stocks of transformed bacteria, *E.coli* were grown in LB to an OD_{600} of 0.5 and then diluted 1:1 with sterile Glycerine (87%). The resulting stock was shock frozen in liquid nitrogen and stored at -80°C.

LB-Medium	
Tryptone	10g
Yeast-Extract	5g
NaCl	10g

SOB-Medium	
Tryptone	10g
Yeast-Extract	2.5g
NaCl	0.25g
KCL	0.093g

7.2. MAMMALIAN CELL CULTURE

7.2.1. HELA CULTURE

Human cervix carcinoma cells (HeLa) were used as a mammalian model system for studying the TNF-R1 pathway. The cell line shows robust, endothelial-like growth, building monolayers in standard growth medium. Cells were cultivated at 5% CO_2 and 37°C in an automatic CO_2 Incubator (Haereus) in Roswell Park Memorial Institute medium 1640 (RPMI; Gibco) supplemented with 10% fetal calf serum (FCS; Gibco), 5% L-Glutamine and 5% Penicillin/Streptomycin (Gibco). Cell growth and viability was regularly checked by microscopic assessment of the tissue flasks (Gibco). Cells were passaged every other day by trypsinization (1x Trypsin/EDTA; PAA) and supplemented with fresh medium. For imaging purposes, HeLa cells were transferred into Lab-Tek chambered cover glass wells (Nunc) at a concentration of $1\text{-}2\cdot10^5$ cells per well. Cells were then allowed to re-attach to the glass surface over night. Fixing cells was done by incubating cells with 4% paraformaldehyde (PFA) for 10 minutes at room temperature.

7.3. CELLULAR LABELING

7.3.1. eDHFR LABELING

$2\cdot10^6$ HeLa cells were transfected with an eDHFR-H2B using the Amaxa Nucleofector System (Lonza), according to the manufacturer's instructions. As a control, H2B-GFP control vector was used in similar vector concentrations. After transfection, cells were allowed to grow in Labtek 8-well chambers (Nunc) over night. A staining solution of $2.5\cdot10^{-8}$ M of TMP-ATTO655 was directly added to the cell culture medium and allowed to react for 1 hr at 37°C and 10% CO_2. Cells were then washed with phosphate buffered saline (PBS; Gibco) and incubated in fresh medium for 1 hr. To avoid unspecific background, cells were detached by trypsination and transferred into a new LabTek chamber. Cells were allowed to reattach for 1-3 hrs. Imaging was done in standard DMEM at room temperature. Alternatively, LabTeks can be coated with 2 M glycine for 30-60 min before cells are entered, to reduce unspecific binding to the glass surface of TMP-ATTO655.

7.3.2. QUANTUM DOT IMMUNOSTAIN

HeLa cells were fixed with 4% PFA at RT for 10 minutes, then washed twice with 1x PBS (Gibco) and subsequently permeabilized with 0.5% Triton-X (v/v) in PBS for 10 min. If membrane receptors were to be observed, no permeabilization was done to achieve a better view of only their outer membrane distribution. To reduce background and unspecific binding, cells were washed twice with 1x PBS, then blocked with 5% Bovine serum albumin (BSA; Sigma) for at least 1 hour at RT and then washed twice with PBS. Primary antibodies were added to the samples and allowed to bind for 2-3 hrs at RT. Cells

were then washed twice with PBS containing 0.05% Triton-X for 5 min. The relevant secondary antibody carrying a QD655 (Invitrogen) was added for 2-3 hours at RT. Samples were again washed with PBS containing 0.05% Triton-X and 4% PFA was added for 10 minutes.

For nuclear staining, $5 \cdot 10^{-4}$ mM Sytox dye (Invitrogen) in PBS was added to the sample for 30 min. To reduce staining of cytosolic RNA, RNAse A (Gibco) can be added and samples. Incubation at 37°C facilitates the enzymatic RNA degradation. Cells were then washed again with PBS and and stored at 4°C.

7.3.3. CELL TRANSFECTION

To introduce plasmid DNA into Helas, FuGene HD transfection reagent (Promega) was used according to protocol. In brief, $5 \cdot 10^{4}$ cells per well were transferred into chamber slides (Nunc) by trypsinization and allowed to reattach over night before transfection. Cells were usually tested for fluorescence 24 hrs after transfection.

7.3.4. LUCIFERASE/RENILLA MEASUREMENT

To test the functionality of the TNF-R1-tdEos fusion, the Dual-Luciferase Reporter Assay System (Promega) was used to monitor gene expression of transfected cells. Here, two luciferases - from the firefly (*Photinus pyralis*) and from the sea pansy (*Renilla reniformis*) - act as reporter genes [257]. As *renilla* expression is constant, it provides a baseline fluorescence of transfected cells. The firefly luciferase is coupled to a κbLuc reporter, which is only expressed in the presence of activated NF-κB. Thus, upon TNFα induction, the activation rates of NF-κB could be monitored by an increase luminescence and compared to the baseline expression level of renilla-luc. As both luciferases need different substrates and can be selectively quenched, a good distinction could be achieved in a Luminometer (Titertek-Berthold).

7.4. MICROSCOPY

7.4.1. *d*STORM SWITCHING BUFFER

To successfully cycle dyes between a light and a dark state, special buffer systems are needed for *d*STORM, the photoswitching buffer for organic dyes contains glucose oxidase, catalase and β-mercaptoethylamine hydrochloride (MEA-HCl). For long-term storage tris(2-carboxyethyl)-phosphine hydrochloride (TCEP) and glycerine are added and aliquots of stock solutions were prepared. For long-term storage, stock solutions were stored at -20°C.

1 mol/l MEA stock solution	
MEA-HCl	1.136g
dH_2O	10ml

Glucose stock solution	
Glucose	5 g
Glycerine	5 ml
dH_2O	45 ml

Enzyme stock solution	
Catalase	100 µl
TCEP (1mol/l)	200 µl
Glycerine	25 ml
KCl (1M)	1.25 ml
Tris-HCl pH 7.5 (1mol/l)	1 ml
Glucose oxidase	50 mg
ddH_2O	22.5ml

For imaging, 50 µl of enzyme stock solution, 400 µl of glucose stock solution and 100 µl MEA stock solution are added to the imaging chamber. The remaining volume (~400 µl) is filled with PBS and the chamber sealed with a coverslip, avoiding air bubbles. As different dyes show different switching behaviors, MEA concentrations and pH must be adjusted to best achieve the performance for each dye (e.g. for Alexa647 pH = 7.5).

7.4.2. CELL PREPARATION

To obtain a uniform appearance and reaction to stimuli or drugs, HeLa cells were cold shocked before imaging, which is thought to reset TNF-R1 back to the cell surface [84]. For this, cells were supplied with fresh medium and incubated at 4°C for 30 min (FIG. 37). Cells were then washed twice with cold medium. For dSTORM experiments, samples were fixed using 4% PFA for 10 min at RT. For live-cell imaging (i.e. sptPALM), cells were supplied with serum- and phenol-free full RPMI to reduce medium influences during measurements. For monitoring signal induction or the response to lipid disruption, 10 ng/ml soluble TNFα (Gibco), 10 mM methyl-β-cyclodextrin (MCD; Sigma) or 50 µM Nystatin (Sigma) were added during the cold reset.

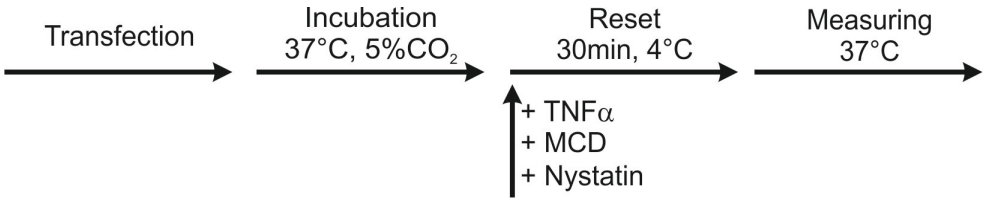

Fig. 37: Setup of an sptPALM experimental setup to image living cells.

7.4.3. CONFOCAL LASER SCANNING MICROSCOPY - QDTI

A commercially available confocal laser scanning microscope (LSM 710; Zeiss) supplied with an argon ion laser (458nm, 488nm, 541nm) and two helium neon lasers (542 nm, 633 nm) together with a 63x oil immersion objective (Plan-Apo, NA 1.40; Zeiss) was used for confocal laser scanning microscopy. The provided software platform was used for image recording and preliminary analysis (Zen; Zeiss). Detection ranges, dichroics, pinhole sizes and detection ranges were adjusted individually for each fluorescent dye or protein accordingly. For QDTI, 458 nm or 488 nm were used as excitation wavelengths and emission detection ranges were set to 580-620 nm (TX) and 650-720 nm (MX, BX), which were operated at the same gain and in parallel. Both detection pinholes were typically adjusted to 1 AU (40-65 µm). To obtain good TX yield, 10x higher laser intensities than for MX and BX were used. Spectral separation was achieved using a 633 nm dichroic beamsplitter. Pixel sizes were adjusted to 60-100 nm (lateral) and 250-350 nm in axial direction. Image analysis was performed

using the 3D Objects counter plugin for ImageJ (NIH), which was first tested on individual QDs immobilized on a glass surface to obtain suitable parameters for optimized images.

7.4.4. *d*STORM AND PALM

The custom-build setup for *d*STORM and sptPALM/PALM imaging consisted of an inverted microscope (Olympus) mounted on a shock-absorbing table (Newport). A multi-line argon-krypton laser (Innova70C; Coherent) provided relevant laser lines for irradiation, which were selected using an acousto-optical tunable filter (AOTF; AAOptics). Clean-up filters in the laser pathway further blocked unspecific wavelengths. UV light for photoactivation in PALM (405 nm) was provided by an UV laser diode (Cube 405-100C; Coherent). Lasers were focused onto the backfocal plane of an 60x oil immersion objective adjustable for RT and 37°C imaging (PlanApo, NA 1.45; Olympus), TIRF or widefield mode could be adjusted by a movable mirror. Before detection, emission light from the sample was spectrally separated from the excitation light using relevant dichroic mirrors, bandpass and longpass filters to further select the signal:

- For *d*STORM using Alexa647 measurements used an 488/568/647 cleanup filter (Chroma) and a 647 longpass filter (Semrock) in concert with a 700/75 bandpass (Chroma) filter to reduce background fluorescence. For live-cell dSTORM using ATTO655 experiments used an 700/75 bandpass filter (Semrock) and a 655 longpass filter (AHF).
- For sptPALM, the 488/568/647 cleanup filter (Chroma), a 610/75 bandpass (Chroma), 633 shortpass (Semrock) and a 586 longpass filter (Semrock) was used. Typical irradiation intensities for live cell imaging were in the range of 1-5 mW (488 nm), 10-20 mW (568 nm) and < 100 µW (405 nm) to minimize possible photodamage to the cell.

For detection of the fluorescent signal, an electron multiplying charge-coupled device (EMCCD) camera (Andor Ixon DU897; Andor) was mounted behind a telescope system improving pixel size (70-160 nm). Camera settings were optimized for each fluorophore and experiment, with frame rates of 20-50 frames per second, adjusted to the corresponding switching behavior of the observed fluorophore. Movies of 4000-9000 frames were recorded. The obtained movies consisting of many single-molecule emissions were analyzed using the open source rapidSTORM software [165]. Here, each image is evaluated for fluorophore emissions, which are fitted by a Gaussian function and its position recorded and analyzed for its quality before image reconstruction. Analyzing a sptPALM was done using a custom-written program for Metamorph (Molecular Devices), that localized spots and calculated trajectories using wavelet segmentation and simulated annealing algorithms [173, 174, 258].

8. ABBREVIATIONS

°C	Degree Celsius
µl	Microlitre
µM	Micromolar
µm	Micrometer
AOTF	Acousto-optic tunable filter
BSA	Bovine serum albumin
CBC	Coordinate-based co-localization
CCP	Clathrin coated pit
cDNA	Complementary DNA
CLSM	Confocal laser scanning microscopy/microscope
DD	Death domain
DISC	Death inducing signaling complex
DMSO	Dimethylsulfoxide
DNA	Deoxyribonucleic acid
***d*STORM**	*Direct* stochastic optical reconstruction microscopy
DTT	Dithiothtreitol
e.g.	Example given
et al.	Et alii
FADD	Fas-associated via death domain
FBS	Fetal bovine serum
FCS	Fluorescence correlation spectroscopy
FP	Fluorescent protein
FRAP	Fluorescence recovery after photobleaching
FRET	Fluorescence resonance energy transfer
GFP	Green fluorescent protein
GSH	Glutathione
HILO	Highly inclined and laminated optical sheet
hr/hrs	Hour/hours
Hrs	Hours
i.e.	id est – that is
IgG	Immunglobuline G
IKK	I kappa B kinase complex

LPS	Lipopolysaccharide
LTα	Lymphotoxin α
MCD	Methyl-β-cyclodextrin
MEA	Mercaptoethylamine
min	Minute
NF-κB	Nuclear factor kappa B
nm	Nanometer
OD	Optical density
PALM	Photoactivated localization microscopy
PBS	Phosphate buffered saline
PFA	Paraformaldehyde
PLAD	Pre-ligand assembly domain
PSF	Point spread function
QD	Quantum dot
QDTI	Quantum dot triexciton imaging
RIP1	Receptor interacting protein 1
RNA	Ribonucleic acid
RT	Room temperature (21°C)
SOFI	Super-resolution optical fluctuation imaging
SPT	Single particle tracking
sptPALM	Single particle tracking photoactivated localization microscopy
STED	Stimulated emission depletion
STORM	Stochastic optical reconstruction microscopy
TIRFM	Total internal reflection fluorescence microscopy
TNF	Tumor necrosis factor
TNF-R1	Tumor necrosis factor receptor 1
TNF-R2	Tumor necrosis factor receptor 2
TNFSF	Tumor necrosis factor superfamily
TRADD	TNF receptor associated Death domain
TRAF2	TNF receptor associated factor

9. LITERATURE

1. Smit, P. and J. Heniger, *Antoni van Leeuwenhoek (1632-1723) and the discovery of bacteria.* Antonie van Leeuwenhoek, 1975. **41**(3): p. 219-28.
2. Hooke, R., *Micrographia: or some Physiological Descriptions of Minute Bodies made by Magnifying Glasses with Observations and Inquiries thereupon* Jo. Martyn and Ja. Allestry, Printers to the Royal Society, London, 1665.
3. Hirschfeld, T., *Optical microscopic observation of single small molecules.* Applied optics, 1976. **15**(12): p. 2965-6.
4. Haitinger, M., *Fluoreszenz-Mikroskopie: Ihre Anwendung in der Histologie und Chemie.* Akad. Verlagsgesellschaft Leipzig, 1938.
5. Coley, W.B., *The treatment of malignant tumors by repeated inoculations of erysipelas. With a report of ten original cases. 1893.* Clinical orthopaedics and related research, 1991(262): p. 3-11.
6. Carswell, E.A., et al., *An endotoxin-induced serum factor that causes necrosis of tumors.* Proceedings of the National Academy of Sciences of the United States of America, 1975. **72**(9): p. 3666-70.
7. Oliff, A., et al., *Tumors secreting human TNF/cachectin induce cachexia in mice.* Cell, 1987. **50**(4): p. 555-63.
8. Tracey, K.J., et al., *Anti-cachectin/TNF monoclonal antibodies prevent septic shock during lethal bacteraemia.* Nature, 1987. **330**(6149): p. 662-4.
9. Sugarman, B.J., et al., *Recombinant human tumor necrosis factor-alpha: effects on proliferation of normal and transformed cells in vitro.* Science, 1985. **230**(4728): p. 943-5.
10. Kolb, W.P. and G.A. Granger, *Lymphocyte in vitro cytotoxicity: characterization of human lymphotoxin.* Proceedings of the National Academy of Sciences of the United States of America, 1968. **61**(4): p. 1250-5.
11. Peter, H.H., R.F. Eife, and J.R. Kalden, *Spontaneous cytotoxicity (SCMC) of normal human lymphocytes against a human melanoma cell line: a phenomenon due to a lymphotoxin-like mediator.* Journal of immunology, 1976. **116**(2): p. 342-8.
12. Aggarwal, B.B., B. Moffat, and R.N. Harkins, *Human lymphotoxin. Production by a lymphoblastoid cell line, purification, and initial characterization.* The Journal of biological chemistry, 1984. **259**(1): p. 686-91.
13. Aggarwal, B.B., et al., *Human tumor necrosis factor. Production, purification, and characterization.* The Journal of biological chemistry, 1985. **260**(4): p. 2345-54.
14. Aggarwal, B.B., T.E. Eessalu, and P.E. Hass, *Characterization of receptors for human tumour necrosis factor and their regulation by gamma-interferon.* Nature, 1985. **318**(6047): p. 665-7.
15. Gray, P.W., et al., *Cloning and expression of cDNA for human lymphotoxin, a lymphokine with tumour necrosis activity.* Nature, 1984. **312**(5996): p. 721-4.
16. Pennica, D., et al., *Human tumour necrosis factor: precursor structure, expression and homology to lymphotoxin.* Nature, 1984. **312**(5996): p. 724-9.
17. Nedwin, G.E., et al., *Human lymphotoxin and tumor necrosis factor genes: structure, homology and chromosomal localization.* Nucleic acids research, 1985. **13**(17): p. 6361-73.
18. Kriegler, M., et al., *A novel form of TNF/cachectin is a cell surface cytotoxic transmembrane protein: ramifications for the complex physiology of TNF.* Cell, 1988. **53**(1): p. 45-53.
19. Black, R.A., et al., *A metalloproteinase disintegrin that releases tumour-necrosis factor-alpha from cells.* Nature, 1997. **385**(6618): p. 729-33.
20. Anklesaria, P., et al., *Cell-cell adhesion mediated by binding of membrane-anchored transforming growth factor alpha to epidermal growth factor receptors promotes cell proliferation.* Proceedings of the National Academy of Sciences of the United States of America, 1990. **87**(9): p. 3289-93.

21. Perez, C., et al., *A nonsecretable cell surface mutant of tumor necrosis factor (TNF) kills by cell-to-cell contact.* Cell, 1990. **63**(2): p. 251-8.
22. Eck, M.J. and S.R. Sprang, *The structure of tumor necrosis factor-alpha at 2.6 A resolution. Implications for receptor binding.* The Journal of biological chemistry, 1989. **264**(29): p. 17595-605.
23. Smith, R.A. and C. Baglioni, *The active form of tumor necrosis factor is a trimer.* The Journal of biological chemistry, 1987. **262**(15): p. 6951-4.
24. Brenner, D.A., et al., *Prolonged activation of jun and collagenase genes by tumour necrosis factor-alpha.* Nature, 1989. **337**(6208): p. 661-3.
25. Hajjar, K.A., et al., *Tumor necrosis factor-mediated release of platelet-derived growth factor from cultured endothelial cells.* The Journal of experimental medicine, 1987. **166**(1): p. 235-45.
26. Jacobsen, H., et al., *Beta interferon subtype 1 induction by tumor necrosis factor.* Molecular and cellular biology, 1989. **9**(7): p. 3037-42.
27. Mukaida, N., Y. Mahe, and K. Matsushima, *Cooperative interaction of nuclear factor-kappa B- and cis-regulatory enhancer binding protein-like factor binding elements in activating the interleukin-8 gene by pro-inflammatory cytokines.* The Journal of biological chemistry, 1990. **265**(34): p. 21128-33.
28. Wride, M.A. and E.J. Sanders, *Potential roles for tumour necrosis factor alpha during embryonic development.* Anatomy and embryology, 1995. **191**(1): p. 1-10.
29. Krueger, J.M., et al., *Sleep. A physiologic role for IL-1 beta and TNF-alpha.* Annals of the New York Academy of Sciences, 1998. **856**: p. 148-59.
30. Aggarwal, B.B., *Structure of tumor necrosis factor and its receptor.* Biotherapy, 1991. **3**(2): p. 113-20.
31. Oh, C.J., K.M. Das, and A.B. Gottlieb, *Treatment with anti-tumor necrosis factor alpha (TNF-alpha) monoclonal antibody dramatically decreases the clinical activity of psoriasis lesions.* Journal of the American Academy of Dermatology, 2000. **42**(5 Pt 1): p. 829-30.
32. Hehlgans, T. and K. Pfeffer, *The intriguing biology of the tumour necrosis factor/tumour necrosis factor receptor superfamily: players, rules and the games.* Immunology, 2005. **115**(1): p. 1-20.
33. Loetscher, H., et al., *Molecular cloning and expression of the human 55 kd tumor necrosis factor receptor.* Cell, 1990. **61**(2): p. 351-9.
34. Armitage, R.J., *Tumor necrosis factor receptor superfamily members and their ligands.* Current opinion in immunology, 1994. **6**(3): p. 407-13.
35. Banner, D.W., et al., *Crystal structure of the soluble human 55 kd TNF receptor-human TNF beta complex: implications for TNF receptor activation.* Cell, 1993. **73**(3): p. 431-45.
36. Branschadel, M., et al., *Dual function of cysteine rich domain (CRD) 1 of TNF receptor type 1: conformational stabilization of CRD2 and control of receptor responsiveness.* Cellular signalling, 2010. **22**(3): p. 404-14.
37. Chan, F.K., et al., *A domain in TNF receptors that mediates ligand-independent receptor assembly and signaling.* Science, 2000. **288**(5475): p. 2351-4.
38. Islam, A., et al., *Extracellular TNFR1 release requires the calcium-dependent formation of a nucleobindin 2-ARTS-1 complex.* The Journal of biological chemistry, 2006. **281**(10): p. 6860-73.
39. Hawari, F.I., et al., *Release of full-length 55-kDa TNF receptor 1 in exosome-like vesicles: a mechanism for generation of soluble cytokine receptors.* Proceedings of the National Academy of Sciences of the United States of America, 2004. **101**(5): p. 1297-302.
40. Grell, M., et al., *Induction of cell death by tumour necrosis factor (TNF) receptor 2, CD40 and CD30: a role for TNF-R1 activation by endogenous membrane-anchored TNF.* The EMBO journal, 1999. **18**(11): p. 3034-43.
41. Vandenabeele, P., et al., *Two tumour necrosis factor receptors: structure and function.* Trends in cell biology, 1995. **5**(10): p. 392-9.

42. Lin, W.W. and S.L. Hsieh, *Decoy receptor 3: a pleiotropic immunomodulator and biomarker for inflammatory diseases, autoimmune diseases and cancer.* Biochemical pharmacology, 2011. **81**(7): p. 838-47.
43. Jiang, Y., et al., *Prevention of constitutive TNF receptor 1 signaling by silencer of death domains.* Science, 1999. **283**(5401): p. 543-6.
44. Ryffel, B. and M.J. Mihatsch, *TNF receptor distribution in human tissues.* International review of experimental pathology, 1993. **34 Pt B**: p. 149-56.
45. Grell, M., et al., *The transmembrane form of tumor necrosis factor is the prime activating ligand of the 80 kDa tumor necrosis factor receptor.* Cell, 1995. **83**(5): p. 793-802.
46. Krippner-Heidenreich, A., et al., *Control of receptor-induced signaling complex formation by the kinetics of ligand/receptor interaction.* The Journal of biological chemistry, 2002. **277**(46): p. 44155-63.
47. Dembic, Z., et al., *Two human TNF receptors have similar extracellular, but distinct intracellular, domain sequences.* Cytokine, 1990. **2**(4): p. 231-7.
48. Mikenberg, I., et al., *TNF-alpha mediated transport of NF-kappaB to the nucleus is independent of the cytoskeleton-based transport system in non-neuronal cells.* European journal of cell biology, 2006. **85**(6): p. 529-36.
49. Nelson, G., et al., *Multi-parameter analysis of the kinetics of NF-kappaB signalling and transcription in single living cells.* Journal of cell science, 2002. **115**(Pt 6): p. 1137-48.
50. Ashkenazi, A. and V.M. Dixit, *Death receptors: signaling and modulation.* Science, 1998. **281**(5381): p. 1305-8.
51. Van Antwerp, D.J., et al., *Suppression of TNF-alpha-induced apoptosis by NF-kappaB.* Science, 1996. **274**(5288): p. 787-9.
52. Malinin, N.L., et al., *MAP3K-related kinase involved in NF-kappaB induction by TNF, CD95 and IL-1.* Nature, 1997. **385**(6616): p. 540-4.
53. Cheng, G. and D. Baltimore, *TANK, a co-inducer with TRAF2 of TNF- and CD 40L-mediated NF-kappaB activation.* Genes & development, 1996. **10**(8): p. 963-73.
54. Rothe, M., et al., *TRAF2-mediated activation of NF-kappa B by TNF receptor 2 and CD40.* Science, 1995. **269**(5229): p. 1424-7.
55. Grech, A.P., et al., *Tumor necrosis factor receptor 2 (TNFR2) signaling is negatively regulated by a novel, carboxyl-terminal TNFR-associated factor 2 (TRAF2)-binding site.* The Journal of biological chemistry, 2005. **280**(36): p. 31572-81.
56. Fotin-Mleczek, M., et al., *Apoptotic crosstalk of TNF receptors: TNF-R2-induces depletion of TRAF2 and IAP proteins and accelerates TNF-R1-dependent activation of caspase-8.* Journal of cell science, 2002. **115**(Pt 13): p. 2757-70.
57. Weiss, T., et al., *Enhancement of TNF receptor p60-mediated cytotoxicity by TNF receptor p80: requirement of the TNF receptor-associated factor-2 binding site.* Journal of immunology, 1997. **158**(5): p. 2398-404.
58. Danielli, J.F. and H. Davson, *A contribution to the theory of permeability of thin films.* Journal of Cellular and Comparative Physiology, 1935. **5**(4): p. 495-508.
59. Bretscher, M.S., *Membrane structure: some general principles.* Science, 1973. **181**(4100): p. 622-9.
60. Capaldi, R.A. and G. Vanderkooi, *The low polarity of many membrane proteins.* Proceedings of the National Academy of Sciences of the United States of America, 1972. **69**(4): p. 930-2.
61. Frye, L.D. and M. Edidin, *The rapid intermixing of cell surface antigens after formation of mouse-human heterokaryons.* Journal of cell science, 1970. **7**(2): p. 319-35.
62. Singer, S.J. and G.L. Nicolson, *The fluid mosaic model of the structure of cell membranes.* Science, 1972. **175**(4023): p. 720-31.
63. Ziparo, E., A. Lemay, and V.T. Marchesi, *The distribution of spectrin along the membranes of normal and echinocytic human erythrocytes.* Journal of cell science, 1978. **34**: p. 91-101.

64. Sato, N., et al., *A gene family consisting of ezrin, radixin and moesin. Its specific localization at actin filament/plasma membrane association sites.* Journal of cell science, 1992. **103 (Pt 1)**: p. 131-43.
65. Brown, R.E., *Sphingolipid organization in biomembranes: what physical studies of model membranes reveal.* Journal of cell science, 1998. **111 (Pt 1)**: p. 1-9.
66. Simons, K. and E. Ikonen, *Functional rafts in cell membranes.* Nature, 1997. **387**(6633): p. 569-72.
67. Karnovsky, M.J., et al., *The concept of lipid domains in membranes.* The Journal of cell biology, 1982. **94**(1): p. 1-6.
68. Simons, K. and D. Toomre, *Lipid rafts and signal transduction.* Nature reviews. Molecular cell biology, 2000. **1**(1): p. 31-9.
69. van Meer, G. and K.N. Burger, *Sphingolipid trafficking--sorted out?* Trends in cell biology, 1992. **2**(11): p. 332-7.
70. Jacobson, K., A. Ishihara, and R. Inman, *Lateral diffusion of proteins in membranes.* Annual review of physiology, 1987. **49**: p. 163-75.
71. Yamada, E., *The fine structure of the gall bladder epithelium of the mouse.* The Journal of biophysical and biochemical cytology, 1955. **1**(5): p. 445-58.
72. Rothberg, K.G., et al., *Caveolin, a protein component of caveolae membrane coats.* Cell, 1992. **68**(4): p. 673-82.
73. Simons, K. and R. Ehehalt, *Cholesterol, lipid rafts, and disease.* The Journal of clinical investigation, 2002. **110**(5): p. 597-603.
74. Rothberg, K.G., et al., *Cholesterol controls the clustering of the glycophospholipid-anchored membrane receptor for 5-methyltetrahydrofolate.* The Journal of cell biology, 1990. **111**(6 Pt 2): p. 2931-8.
75. Rodal, S.K., et al., *Extraction of cholesterol with methyl-beta-cyclodextrin perturbs formation of clathrin-coated endocytic vesicles.* Molecular biology of the cell, 1999. **10**(4): p. 961-74.
76. Friedrichson, T. and T.V. Kurzchalia, *Microdomains of GPI-anchored proteins in living cells revealed by crosslinking.* Nature, 1998. **394**(6695): p. 802-5.
77. Brown, D.A. and J.K. Rose, *Sorting of GPI-anchored proteins to glycolipid-enriched membrane subdomains during transport to the apical cell surface.* Cell, 1992. **68**(3): p. 533-44.
78. Harder, T., et al., *Lipid domain structure of the plasma membrane revealed by patching of membrane components.* The Journal of cell biology, 1998. **141**(4): p. 929-42.
79. Wilson, B.S., J.R. Pfeiffer, and J.M. Oliver, *Observing FcepsilonRI signaling from the inside of the mast cell membrane.* The Journal of cell biology, 2000. **149**(5): p. 1131-42.
80. Elson, E.L., et al., *Measurement of lateral transport on cell surfaces.* Progress in clinical and biological research, 1976. **9**: p. 137-47.
81. Jacobson, K., E. Wu, and G. Poste, *Measurement of the translational mobility of concanavalin A in glycerol-saline solutions and on the cell surface by fluorescence recovery after photobleaching.* Biochimica et biophysica acta, 1976. **433**(1): p. 215-22.
82. Pralle, A., et al., *Sphingolipid-cholesterol rafts diffuse as small entities in the plasma membrane of mammalian cells.* The Journal of cell biology, 2000. **148**(5): p. 997-1008.
83. Varma, R. and S. Mayor, *GPI-anchored proteins are organized in submicron domains at the cell surface.* Nature, 1998. **394**(6695): p. 798-801.
84. Schneider-Brachert, W., et al., *Compartmentalization of TNF receptor 1 signaling: internalized TNF receptosomes as death signaling vesicles.* Immunity, 2004. **21**(3): p. 415-28.
85. Varadhachary, A.S., et al., *Phosphatidylinositol 3'-kinase blocks CD95 aggregation and caspase-8 cleavage at the death-inducing signaling complex by modulating lateral diffusion of CD95.* Journal of immunology, 2001. **166**(11): p. 6564-9.
86. Pullen, S.S., et al., *High-affinity interactions of tumor necrosis factor receptor-associated factors (TRAFs) and CD40 require TRAF trimerization and CD40 multimerization.* Biochemistry, 1999. **38**(31): p. 10168-77.

87. Naismith, J.H., et al., *Crystallographic evidence for dimerization of unliganded tumor necrosis factor receptor.* The Journal of biological chemistry, 1995. **270**(22): p. 13303-7.
88. Sukits, S.F., et al., *Solution structure of the tumor necrosis factor receptor-1 death domain.* Journal of molecular biology, 2001. **310**(4): p. 895-906.
89. Bazzoni, F. and B. Beutler, *The tumor necrosis factor ligand and receptor families.* The New England journal of medicine, 1996. **334**(26): p. 1717-25.
90. Boschert, V., et al., *Single chain TNF derivatives with individually mutated receptor binding sites reveal differential stoichiometry of ligand receptor complex formation for TNFR1 and TNFR2.* Cellular signalling, 2010. **22**(7): p. 1088-96.
91. Sandu, C., et al., *FADD self-association is required for stable interaction with an activated death receptor.* Cell death and differentiation, 2006. **13**(12): p. 2052-61.
92. Ranzinger, J., et al., *Nanoscale arrangement of apoptotic ligands reveals a demand for a minimal lateral distance for efficient death receptor activation.* Nano letters, 2009. **9**(12): p. 4240-5.
93. Schutze, S., V. Tchikov, and W. Schneider-Brachert, *Regulation of TNFR1 and CD95 signalling by receptor compartmentalization.* Nature reviews. Molecular cell biology, 2008. **9**(8): p. 655-62.
94. Legler, D.F., et al., *Recruitment of TNF receptor 1 to lipid rafts is essential for TNFalpha-mediated NF-kappaB activation.* Immunity, 2003. **18**(5): p. 655-64.
95. D'Alessio, A., et al., *Caveolae participate in tumor necrosis factor receptor 1 signaling and internalization in a human endothelial cell line.* The American journal of pathology, 2005. **166**(4): p. 1273-82.
96. Gerken, M., et al., *Fluorescence correlation spectroscopy reveals topological segregation of the two tumor necrosis factor membrane receptors.* Biochimica et biophysica acta, 2010. **1798**(6): p. 1081-9.
97. Herschel, J.F.W., *On a Case of Superficial Colour Presented by a Homogeneous Liquid Internally Colourless.* Philosophical Transactions of the Royal Society of London 1845. **135 (1845)**: p. 143-145.
98. Stokes, G.G., *On the Change of Refrangibility of Light.* Philosophical Transactions of the Royal Society of London, 1852. **142 (1852)**: p. 463-562.
99. Abbe, E., *Beiträge zur Theorie des Mikroskops und der mikroskopischen Wahrnehmung.* Archiv für Mikroskopische Anatomie, 1873. **9**: p. 411-468.
100. Rayleigh, L., *On the Theory of Optical Images, with special reference to the Microscope.* Journal of the Royal Microscopical Society, 1903. **23**: p. 474–482.
101. Shannon, C.E., *Ccommunication in the presence of noise.* Proc. IRE, 1949. **37**(10): p. 10-21.
102. Jablonski, A., *Efficiency of Anti-Stokes Fluorescence in Dyes.* Nature, 1933. **131**: p. 839-840.
103. Axelrod, D., *Cell-substrate contacts illuminated by total internal reflection fluorescence.* The Journal of cell biology, 1981. **89**(1): p. 141-5.
104. Tokunaga, M., N. Imamoto, and K. Sakata-Sogawa, *Highly inclined thin illumination enables clear single-molecule imaging in cells.* Nature methods, 2008. **5**(2): p. 159-61.
105. Minsky, M., *Microscopy apparatus, Patent no. 3013467.* US Patent 1957.
106. Sandison, D.R., et al., *Quantitative comparison of background rejection, signal-to-noise ratio, and resolution in confocal and full-field laser scanning microscopes.* Applied optics, 1995. **34**(19): p. 3576-88.
107. Wilson, T., *Optical sectioning in fluorescence microscopy.* Journal of microscopy, 2011. **242**(2): p. 111-6.
108. Klar, T.A., et al., *Fluorescence microscopy with diffraction resolution barrier broken by stimulated emission.* Proceedings of the National Academy of Sciences of the United States of America, 2000. **97**(15): p. 8206-10.
109. Rust, M.J., M. Bates, and X. Zhuang, *Sub-diffraction-limit imaging by stochastic optical reconstruction microscopy (STORM).* Nature methods, 2006. **3**(10): p. 793-5.

110. Heilemann, M., et al., *Carbocyanine dyes as efficient reversible single-molecule optical switch.* Journal of the American Chemical Society, 2005. **127**(11): p. 3801-6.
111. Betzig, E., et al., *Imaging intracellular fluorescent proteins at nanometer resolution.* Science, 2006. **313**(5793): p. 1642-5.
112. Thompson, R.E., D.R. Larson, and W.W. Webb, *Precise nanometer localization analysis for individual fluorescent probes.* Biophysical journal, 2002. **82**(5): p. 2775-83.
113. van de Linde, S., et al., *The effect of photoswitching kinetics and labeling densities on super-resolution fluorescence imaging.* Journal of biotechnology, 2010. **149**(4): p. 260-6.
114. Heilemann, M., et al., *Subdiffraction-resolution fluorescence imaging with conventional fluorescent probes.* Angewandte Chemie, 2008. **47**(33): p. 6172-6.
115. Wolter, S., et al., *Measuring localization performance of super-resolution algorithms on very active samples.* Optics express, 2011. **19**(8): p. 7020-33.
116. Jablonski, A., *Über den mechanismus der Photolumineszenz von Farbstoffphosphoren.* Zeitschrift für Physik A Hadrons and Nuclei, 1935. **94**(1): p. 38-46.
117. van de Linde, S., et al., *Photoinduced formation of reversible dye radicals and their impact on super-resolution imaging.* Photochemical & photobiological sciences : Official journal of the European Photochemistry Association and the European Society for Photobiology, 2011. **10**(4): p. 499-506.
118. Heilemann, M., et al., *Super-resolution imaging with small organic fluorophores.* Angewandte Chemie, 2009. **48**(37): p. 6903-8.
119. Smith, A.M., X. Gao, and S. Nie, *Quantum dot nanocrystals for in vivo molecular and cellular imaging.* Photochemistry and photobiology, 2004. **80**(3): p. 377-85.
120. Alivisatos, A.P., *Perspectives on the physical chemistry of semiconductor nanocrystals.* Journal of Physical Chemistry, 1996. **100**(31): p. 13226-13239.
121. Nirmal, M., et al., *Fluorescence intermittency in single cadmium selenide nanocrystals.* Nature, 1996. **383**(6603): p. 802-804.
122. Fisher, B., et al., *Multiexciton fluorescence from semiconductor nanocrystals.* Chemical Physics, 2005. **318**(1-2): p. 71-81.
123. Sheppard, C.J.R., *Image formation in three-photon fluorescence microscopy.* . Bioimaging, , 1996. **4**: p. 124–128.
124. Denk, W., J.H. Strickler, and W.W. Webb, *Two-photon laser scanning fluorescence microscopy.* Science, 1990. **248**(4951): p. 73-6.
125. Franceschetti, A. and M.C. Troparevsky, *Radiative recombination of triexcitons in CdSe colloidal quantum dots.* Journal of Physical Chemistry C, 2007. **111**(17): p. 6154-6157.
126. Zipfel, W.R., R.M. Williams, and W.W. Webb, *Nonlinear magic: multiphoton microscopy in the biosciences.* Nature biotechnology, 2003. **21**(11): p. 1369-77.
127. Ormo, M., et al., *Crystal structure of the Aequorea victoria green fluorescent protein.* Science, 1996. **273**(5280): p. 1392-5.
128. Prasher, D.C., et al., *Primary structure of the Aequorea victoria green-fluorescent protein.* Gene, 1992. **111**(2): p. 229-33.
129. Tsien, R.Y., *The green fluorescent protein.* Annual review of biochemistry, 1998. **67**: p. 509-44.
130. Shaner, N.C., P.A. Steinbach, and R.Y. Tsien, *A guide to choosing fluorescent proteins.* Nature methods, 2005. **2**(12): p. 905-9.
131. Wiedenmann, J., et al., *EosFP, a fluorescent marker protein with UV-inducible green-to-red fluorescence conversion.* Proceedings of the National Academy of Sciences of the United States of America, 2004. **101**(45): p. 15905-10.
132. Patterson, G.H. and J. Lippincott-Schwartz, *A photoactivatable GFP for selective photolabeling of proteins and cells.* Science, 2002. **297**(5588): p. 1873-7.
133. Lukyanov, K.A., et al., *Innovation: Photoactivatable fluorescent proteins.* Nature reviews. Molecular cell biology, 2005. **6**(11): p. 885-91.

134. Adam, V., et al., *Structural characterization of IrisFP, an optical highlighter undergoing multiple photo-induced transformations.* Proceedings of the National Academy of Sciences of the United States of America, 2008. **105**(47): p. 18343-8.
135. Nienhaus, G.U., et al., *Photoconvertible fluorescent protein EosFP: biophysical properties and cell biology applications.* Photochemistry and photobiology, 2006. **82**(2): p. 351-8.
136. Nienhaus, K., et al., *Structural basis for photo-induced protein cleavage and green-to-red conversion of fluorescent protein EosFP.* Proceedings of the National Academy of Sciences of the United States of America, 2005. **102**(26): p. 9156-9.
137. Brown, R., *A Brief account of microscopical observations made in the months of June, July and August 1827 on the particles contained in the pollen of plants.* Ann. Phys. Chem. , 1828. **14 (1828)** p. 294.
138. Saxton, M.J. and K. Jacobson, *Single-particle tracking: applications to membrane dynamics.* Annual review of biophysics and biomolecular structure, 1997. **26**: p. 373-99.
139. Arcizet, D., et al., *Temporal analysis of active and passive transport in living cells.* Physical review letters, 2008. **101**(24): p. 248103.
140. Axelrod, D., et al., *Mobility measurement by analysis of fluorescence photobleaching recovery kinetics.* Biophysical journal, 1976. **16**(9): p. 1055-69.
141. Yguerabide, J., J.A. Schmidt, and E.E. Yguerabide, *Lateral mobility in membranes as detected by fluorescence recovery after photobleaching.* Biophysical journal, 1982. **40**(1): p. 69-75.
142. Magde, D., E. Elson, and W.W. Webb, *Thermodynamic Fluctuations in a Reacting System—Measurement by Fluorescence Correlation Spectroscopy.* Phys. Rev. Lett., 1972(29): p. 705–708
143. Schwille, P., J. Korlach, and W.W. Webb, *Fluorescence correlation spectroscopy with single-molecule sensitivity on cell and model membranes.* Cytometry, 1999. **36**(3): p. 176-82.
144. Magde, D., E.L. Elson, and W.W. Webb, *Fluorescence correlation spectroscopy. II. An experimental realization.* Biopolymers, 1974. **13**(1): p. 29-61.
145. Bonnet, G., O. Krichevsky, and A. Libchaber, *Kinetics of conformational fluctuations in DNA hairpin-loops.* Proceedings of the National Academy of Sciences of the United States of America, 1998. **95**(15): p. 8602-6.
146. Torres, T. and M. Levitus, *Measuring conformational dynamics: a new FCS-FRET approach.* The journal of physical chemistry. B, 2007. **111**(25): p. 7392-400.
147. Schwille, P., F.J. Meyer-Almes, and R. Rigler, *Dual-color fluorescence cross-correlation spectroscopy for multicomponent diffusional analysis in solution.* Biophysical journal, 1997. **72**(4): p. 1878-86.
148. De Brabander, M., et al., *Probing microtubule-dependent intracellular motility with nanometre particle video ultramicroscopy (nanovid ultramicroscopy).* Cytobios, 1985. **43**(174S): p. 273-83.
149. Kucik, D.F., E.L. Elson, and M.P. Sheetz, *Cell migration does not produce membrane flow.* The Journal of cell biology, 1990. **111**(4): p. 1617-22.
150. Michalet, X., et al., *Quantum dots for live cells, in vivo imaging, and diagnostics.* Science, 2005. **307**(5709): p. 538-44.
151. Schutz, G.J., et al., *Properties of lipid microdomains in a muscle cell membrane visualized by single molecule microscopy.* The EMBO journal, 2000. **19**(5): p. 892-901.
152. Barak, L.S. and W.W. Webb, *Fluorescent low density lipoprotein for observation of dynamics of individual receptor complexes on cultured human fibroblasts.* The Journal of cell biology, 1981. **90**(3): p. 595-604.
153. de Bruin, K., et al., *Cellular dynamics of EGF receptor-targeted synthetic viruses.* Molecular therapy : the journal of the American Society of Gene Therapy, 2007. **15**(7): p. 1297-305.
154. Manley, S., et al., *High-density mapping of single-molecule trajectories with photoactivated localization microscopy.* Nature methods, 2008. **5**(2): p. 155-7.
155. Subach, F.V., et al., *Photoactivatable mCherry for high-resolution two-color fluorescence microscopy.* Nature methods, 2009. **6**(2): p. 153-9.

156. Gurskaya, N.G., et al., *Engineering of a monomeric green-to-red photoactivatable fluorescent protein induced by blue light.* Nature biotechnology, 2006. **24**(4): p. 461-5.
157. Sharonov, A. and R.M. Hochstrasser, *Wide-field subdiffraction imaging by accumulated binding of diffusing probes.* Proceedings of the National Academy of Sciences of the United States of America, 2006. **103**(50): p. 18911-6.
158. Giannone, G., et al., *Dynamic superresolution imaging of endogenous proteins on living cells at ultra-high density.* Biophysical journal, 2010. **99**(4): p. 1303-10.
159. Schoen, I., et al., *Binding-activated localization microscopy of DNA structures.* Nano letters, 2011. **11**(9): p. 4008-11.
160. Pitha, J., et al., *Drug solubilizers to aid pharmacologists: amorphous cyclodextrin derivatives.* Life sciences, 1988. **43**(6): p. 493-502.
161. Kwik, J., et al., *Membrane cholesterol, lateral mobility, and the phosphatidylinositol 4,5-bisphosphate-dependent organization of cell actin.* Proceedings of the National Academy of Sciences of the United States of America, 2003. **100**(24): p. 13964-9.
162. Ilangumaran, S. and D.C. Hoessli, *Effects of cholesterol depletion by cyclodextrin on the sphingolipid microdomains of the plasma membrane.* The Biochemical journal, 1998. **335 (Pt 2)**: p. 433-40.
163. Keppler, A., et al., *A general method for the covalent labeling of fusion proteins with small molecules in vivo.* Nature biotechnology, 2003. **21**(1): p. 86-9.
164. Miller, L.W., et al., *In vivo protein labeling with trimethoprim conjugates: a flexible chemical tag.* Nature methods, 2005. **2**(4): p. 255-7.
165. Wolter, S., et al., *Real-time computation of subdiffraction-resolution fluorescence images.* Journal of microscopy, 2010. **237**(1): p. 12-22.
166. Henriques, R., et al., *QuickPALM: 3D real-time photoactivation nanoscopy image processing in ImageJ.* Nature methods, 2010. **7**(5): p. 339-40.
167. Geerts, H., et al., *Nanovid tracking: a new automatic method for the study of mobility in living cells based on colloidal gold and video microscopy.* Biophysical journal, 1987. **52**(5): p. 775-82.
168. Schnapp, B.J., J. Gelles, and M.P. Sheetz, *Nanometer-scale measurements using video light microscopy.* Cell motility and the cytoskeleton, 1988. **10**(1-2): p. 47-53.
169. Kalaidzidis, Y., *Multiple objects tracking in fluorescence microscopy.* Journal of mathematical biology, 2009. **58**(1-2): p. 57-80.
170. Bonneau S , Dahan M , and C. LD, *Single Quantum Dot Tracking based on Perceptual Grouping using Minimal Paths in a Spatio-Temporal Volume.* IEEE Trans Image Process, 2005. **14**(1384–1395).
171. Fortmann, T.E., Bar-Shalom, Y., Scheffe, M., *Multi-target tracking using joint probabilistic data association.* 19th IEEE Conference on, 1980. **19**(807-812).
172. Reid, D., *An Algorithm for Tracking Multiple Targets.* IEEE Transactions Automatic Control, 1979. **24**(6): p. 843- 854.
173. Racine, V., et al., *Multiple-target tracking of 3D fluorescent objects based on simulated annealing* 2006 IEEE International Symposium on Biomedical Imaging (ISBI 2006), April 6–9, 2006, Arlington, VA, 2006.
174. Racine, V., et al., *Visualization and quantification of vesicle trafficking on a three-dimensional cytoskeleton network in living cells.* Journal of microscopy, 2007. **225**(Pt 3): p. 214-28.
175. Ram, S., et al., *Improved single particle localization accuracy with dual objective multifocal plane microscopy.* Optics express, 2009. **17**(8): p. 6881-98.
176. Huang, B., et al., *Three-dimensional super-resolution imaging by stochastic optical reconstruction microscopy.* Science, 2008. **319**(5864): p. 810-3.
177. Coons, A.H. and M.H. Kaplan, *Localization of antigen in tissue cells; improvements in a method for the detection of antigen by means of fluorescent antibody.* The Journal of experimental medicine, 1950. **91**(1): p. 1-13.

178. Gallagher, S.S., et al., *An in vivo covalent TMP-tag based on proximity-induced reactivity.* ACS chemical biology, 2009. **4**(7): p. 547-56.
179. Stohr, K., et al., *Quenched substrates for live-cell labeling of SNAP-tagged fusion proteins with improved fluorescent background.* Analytical chemistry, 2010. **82**(19): p. 8186-93.
180. Hennig, S., et al., *Quantum dot triexciton imaging with three-dimensional subdiffraction resolution.* Nano letters, 2009. **9**(6): p. 2466-70.
181. Chan, W.C.W. and S.M. Nie, *Quantum dot bioconjugates for ultrasensitive nonisotopic detection.* Science, 1998. **281**(5385): p. 2016-2018.
182. Bannai, H., et al., *Imaging the lateral diffusion of membrane molecules with quantum dots.* Nature protocols, 2006. **1**(6): p. 2628-34.
183. Bruchez, M., Jr., et al., *Semiconductor nanocrystals as fluorescent biological labels.* Science, 1998. **281**(5385): p. 2013-6.
184. Widera, D., et al., *Schwann Cells can be reprogrammed to multipotency by culture.* Stem cells and development, 2011.
185. Heidbreder, M., et al., *Subdiffraction fluorescence imaging of biomolecular structure and distributions with quantum dots.* Biochimica et biophysica acta, 2010. **1803**(10): p. 1224-9.
186. Cai, W., et al., *Peptide-labeled near-infrared quantum dots for imaging tumor vasculature in living subjects.* Nano letters, 2006. **6**(4): p. 669-76.
187. Dahan, M., et al., *Diffusion dynamics of glycine receptors revealed by single-quantum dot tracking.* Science, 2003. **302**(5644): p. 442-5.
188. Lidke, D.S., et al., *Quantum dot ligands provide new insights into erbB/HER receptor-mediated signal transduction.* Nature biotechnology, 2004. **22**(2): p. 198-203.
189. Shroff, H., et al., *Live-cell photoactivated localization microscopy of nanoscale adhesion dynamics.* Nature methods, 2008. **5**(5): p. 417-23.
190. Endesfelder, U., et al., *Subdiffraction-resolution fluorescence microscopy of myosin-actin motility.* Chemphyschem : a European journal of chemical physics and physical chemistry, 2010. **11**(4): p. 836-40.
191. van de Linde, S., et al., *Direct stochastic optical reconstruction microscopy with standard fluorescent probes.* Nature protocols, 2011. **6**(7): p. 991-1009.
192. Triller, A. and D. Choquet, *New concepts in synaptic biology derived from single-molecule imaging.* Neuron, 2008. **59**(3): p. 359-74.
193. Fujiwara, T., et al., *Phospholipids undergo hop diffusion in compartmentalized cell membrane.* The Journal of cell biology, 2002. **157**(6): p. 1071-81.
194. Dietrich, C., et al., *Relationship of lipid rafts to transient confinement zones detected by single particle tracking.* Biophysical journal, 2002. **82**(1 Pt 1): p. 274-84.
195. Sheets, E.D., et al., *Transient confinement of a glycosylphosphatidylinositol-anchored protein in the plasma membrane.* Biochemistry, 1997. **36**(41): p. 12449-58.
196. Kusumi, A. and Y. Sako, *Cell surface organization by the membrane skeleton.* Current opinion in cell biology, 1996. **8**(4): p. 566-74.
197. Alecio, M.R., et al., *Use of a fluorescent cholesterol derivative to measure lateral mobility of cholesterol in membranes.* Proceedings of the National Academy of Sciences of the United States of America, 1982. **79**(17): p. 5171-4.
198. Wu, E.S., K. Jacobson, and D. Papahadjopoulos, *Lateral diffusion in phospholipid multibilayers measured by fluorescence recovery after photobleaching.* Biochemistry, 1977. **16**(17): p. 3936-41.
199. Axelrod, D., et al., *Lateral motion of fluorescently labeled acetylcholine receptors in membranes of developing muscle fibers.* Proceedings of the National Academy of Sciences of the United States of America, 1976. **73**(12): p. 4594-8.
200. Venkatakrishnan, G., et al., *Lateral diffusion of nerve growth factor receptor: modulation by ligand-binding and cell-associated factors.* Cell regulation, 1990. **1**(8): p. 605-14.

201. Ellenberg, J., et al., *Nuclear membrane dynamics and reassembly in living cells: targeting of an inner nuclear membrane protein in interphase and mitosis.* The Journal of cell biology, 1997. **138**(6): p. 1193-206.
202. Cole, N.B., et al., *Diffusional mobility of Golgi proteins in membranes of living cells.* Science, 1996. **273**(5276): p. 797-801.
203. Schaaf, M.J., et al., *The relationship between intranuclear mobility of the NF-kappaB subunit p65 and its DNA binding affinity.* The Journal of biological chemistry, 2006. **281**(31): p. 22409-20.
204. Meffert, M.K., et al., *NF-kappa B functions in synaptic signaling and behavior.* Nature neuroscience, 2003. **6**(10): p. 1072-8.
205. Meissner, O. and H. Haberlein, *Lateral mobility and specific binding to GABA(A) receptors on hippocampal neurons monitored by fluorescence correlation spectroscopy.* Biochemistry, 2003. **42**(6): p. 1667-72.
206. Wohland, T., et al., *Study of ligand-receptor interactions by fluorescence correlation spectroscopy with different fluorophores: evidence that the homopentameric 5-hydroxytryptamine type 3As receptor binds only one ligand.* Biochemistry, 1999. **38**(27): p. 8671-81.
207. Klingler, J. and T. Friedrich, *Site-specific interaction of thrombin and inhibitors observed by fluorescence correlation spectroscopy.* Biophysical journal, 1997. **73**(4): p. 2195-200.
208. Bacia, K., et al., *Fluorescence correlation spectroscopy relates rafts in model and native membranes.* Biophysical journal, 2004. **87**(2): p. 1034-43.
209. Eggeling, C., et al., *Direct observation of the nanoscale dynamics of membrane lipids in a living cell.* Nature, 2009. **457**(7233): p. 1159-62.
210. Chen, Y., et al., *Methods to measure the lateral diffusion of membrane lipids and proteins.* Methods, 2006. **39**(2): p. 147-53.
211. Qian, H., M.P. Sheetz, and E.L. Elson, *Single particle tracking. Analysis of diffusion and flow in two-dimensional systems.* Biophysical journal, 1991. **60**(4): p. 910-21.
212. Dembo, M. and A.K. Harris, *Motion of particles adhering to the leading lamella of crawling cells.* The Journal of cell biology, 1981. **91**(2 Pt 1): p. 528-36.
213. Niu, L. and J. Yu, *Investigating intracellular dynamics of FtsZ cytoskeleton with photoactivation single-molecule tracking.* Biophysical journal, 2008. **95**(4): p. 2009-16.
214. McFarlane, S.M., et al., *Differential activation of nuclear factor-kappa B by tumour necrosis factor receptor subtypes. TNFR1 predominates whereas TNFR2 activates transcription poorly.* FEBS letters, 2002. **515**(1-3): p. 119-126.
215. Richter, C., et al., *The Tumor Necrosis Factor Receptor Stalk Regions Define Responsiveness to Soluble versus Membrane-Bound Ligand.* Molecular and cellular biology, 2012. **32**(13): p. 2515-29.
216. Fiers, W., *Tumor necrosis factor. Characterization at the molecular, cellular and in vivo level.* FEBS letters, 1991. **285**(2): p. 199-212.
217. Yang, Z., et al., *Serum components enhance bacterial lipopolysaccharide-induced tissue factor expression and tumor necrosis factor-alpha secretion by bovine alveolar macrophages in vitro.* Journal of leukocyte biology, 1994. **55**(4): p. 483-8.
218. Wombacher, R., et al., *Live-cell super-resolution imaging with trimethoprim conjugates.* Nature methods, 2010. **7**(9): p. 717-9.
219. Woodcock, C.L., et al., *A Chromatin Folding Model That Incorporates Linker Variability Generates Fibers Resembling the Native Structures.* Proceedings of the National Academy of Sciences of the United States of America, 1993. **90**(19): p. 9021-9025.
220. Heun, P., et al., *Chromosome dynamics in the yeast interphase nucleus.* Science, 2001. **294**(5549): p. 2181-6.
221. Kimura, H. and P.R. Cook, *Kinetics of core histones in living human cells: little exchange of H3 and H4 and some rapid exchange of H2B.* The Journal of cell biology, 2001. **153**(7): p. 1341-53.

222. Workman, J.L. and R.E. Kingston, *Alteration of nucleosome structure as a mechanism of transcriptional regulation.* Annual review of biochemistry, 1998. **67**: p. 545-79.
223. Wolffe, A.P. and J.J. Hayes, *Chromatin disruption and modification.* Nucleic acids research, 1999. **27**(3): p. 711-20.
224. Abulrob, A., et al., *Interactions of EGFR and caveolin-1 in human glioblastoma cells: evidence that tyrosine phosphorylation regulates EGFR association with caveolae.* Oncogene, 2004. **23**(41): p. 6967-79.
225. Grassme, H., et al., *CD95 signaling via ceramide-rich membrane rafts.* The Journal of biological chemistry, 2001. **276**(23): p. 20589-96.
226. Heidbreder, M., et al., *TNF-alpha influences the lateral dynamics of TNF receptor I in living cells.* Biochimica et biophysica acta, 2012.
227. Ruthardt, N., D.C. Lamb, and C. Brauchle, *Single-particle tracking as a quantitative microscopy-based approach to unravel cell entry mechanisms of viruses and pharmaceutical nanoparticles.* Molecular therapy : the journal of the American Society of Gene Therapy, 2011. **19**(7): p. 1199-211.
228. Parton, R.G. and A.A. Richards, *Lipid rafts and caveolae as portals for endocytosis: new insights and common mechanisms.* Traffic, 2003. **4**(11): p. 724-38.
229. Yarar, D., C.M. Waterman-Storer, and S.L. Schmid, *A dynamic actin cytoskeleton functions at multiple stages of clathrin-mediated endocytosis.* Molecular biology of the cell, 2005. **16**(2): p. 964-75.
230. Pelkmans, L. and A. Helenius, *Endocytosis via caveolae.* Traffic, 2002. **3**(5): p. 311-20.
231. Gajate, C. and F. Mollinedo, *Cytoskeleton-mediated death receptor and ligand concentration in lipid rafts forms apoptosis-promoting clusters in cancer chemotherapy.* The Journal of biological chemistry, 2005. **280**(12): p. 11641-7.
232. Cottin, V., J.E. Doan, and D.W. Riches, *Restricted localization of the TNF receptor CD120a to lipid rafts: a novel role for the death domain.* Journal of immunology, 2002. **168**(8): p. 4095-102.
233. Lotocki, G., et al., *Tumor necrosis factor receptor 1 and its signaling intermediates are recruited to lipid rafts in the traumatized brain.* The Journal of neuroscience : the official journal of the Society for Neuroscience, 2004. **24**(49): p. 11010-6.
234. Fischer, R., et al., *Ligand-induced internalization of TNF receptor 2 mediated by a di-leucin motif is dispensable for activation of the NFkappaB pathway.* Cellular signalling, 2011. **23**(1): p. 161-70.
235. Briggs, J.A., et al., *The stoichiometry of Gag protein in HIV-1.* Nature structural & molecular biology, 2004. **11**(7): p. 672-5.
236. Subach, F.V., et al., *Bright monomeric photoactivatable red fluorescent protein for two-color super-resolution sptPALM of live cells.* Journal of the American Chemical Society, 2010. **132**(18): p. 6481-91.
237. Ichinose, J., et al., *EGF signalling amplification induced by dynamic clustering of EGFR.* Biochemical and biophysical research communications, 2004. **324**(3): p. 1143-9.
238. Lambert, S., et al., *Ligand-independent activation of the EGFR by lipid raft disruption.* The Journal of investigative dermatology, 2006. **126**(5): p. 954-62.
239. Schoeberl, B., E.D. Gilles, and P. Scheurich, *A mathematical vision of TNF receptor interaction.* In Proceedings of 2nd International Conference on Systems Biology, 2001. **ICSB2001**: p. pp. 158-67.
240. Guicciardi, M.E. and G.J. Gores, *Life and death by death receptors.* FASEB journal : official publication of the Federation of American Societies for Experimental Biology, 2009. **23**(6): p. 1625-37.
241. Endesfelder, U., et al., *Chemically induced photoswitching of fluorescent probes-a general concept for super-resolution microscopy.* Molecules, 2011. **16**(4): p. 3106-18.

242. Sengupta, P. and J. Lippincott-Schwartz, *Quantitative analysis of photoactivated localization microscopy (PALM) datasets using pair-correlation analysis.* BioEssays : news and reviews in molecular, cellular and developmental biology, 2012. **34**(5): p. 396-405.
243. Malkusch, S., et al., *Coordinate-based colocalization analysis of single-molecule localization microscopy data.* Histochemistry and cell biology, 2012. **137**(1): p. 1-10.
244. Zhang, W., et al., *Single-molecule imaging reveals transforming growth factor-beta-induced type II receptor dimerization.* Proceedings of the National Academy of Sciences of the United States of America, 2009. **106**(37): p. 15679-83.
245. Weiss, S., *Fluorescence spectroscopy of single biomolecules.* Science, 1999. **283**(5408): p. 1676-83.
246. Kapanidis, A.N., et al., *Fluorescence-aided molecule sorting: analysis of structure and interactions by alternating-laser excitation of single molecules.* Proceedings of the National Academy of Sciences of the United States of America, 2004. **101**(24): p. 8936-41.
247. Dertinger, T., et al., *Fast, background-free, 3D super-resolution optical fluctuation imaging (SOFI).* Proceedings of the National Academy of Sciences of the United States of America, 2009. **106**(52): p. 22287-92.
248. Dertinger, T., et al., *Superresolution optical fluctuation imaging with organic dyes.* Angewandte Chemie, 2010. **49**(49): p. 9441-3.
249. Terskikh, A., et al., *"Fluorescent timer": protein that changes color with time.* Science, 2000. **290**(5496): p. 1585-8.
250. Kneen, M., et al., *Green fluorescent protein as a noninvasive intracellular pH indicator.* Biophysical journal, 1998. **74**(3): p. 1591-9.
251. Bosisio, D., et al., *A hyper-dynamic equilibrium between promoter-bound and nucleoplasmic dimers controls NF-kappaB-dependent gene activity.* The EMBO journal, 2006. **25**(4): p. 798-810.
252. Levsky, J.M. and R.H. Singer, *Fluorescence in situ hybridization: past, present and future.* Journal of cell science, 2003. **116**(Pt 14): p. 2833-8.
253. Kolb, H.C. and K.B. Sharpless, *The growing impact of click chemistry on drug discovery.* Drug discovery today, 2003. **8**(24): p. 1128-37.
254. Mikenberg, I., et al., *Transcription factor NF-kappaB is transported to the nucleus via cytoplasmic dynein/dynactin motor complex in hippocampal neurons.* PloS one, 2007. **2**(7): p. e589.
255. Zander, C., et al., *Retrograde, dynein-mediated transport of NF-kappaB p65 in hippocampal neurons occurs via heterocomplex formation with HSP90/Hsc70 protein chaperones.* Journal of Neuroscience 2012.
256. Henke, W., et al., *Betaine improves the PCR amplification of GC-rich DNA sequences.* Nucleic acids research, 1997. **25**(19): p. 3957-8.
257. Gould, S.J. and S. Subramani, *Firefly luciferase as a tool in molecular and cell biology.* Analytical biochemistry, 1988. **175**(1): p. 5-13.
258. Izeddin, I., et al., *Wavelet analysis for single molecule localization microscopy.* Optics express, 2012. **20**(3): p. 2081-95.

10. ACKNOWLEDGEMENTS

I would like to thank my supervisor Mike Heilemann for giving me the great opportunity to start working in super-resolution microscopy - I am very grateful for all the invaluable support, challenges, opportunities and encouragement you offered throughout the last three years.
I would also like to thank Christian Kaltschmidt, Barbara Kaltschmidt and Darius Widera who started me on my path researching the TNFSF in the first place, and who always had an open ear for questions, scientific discussions and pleas for help (Darius - I still owe you that beer!).

None of this work would have been possible without the help and advice of our interdisciplinary collaborators:

I thank Jean-Baptiste Sibarita, Deepak Nair and Daniel Choquet for the chance to work at the Interdisciplinary Institute for Neuroscience (IINS) in Bordeaux and for offering their unconditional support at all times. Many thanks also go to Christin Zander for being such an excellent colleague and traveling companion during rainy French nights.

Many thanks to Markus Sauer, Virginia W. Cornish and Richard Wombacher for supplying invaluable input, knowledge and help. Thank you also to everyone in the Sauer Group - especially Sebastian van de Linde, Anna Löschberger, Teresa Klein, Steve Wolter and Simon Hennig - for such a great working atmosphere and unlimited support.

Of course I would also like to thank everyone in the Heilemann Group; we started out small, but so many people have since enriched our little *Reisegruppe Heilemann*. I especially want to thank Sebastian Malkusch, Ulrike Endesfelder and Marina Dietz for fruitful office discussions and help - be it scientific or completely off-topic - in every situation of life. Thanks for bearing with the biologist. Ulrike and Sebastian, thank you also for the best flat share in the history of Reichenberg.

Last but *definetly* not least, I would like to thank my family and friends for their constant, compassionate love and faithful support - despite having no concept of the scientific problems I was talking about most of the time. Alexander - I love you; it's your turn to graduate now!

It's been a rollercoaster ride that started in Bielefeld and led us to Würzburg - as the proverb says: the way is the goal. Thanks to everyone who shared it with me.